On 0-dimensional Modeling of Combustion and Pollutant Formation in Diesel Engines

Author:

Dipl.-Ing. Christoph Pötsch

Institut für Verbrennungskraftmaschinen und Thermodynamik

Graz University of Technology

Chairman:

Univ.-Prof. Dipl.-Ing. Dr. techn. Helmut Eichlseder

Supervisor:

Ao. Univ.-Prof. Dipl.-Ing. Dr. techn. Andreas Wimmer

Approved by:

Prof. Dr.-Ing. habil. Günter P. Merker

External Supervisor:

Dr. Herwig Ofner, AVL List GmbH

Graz, June 2012

If it disagrees with experiment it is wrong.
Richard P. Feynman

Acknowledgements

I would like to thank Prof. Andreas Wimmer for giving me the opportunity to engage in this interesting and challenging topic, and for his scientific support.

Also, I want to extend my thanks to Prof. Günter Merker for evaluating this work.

I want to thank my family and my friends, among them former colleagues, for their support during these years and for the distraction apart from work and studies.

Finally, I would like to say a special word of thanks to Dr. Herwig Ofner. Not only did he initiate and establish the modeling approach that lead to the present work in the research consortium. He made his dedication to the topic express in inspiring discussions, giving advice and support, and his personal contribution far beyond common working hours. Without his commitment, this work would not have been possible.

The present work was carried out during my occupation as research engineer at the K2 Mobility Competence Center as well as during my work as development engineer at AVL List GmbH. In the course of this work two publications were derived which are cited below. The main results of these papers are also documented in the present work.

Poetsch, C., Ofner, H. and Schutting, E., "*Assessment of a Multi Zone Combustion Model for Analysis and Prediction of CI Engine Combustion and Emissions*" SAE Technical Paper, doi:10.4271/2011-01-1439

Poetsch, C., Ofner, H. and Cartellieri, W., "*Analysis of Thermodynamic Characteristics of Diesel Engine Emission Control Strategies Using a Multi-Zone Combustion Model*" SAE Int. Journal of Engines 5(3):2012, doi: 10.4271/2012-01-1340

Deutsche Fassung:
Beschluss der Curricula-Kommission für Bachelor-, Master- und Diplomstudien vom 10.11.2008
Genehmigung des Senates am 1.12.2008

EIDESSTATTLICHE ERKLÄRUNG

Ich erkläre an Eides statt, dass ich die vorliegende Arbeit selbstständig verfasst, andere als die angegebenen Quellen/Hilfsmittel nicht benutzt, und die den benutzten Quellen wörtlich und inhaltlich entnommenen Stellen als solche kenntlich gemacht habe.

Graz, am …… ……..
(Unterschrift)

Englische Fassung:

STATUTORY DECLARATION

I declare that I have authored this thesis independently, that I have not used other than the declared sources / resources, and that I have explicitly marked all material which has been quoted either literally or by content from the used sources.

…… ……..
date (signature)

Abstract

In the course of the present work, a 0-dimensional crank-angle resolved combustion model for the analysis and prediction of the combustion process in Diesel engines is developed. The model calculates heat release and pollutant formation on the basis of the injection characteristics.

The modeling conception is based on the well-established multi-zone package approach. In this type of model the injection spray is sub-divided into a high number of reaction zones. Doing so, the model considers a heterogeneous distribution of states and composition in the injection spray which is seen as a prerequisite for the simultaneous simulation of NO_x and soot emissions. The model takes the main relevant physical mechanisms for the description of the combustion process into account: fuel evaporation, fuel/air mixing (air entrainment) and chemical reactions for heat release and pollutant formation. These mechanisms are calculated as continuous processes within the individual reaction zones. Thus, the model offers a high degree of general validity.

A few modeling extensions are suggested that supplement the genuine multi-zone approach. These especially concern the heat and mass transfer processes between the spray zones. One main advancement is achieved by the introduction of a new distinguished zone that summarizes all burned spray zones. These combustion products are then, together with the fresh charge, recycled into the injection spray. This so-called Re-Entrainment mechanism is crucial for the combustion process in high load operating points and for the prediction of soot emissions.

A systematic method is then presented which identifies the combustion and emission model parameters. This is done in two subsequent steps. First, the combustion model is calibrated by using a new method for a multi-zone pressure trace analysis. On the basis of the predefined combustion process the emission model parameters are then identified. A statistical analysis of the identified parameters allows an assessment of the modeling sophistication.

The model is able to predict engine performance and emissions for different load points and changing operating conditions, such as variations of EGR, turbocharging or injection characteristics with very good accuracy. Therefore, the multi-zone model is used to analyze the impact of different engine settings on the combustion and pollutant formation process. The analysis of these effects concentrates on the fundamental characteristics of the combustion in Diesel engines on the basis of the physical, thermodynamic and reaction kinetic mechanisms.

Kurzfassung

Die vorliegende Arbeit beschäftigt sich mit der Entwicklung eines 0-dimensionalen, kurbelwinkelaufgelösten Berechnungsmodells zur Analyse und Simulation der Verbrennung im Dieselmotor. Das Modell berechnet Wärmefreisetzung und Emissionsentstehung auf Basis des Zylinderzustands und des Einspritzverlaufs.

Das Modell basiert auf dem weit verbreiteten Mehr-Zonen Paket Modellansatz. Bei diesem wird der Einspritzstrahl in eine Vielzahl von Reaktionszonen untereilt. Dadurch ist es möglich, eine heterogene Verteilung von Ladungs-Zusammensetzung und Zustand zu generieren. Dies wird als Grundvoraussetzung für die simultane Berechnung von Stickoxid und Ruß Emissionen gesehen. Der Modellansatz beschreibt die wesentlichen relevanten Mechanismen der Gemischbildung und Verbrennung im Dieselmotor. Dies sind: Kraftstoffverdampfung, Mischung von Luft und Kraftstoff (Entrainment) sowie die chemischen Reaktionen der Verbrennung und Emissionsentstehung. Diese Mechanismen werden als kontinuierliche Prozesse in den einzelnen Reaktionszonen berechnet. Der hohe Grad der Allgemeingültigkeit in der physikalischen Modellierung spiegelt sich darin wieder, dass trotz der komplexen physikalischen Zusammenhänge während der Verbrennung auf Fallunterscheidungen zwischen einzelnen Verbrennungsphasen verzichtet werden kann.

Es werden einige Modellerweiterungen in Ergänzung zum ursprünglichen Modellansatz vorgeschlagen. Diese nehmen vor allem auf die Einschränkung Bezug, dass zwischen einzelnen Reaktionszonen kein Stoff- und Wärmetransport berücksichtigt wird. Eine wesentliche Erweiterung betrifft die Berücksichtigung der Interaktion des Einspritzstrahls mit bereits verbrannten Verbrennungsprodukten über den sogenannten Re-Entrainment Mechanismus. Bei diesem werden die Produkte der vollständig verbrannten Sprayzonen in einer neuen, ausgezeichnet Verbrennungszone gesammelt und über den Entrainment Mechanismus kontinuierlich in den Strahl gemischt. Dieser Mechanismus ist entscheidend für die Simulation von hoch-last Betriebspunkten und für die Vorhersage der Trends der Rußemissionen.

Im anwendungsbezogenen Teil der Arbeit wird eine systematische Methode zur Identifikation der Modellparameter präsentiert. Bei dieser werden zuerst die Parameter des Verbrennungsmodells abgestimmt. Die Grundlage dafür bildet ein neu entwickelter Ansatz für eine mehr-zonige Druckverlaufsanalyse auf Basis des Spraymodells. Auf Basis der vorabgestimmten Verbrennung werden die Paramater der Emissionsmodelle identifiziert. Die Methodik dafür basiert auf einer statistischen Auswertung einer Mehrzahl von eindeutig identifizierten Parameterkombinationen, welche sowohl das Erkennen von Messungenauigkeiten ermöglicht, als auch eine Bewertung der Modellgüte erlaubt.

Mit dem Modell ist es möglich Wärmefreisetzung und Emissionen in einem weiten Kennfeldbereich mit guter Genauigkeit zu berechnen. Dies ermöglicht es, das mehr-zonen Modell für detaillierte Analysen der Einflüsse von unterschiedlichen Betriebsparametern auf die Verbrennung und Schadstoffentstehung einzusetzen. Es wurden Variationen von AGR, Ladedruck, Einspritzzeitpunkt und Einspritzdruck im Detail betrachtet. Die Analyse konzentriert sich auf grundlegende physikalische, thermodynamische und reaktionskinetische Zusammenhänge.

Table of Contents

List of Figures

List of Tables

List of Abbreviations

A	Area, m²
$A, B, \ldots$	Model Coefficients
$[A], [B], \ldots$	Species Fraction
AF_{st}	Stoichiometric Air to Fuel Ratio, kg_{air}/kg_{fuel}
c_D	Discharge Coefficient of Injection Nozzle
c_p	Specific Heat Capacity, J/kg/K
C	Model Constant
$C_{Entrain}$	Charge Entrainment Correction Parameter
C_{Evap}	Evaporation Correction Parameter
C_{IgnDel}	Ignition Delay Correction Parameter
ChF_{st}	Stoichiometric Charge to Fuel Ratio, kg_{charge}/kg_{fuel}
d_{32}	Initial Sauter Mean Diameter, m
d_{inj}	Injector Hole Diameter, m
D_v	Diffusion Coefficient, m²/s
E_a	Activation Energy, kJ/kmol
h_v	Heat of Vaporization, J/kg
H	Absolute Enthalpy, J
H_R	Reaction Enthalpy, kJ/kmol
i	Zone Index
k	Reaction Rate Constant
K_b	Combustion Reaction Correction Parameter
l_n	Needle Lift, m
L	Characteristic Length, m
m	Mass, kg
$\dot{m}$	Massflow, kg/s
n	Engine Speed, min^{-1}
nr	Number of Zones in radial direction
O_2F_{st}	Stoichiometric Oxygen Demand, kg_{O2}/kg_{fuel}
p	Pressure, Pa
p_s	Saturation Pressure, Pa
Q	Thermal Energy, J
R	Gas Constant, kJ/kmol/K
t	Time, s
t_b	Breakup Time, s
T	Temperature, K
u	Specific Internal Energy, J/kg
v	Velocity, m/s
v_{tip}	Tip Penetration Velocity, m/s
V	Volume, m³
w	Species
x	Mass Fraction
X_{egr}, X_{rg}	Residual Gas Fraction
Y	Stoichiometric Ratio, $kg_{species}/kg_{fuel}$

Dimensionless Groups

Nu	Nusselt Number
Sh	Sherwood Number
Re	Reynolds Number
Da	Damköhler Number
Oh	Ohnesorge Number
We	Weber Number

Greek

φ	Crank-Angle Position
σ	Surface Tension, N/m
υ	Kinematic Viscosity, m^2/s
ρ	Density, kg/m^3
λ	Lambda Value; Thermal Conductivity, W/m/K
μ	Molar Fraction, mol/mol
ζ	Flow Coefficient

Subscripts

ax	Axial Position
b	Burned
c	Spray Center
ch	Cylinder Charge
comb	Combustion
cp	Combustion Products
cyl	Cylinder
ex	Exhaust
f	Formation; Forward Reaction
fb	Fuel Burned
fv	Fuel Vapor
g	Global
i	Zone Index
in	Intake
inj	Injection
j	Species Index
l	Liquid
L	Local (Lambda)
m	Mean Value
max	Peak Value
NH	Nozzle Hole
NS	Needle Seat
rad	Radial Position
rg	Residual Gas

r	Backward Reaction
s	Soot, Saturation
sc	Scavenging
st	Stoichiometric
t	Trapped
ub	Unburned
wt	Weight
z	Zone

Abbreviations

CI	Compression Ignition
CFD	Computational Fluid Dynamics
CR	Common Rail
CRFD	Computational Reacting Fluid Dynamics
DI	Direct Injection
EGR	Exhaust Gas Recirculation
EOI	End of Injection
EVO	Exhaust Valve Opening
HCCI	Homogeneous Charge Compression Ignition
HP	High Pressure
ICE	Internal Combustion Engine
IMEP	Indicated Mean Effective Pressure
IVC	Intake Valve Closing
MFB	Mass of Fuel Burned
MZCM	Multi-Zone Combustion Model
OP	Operating Point
PTA	Pressure Trace Analysis
ROHR	Rate of Heat Release
ROI	Rate of Injection
SHP	Start of High Pressure
SI	Spark Ignited
SMD	Sauter Mean Diameter
SOC	Start of Combustion
SOI	Start of Injection
WPC	Working-process Calculation
wt	Weight

1 Introduction

1.1 Motivation

Today's engine development process is characterized by tightening of emission regulations and reducing fuel consumption targets. These topics do not only concern the sustainability in an environment of growing demands in propulsion but also gain increasing public attention. The ambitious development targets at the limits of technical feasibility result in a growing complexity of the engine and periphery systems. Electronically controlled common-rail injection systems, multi-stage variable turbochargers, and controlled EGR and cooling systems result in an increasing number of degrees of freedom. In this context, highly accurate simulation tools play an important role in minimizing of development time and optimizing cost efficiency.

Today, it is common practice to apply 1-dimensional model codes for engine cycle simulations that describe the thermo- and fluid dynamic processes in the engine and periphery with high accuracy. These models consider the relevant variables, such as the gas exchange process of the multi-cylinder arrangement with its pipes and volumes, turbocharger(s), charge air cooler(s), exhaust gas recirculation, valve timing, exhaust after-treatment volumes, etc. An essential part of these full cycle simulation codes is the description of the in-cylinder combustion and pollutant formation processes for changing operating conditions. For this purpose predictive 0-dimensional, crank angle resolved combustion models are commonly applied as they provide a high content of information within short computational time.

In Diesel engines the combustion process and pollutant formation is characterized by a dynamic interrelation of physical and chemical processes. Liquid fuel is injected into the compressed charge of the engine where it evaporates and mixes with the oxygen containing charge. Due to the structure of the fuel jet the distribution of reactants is highly heterogeneous. Chemical processes govern the local auto ignition process and the reaction of fuel and oxygen. Today, 0-dimensional simulation codes are available that predict rate of heat release and NO_x emissions with reasonably good accuracy. Still, especially the very sophisticated task of predicting soot emissions provides room for improvement.

1.2 Definition and Delimitation of Research Objectives

Subject of the present work is the development of a 0-dimensional combustion model that simulates the combustion process in direct-injection diesel engines. The modeling approach aims at describing the rate of heat release on a physical basis as generally valid as possible, nevertheless the focus lies on conventional combustion concepts (in contrast to low temperature combustion concepts e.g. HCCI). Furthermore, the model is intended to predict engine out emissions with focus on NO_x and soot. The calculation time is supposed to be in the order of magnitude of existing 0D/1D codes.

For the modeling of pollutant formation, especially the simultaneous calculation of NO_x and soot, it is seen as a prerequisite to consider a heterogeneous distribution of states and composition in the injection spray. This can be achieved by sub-dividing the cylinder volume into a high number of reaction zones, which have their own history of thermodynamic state and composition. Within these zero-dimensional multi-zone models, the package approach of Hiroyasu has proven its applicability for the prediction of Diesel engine combustion. The modeling conception offers a very high modeling depth for 0-dimensional modeling, as it considers all relevant physical mechanisms: fuel evaporation, fuel/air mixing (air entrainment) and the chemical reaction. All these mechanisms are modeled as integrated and continuous processes, which indicates a high degree of general validity.

As a starting point for the development, a general thermodynamic calculation platform is set up. The combustion model is implemented on the basis of well-established state-of-the-art multi-zone models. The model is validated by a continuous comparison of results with engine testbed measurement data. Therefore a reasonable range of operating conditions is selected, including different engine speeds and loads as well as variations of operation settings in single operating points. The target of this process is to show whether certain modeling assumptions and simplifications, such as the neglecting of heat and mass transfer between the spray zones, are still valid for modern combustion concepts. The findings of this permanent development and validation process are the basis for the modeling extensions, which supplement the current state-of-the-art models. Extensions are introduced, only if absolutely necessary and when the hypotheses of the new approaches are confirmed by the physical principles of the combustion process.

Questions regarding model development and validation:

- Q I.1: Are the assumptions and simplifications of the modeling approach, e.g. neglecting of heat and mass transfer between zones still valid for modern combustion concepts?
- Q I.2: Or: Are there reasonable modeling extensions to overcome any limitations observed during the validation?
- Q I.3: Is it possible or not to predict engine performance and emissions (NO_x and soot) in a reasonable range of operating conditions?

The individual processes in the multi-zone model are described by phenomenological sub-models. Due to several simplifications these models are usually calibrated to a specific engine configuration by empirical parameters, which need to be identified from measurements. To assure a certain degree of general applicability but also to ensure the usability of the model, it is necessary to reduce the number of parameters to a minimum. Consequently, the aim is to develop a systematic procedure for automatic parameter identification which delivers unambiguous solutions for the set of model parameters. Finally, the spreading of the identified parameters allows an assessment of the modeling sophistication.

Questions regarding model parameterization and usability:

- Q II.1: Which are the main relevant parameters for the combustion and emission models?
- Q II.2: How many parameters are required overall to tune the model to one specific engine?
- Q II.3: (How) Is it possible to automatically identify the parameters on the basis of measurements?
- Q II.4: What is the spreading of the parameter solutions for one engine and for different engines?
- Q II.5: Is it possible to transfer an unambiguously identified set of model parameters from one engine to another?

Diesel engine emissions are controlled by various engine operating conditions, such as EGR and turbocharging, and the injection characteristics: injection pressure and timing. From a physical point of view, these measures have a fundamentally different causal impact on the combustion and pollutant formation processes. The multi-zone model is used to analyze these measures on the basis of their causal physical effects. Therefore, well directed measurements are conducted and systematically analyzed.

Questions regarding application of the model for analysis purposes:

- Q III.1: Which are the main boundary conditions for the combustion and pollutant formation in diesel engines?
- Q III.2: How do these boundary conditions affect the process from a basic physical point of view?
- Q III.3: How are the changes represented in the multi-zone model?
- Q III.4: When and under which conditions are emissions predominantly formed in the multi-zone model?

2 Fundamentals of Combustion with Focus on Diesel Engines

The combustion process in engines is governed mainly by three different combustion regimes. An overview of these regimes and a classification of several combustion concepts is exemplarily shown in Figure 1. In this triangular plot, the corners mark the individual combustion regimes. In modern engines, with alternative approaches for Diesel and Spark-Ignited (SI) combustion concepts, a clear separation in-between these distinct regimes is not possible anymore, so that in reality, usually a combination exists. Thus, the classification of combustion concepts within this plot usually leads to an assignment on the axes between two relevant regimes.

In the classic Flame-Front combustion (lower right corner), the mixture is homogeneously premixed at the beginning of the combustion. However, the present thermodynamic conditions do not lead to auto-ignition in the available time. Combustion is induced by an external energy source. Then the flame-front progresses trough the homogeneous mixture as the unburned fuel is ignited by the heat up from the adjacent hot combustion gas. If the conditions in the unburned region are near auto-ignition, the heat up and compression due to the combustion can lead to an immediate auto-ignition (detonation) in the unburned mixture. This phenomenon is known as knocking combustion in SI-Engines.

In the classic Diesel combustion the boundary conditions (pressure and temperature) generated by the compression stroke are sufficient for auto-ignition. However the reactants fuel and oxygen are initially unmixed. Combustion requires two steps: (1) the forming of a combustible mixture by physical mixing and (2) the chemical reaction. Depending on the operating conditions either of these steps can limit the heat release. In the distinct case of diffusion combustion (lower left corner), the chemical reaction is a lot faster than the physical mixing process. This is the case for example in direction injection Diesel engines with pilot injections, which generate conditions that enhance the chemical reactivity for the main injection.

If the chemical reaction is slow, the ignition delay enhances and the homogeneously premixed fraction increases. In this case, the chemical reaction controls the heat release and the combustion regime moves upwards on the left axis. The most distinguished form of homogeneous auto-ignition (upper corner) exists, if the entire mixture ignites almost simultaneously and is spatially distributed, without a previous flame-front or diffusion combustion phase. The related combustion concept is applied for both diesel and gasoline fuels and is commonly described as Homogeneous Charge Compression Ignition (HCCI).

In stratified SI combustion concepts, assigned to the bottom axis, the combustion is induced externally at a moment when the mixture is only partially mixed. Hence, the flame front progresses through both, fuel lean and fuel rich areas. In the rich regions part of the fuel remains un-oxidized after the flame-front. This partially burned fuel consequently oxidizes in a postponed diffusion type combustion phase.

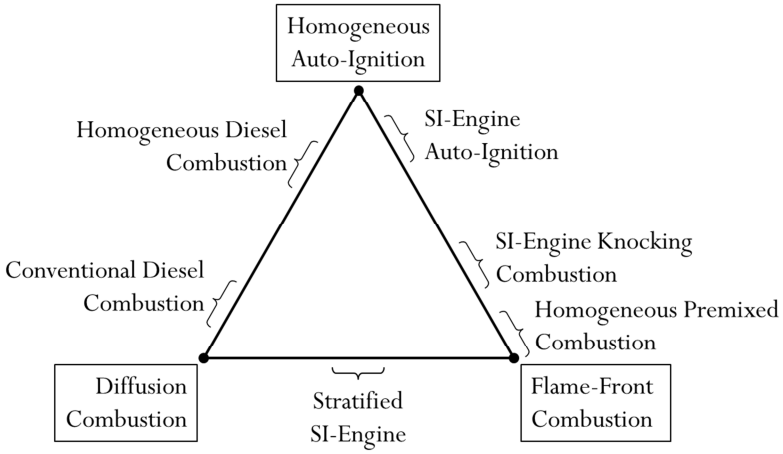

Figure 1: Overview of Combustion Mechanisms and Technologies acc. to [1]

In reality, the processes of turbulent mixing and heat transfer, as well as the chemical reaction always run simultaneously. A quantitative measure for describing which of the processes is predominant is given by the dimensionless Damköhler-Number (*Da*), which is defined as the ratio of the timescale of the turbulent flow to the timescale of the chemical reaction:

$$Da = \frac{\tau_{turb}}{\tau_{chem}} \tag{2-1}$$

Some simulation approaches take advantage of high Damköhler-Numbers ($Da>>1$) by assuming that the turbulent mixing is predominant for the heat release and thus the modeling of the chemical reaction cancels. [1]

2.1 Chemical Reaction

2.1.1 Fundamentals

A chemical reaction of the educts *A, B, C, …* and the products *D, E, F, …* is described by eq. (2-2). Here, the ν_i represent the stoichiometric coefficients of the reaction. On the microscopic scale forward and backward reaction always run simultaneously, as indicated by the bidirectional arrows. The macroscopically observed reaction is the difference between forward and backward reaction. In the special case of chemical equilibrium, both forward and backward reaction rates are equal so that no macroscopic reaction can be observed.

$$-\nu_A \cdot [A] - \nu_B \cdot [B] - \nu_C \cdot [C] - \ldots \underset{k^{(r)}}{\overset{k^{(f)}}{\rightleftharpoons}} \nu_D \cdot [D] + \nu_E \cdot [E] + \nu_F \cdot [F] + \ldots \tag{2-2}$$

The temporal development of the reaction is described by chemical reaction kinetics. Any reaction runs towards chemical equilibrium. The development of the concentrations is given by the temporal evolution of the rate constants $k^{(f)}$ and $k^{(r)}$ and the species balance. For reaction (2-2) the derivative of the concentration of an individual species (e.g. *[A]*) is described by the empirical approach:

$$\frac{d[A]}{dt} = -k^{(f)} \cdot [A]^a \cdot [B]^b \cdot [C]^c \cdot \ldots \tag{2-3}$$

The number of involved atoms and molecules defines the molecularity of a reaction. *a, b, c, …* denote the reaction order of the species *A, B, C,….* Only for elementary reactions (which are defined as running in a single reaction step) the reaction order equals the molecularity. In general, the reaction order needs to be estimated from measurements. The overall order of the reaction is defined by the sum of the sub-reactions ($n=a+b+c+\ldots$).

The reaction rate constants in $k^{(i)}$ are highly temperature-dependent. One relevant factor for the reaction velocity is the frequency of collisions between the involved molecules, which increases with temperature. Additionally, there is a certain threshold of kinetic energy required to let the molecules react in case of a collision which is known as activation energy. The temperature characteristics of the reaction rate constant are often described by the empirical function (2-4), which is known as Arrhenius approach. Here, *B* is the frequency factor which describes the number of collisions per time. The exponential term represents the temperature characteristics due to the required activation energy. Additionally, the temperature can be considered in a pre-exponential term T^n. [2], [3], [4]

$$k(T) = B \cdot T^n \cdot e^{\frac{-E_a}{R \cdot T}} \tag{2-4}$$

2.1.2 Hydrocarbon Oxidation

Stoichiometry

In the case of complete combustion, a hydrocarbon compound $C_cH_hO_o$ is oxidized to carbon dioxide CO_2 and water vapor $H_2O^{(v)}$. The corresponding reaction equation is given by (2-5). The energy released during the exothermic reaction is expressed by the reaction enthalpy ΔH_R.

$$C_cH_hO_o + \left(c + \frac{h}{4} - \frac{o}{2}\right) \cdot O_2 + \longleftrightarrow c \cdot CO_2 + \left(\frac{h}{2}\right) \cdot H_2O + \Delta H_R \tag{2-5}$$

From the reaction equation it is possible to calculate the stoichiometric oxygen demand for a given 'Model Fuel'. It only depends on the composition of the hydrocarbon compound (defined by the molar fractions of C, H, and O in $kmol/kmol_{Fuel}$) and on the fuels molar weight. In the present case, the stoichiometric ratios are defined mass related.

The 'Model Air' is defined by the mass fractions of O_2, N_2, and Ar. The oxygen concentration thus defines the stoichiometric air-to-fuel ratio for fresh air by eq. (2-7). For engines the composition of the working gas (=cylinder charge at IVC) usually differs from fresh air due to the dilution with residual gas from the gas exchange (internal EGR) and external EGR. Therefore, the more descriptive charge-to-fuel ratio is defined by eq. (2-8) which considers the oxygen concentration of the cylinder charge x_{O2}^{ch}.

$$O_2F_{st} = \underbrace{\left(c + \frac{h}{4} - \frac{o}{2}\right) \cdot \frac{M_{O_2}}{M_{fuel}}}_{\text{'Model Fuel'}} \tag{2-6}$$

$$AF_{st} = O_2F_{st} \cdot \underbrace{\frac{1}{x_{O_2}^{air}}}_{\text{'Model Air'}} \tag{2-7}$$

$$ChF_{st} = \frac{O_2F_{st}}{x_{O_2}^{ch}} \tag{2-8}$$

Species Balance for Products of Complete Combustion

For stoichiometric conditions the mass fractions of m species (products of complete combustion) are unambiguously defined by a number of m equations. These are the stoichiometric ratios of all relevant species defined by the composition of model air and model fuel, analogous to eq. (2-6).

Usually, the combustion process does not take place under stoichiometric conditions. Therefore, an additional equation is required to define the species concentrations. This $m+1^{st}$ equation is expressed by the lambda[1] value. Generally speaking, it is defined as the ratio of actual oxygen to stoichiometric oxygen (2-9). In practical use this definition is interpreted ambivalently.

One definition refers to the values available from testbed measurements, where intake air massflow and fuel massflow are measured. The resulting lambda value is defined by the ratio of oxygen in the intake air to fuel mass (2-10). Due to mass conservation, this value represents the composition of the exhaust

[1] The value which is defined here is often denoted as 'air-excess ratio'. However, since in the present work this definition is used in a more general context, the term 'lambda' is preferred.

gas combustion products (for steady state operation). In the present work, this value is denoted as 'global' lambda value λ_g.

General: $$\lambda = \frac{m_{O_2}}{m_{O_2^{st}}} = \frac{m_{O_2}}{m_{fuel} \cdot O_2 F_{st}} \tag{2-9}$$

Measurement $$\lambda_g = \frac{m_{O_2}}{m_{O_2^{st}}} = \frac{m_{air} \cdot x_{o_2}^{air}}{m_{fuel} \cdot O_2 F_{st}} = \frac{m_{air}}{m_{fuel} \cdot AF_{st}} \tag{2-10}$$

In the case of $\lambda_g \neq 1$ the combustion products contain either unburned fuel or oxygen. If exhaust gas is recirculated, the actual in-cylinder lambda value at IVC is not reflected by the global lambda value. Therefore, a so-called 'combustion' lambda value λ_{comb} is defined, which is expressed by eq. (2-11). This value represents the in-cylinder conditions at IVC which are relevant for the combustion process.

In-Cylinder $$\lambda_{comb} = \frac{m_{o_2}^{ch}}{m_{O_2^{st}}} = \frac{m_{air} \cdot x_{o_2}^{air} + m_{cp} \cdot x_{O_2}^{cp}}{\left(m_{fuel} + m_{cp} \cdot x_{fuel}^{cp}\right) \cdot O_2 F_{st}} = \frac{m_{air} \cdot \left(x_{o_2}^{air} + x_{cp} \cdot x_{O_2}^{cp}\right)}{m_{fuel} \cdot \left(1 + \lambda_g \cdot x_{cp} \cdot x_{fuel}^{cp}\right) \cdot O_2 F_{st}} \tag{2-11}$$

As indicated by equation (2-11), the recirculated combustion products lead to an additional degree of freedom in defining the composition of the working gas at IVC. The required $m+2^{nd}$ equation is expressed by the combustion products concentration $x_{cp}=m_{cp}/m_{air}$. As the species concentrations in the recirculated combustion products are known (2-12), the data pair lambda global λ_g and residual gas concentration x_{cp} unambiguously defines the charge oxygen concentration x_{O2}^{ch} and combustion lambda λ_{comb} at IVC. The calculation of the combustion products concentration from measurement data is discussed in chapter 3.2.1.

The species concentrations in the exhaust gas are calculated from stoichiometry as a function of the global lambda value using eq. (2-12). The equation uses the mass fraction of the individual species in the intake air $x_{Y_j}^{air}$ and the stoichiometric ratio Y_j^{st}. To enable a consistent treatment of both products and educts of the reaction, the stoichiometric ratios of species, which are consumed by the reaction (such as O_2), are defined with negative prefixes while coefficients of the products (CO_2 and H_2O) are positive.

$$x_{Y_j}^{cp} = \frac{x_{Y_j}^{air} \cdot \lambda_g \cdot AF_{st} + Y_j^{st}}{1 + \lambda_g \cdot AF_{st}} \tag{2-12}$$

Figure 2 illustrates the interrelations between lambda, residual gas and charge composition by means of an example. The figure refers to a local area (or zone) of the cylinder. In the case of heterogeneous mixture formation, the local combustion conditions do not necessarily represent the global values. The charge mass is composed from fresh air and residual gases, the composition of which is defined by the global lambda. It is assumed that fuel, air and residual gasses are perfectly mixed.

Before combustion begins, the lambda value of this zone λ_Z results from the fractions of fuel and oxygen. With these values the composition of the zone is unambiguously defined. For a closed system the lambda value needs to be constant during combustion although the species concentrations change significantly. Therefore, a general definition of the lambda value that is independent from the combustion progress similar to the mixture ratio, is required.

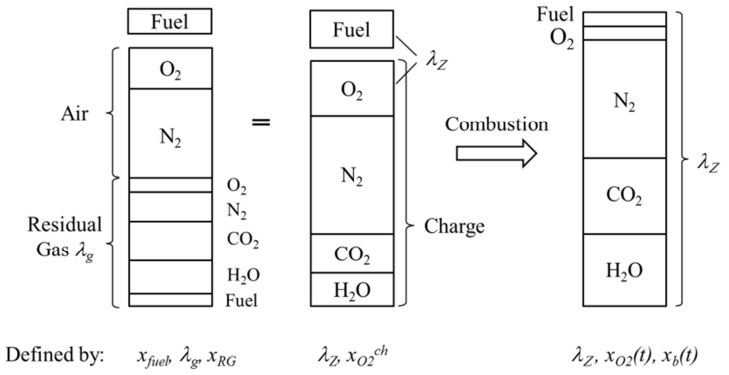

Figure 2: Schematic representation of working gas species concentrations during combustion

As stated above the species conversion during combustion causes another degree of freedom for the definition of composition. The formation and consumption of the individual species is directly related to the combustion progress by the stoichiometric ratios. Therefore, as an additional relation the value x_b is introduced, defined as the ratio of burned fuel to overall fuel. The species concentrations at an arbitrary instant t can now be calculated from the balance equations of the individual components. For a closed system with initial composition defined by λ_Z and x_{O2}^{ch}, the evolution of species concentrations during the process is expressed by eq. (2-13) (exemplarily shown for oxygen). Vice versa, the lambda value of a system λ_Z can be calculated from the instantaneous concentration of an arbitrary species and the fuel burned fraction (2-14).

$$x_{O_2}(t) = \frac{\lambda_Z \cdot ChF_{st} \cdot x_{O_2}^{ch} + O_2^{st} \cdot x_b(t)}{1 + \lambda_Z \cdot ChF_{st}} \tag{2-13}$$

$$\lambda_Z = \frac{1}{ChF_{st}} \frac{x_{O_2}(t) \cdot O_2^{st} \cdot x_b(t)}{x_{O_2}^{ch} - x_{O_2}(t)} \tag{2-14}$$

In summary it can be said that for an arbitrary combustion system the species concentrations are defined by the stoichiometric ratios (which are constant for a given model air and model fuel) and three independent values λ_Z, x_{O2}^{ch} and x_b.

The considerations made above assume a complete combustion of the available fuel and oxygen. However, even if there is plenty of time, the reaction would only proceed until chemical equilibrium is reached. So in reality there is always a small fraction of fuel and oxygen that remains unburned.

Detailed Chemical Reaction

For some purposes a detailed description of the hydrocarbon combustion mechanism is desired, including especially the temporal development of species concentrations, which can be important for the simulation of pollutant formation. In this case, the overall reaction has to be split up into a complex reaction scheme which involves a high number of elementary reactions. The relevant reaction paths and their temperature characteristics must be identified from measurements.

Figure 3 shows a schematic representation of the temporal evolution of concentrations for hydrocarbon oxidation given in [1], [5]. The results derive from calculations with detailed chemical reaction kinetics for several intermediate species. Initially, a detraction of the more volatile hydrogen atoms occurs, which leads to a dehydration and a lowering of the H/C ratio with the formation of Methane, Ethane but also Acetylene. In this early stage, only about 15% of the overall fuel energy is released. Via the intermediate step of Aldehyde formation, the species CO and H_2O are formed. This step releases

another 45% of the energy. A substantial fraction of about 40% of the overall fuel energy is released in the last step, which is the oxidation of CO to CO_2.

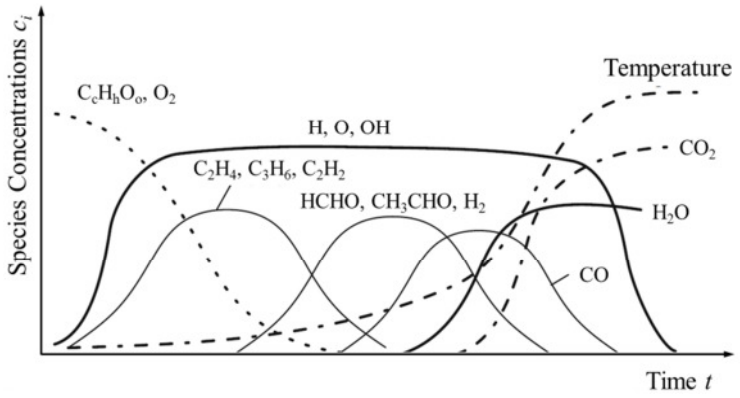

Figure 3: Temporal Evolution of Concentrations during Combustion of Hydrocarbons [1]

2.2 Phenomenology of Mixture Formation and Combustion in Diesel Sprays

In conventional Diesel engine combustion concepts the combustion process is characterized by internal mixture preparation which leads to diffusion type combustion of a heterogeneous mixture. The fuel is injected directly into the cylinder with a high velocity around firing top dead center (TDC). After the nozzle hole exit the liquid fuel breaks up and forms a cone-shaped spray. The spray geometry, characterized by spray angle and penetration length, depends on nozzle geometry and operating parameters such as injection pressure or cylinder backpressure. The initially liquid fuel is dispersed to small droplets due to mechanisms known as primary and secondary breakup. The breakup determines the droplet size distribution, which varies within the different regions the spray. A very detailed description of these mechanisms is given e.g. in [6], [7] and [8].

The different types of breakup mechanisms depend on the fluid mechanic properties of the fuel, and on injection properties, such as spray geometry or injection velocity. They can be classified by means of similarity law considerations. The primary breakup describes the initial decomposition of the condensed liquid core to single droplets. It is mainly caused by turbulence and cavitation phenomena in the injector nozzle hole and after the nozzle exit. The corresponding dimensionless measure would be the Reynolds-Number (*Re*), which is defined as the ratio between inertial forces and viscous forces. [9], [10] Secondary breakup describes the disintegration of existing droplets due to aerodynamic forces, resulting from the velocity difference between droplet and cylinder charge. It can be characterized by means of the Weber-Number (*We*), which defines the ratio between inertia and surface tension. [11], [12] The Ohnesorge-Number (*Oh*) can be thought of as the ratio between surface forces and viscous forces. It is used to characterize different spray breakup regimes. At conditions typical for modern diesel injection systems, the injection is characterized by very high Re-Numbers and Oh-Numbers which leads to an atomization type breakup of the spray. [1], [6]

$$Re = \frac{v \cdot L}{\upsilon} \tag{2-15}$$

$$We = \frac{\rho \cdot v^2 \cdot L}{\sigma} \tag{2-16}$$

$$Oh = \frac{\sqrt{We}}{Re} \tag{2-17}$$

Due to the high temperatures of the surrounding air, the droplets heat up and evaporate. Aside from fuel properties and the thermodynamic conditions in the cylinder (pressure and temperature), another criterion for the evaporation rate is the surface area of the droplets, which is then again determined by the break-up mechanisms. The required energy for the heat-up and vaporization is detracted from the surrounding charge.

Fuel droplets and fuel vapor penetrate the cylinder and distribute within the surrounding charge. Due to the high momentum of the injection, the cylinder charge is entrained into the fuel spray. This leads to a mixing of the reactants, fuel and oxygen. Aside from the momentum impinged by the injection, the mixture formation is additionally enhanced by the interaction between the injection spray and the macroscopic flow field in the cylinder, especially swirl and squish. Inlet design for high swirl usually negatively affects the intake flow coefficients causing deterioration of cylinder filling and efficiency. The swirl motion depends on the design of the inlet system and operating conditions, especially engine speed. To prevent interaction of injection sprays, it is necessary to match the swirl level to combustion system parameters, such as the number of injector holes and the spray angle. An optimization of the swirl level in a wide range of engine operating conditions requires a variability in the inlet system, which can be achieved e.g. by switchable throttle valves. Other macroscopic flows, especially the tumble flow have minor impact on Diesel engines, as they would collapse during the compression stroke.

As soon as a combustible mixture has been formed, the auto-ignition processes begin and run until combustion starts. The precursor steps that lead to ignition are characterized by complex reaction kinetic processes and branching mechanisms in the hydrocarbon chains. Two common modeling conceptions for this process are the thermal and the chemical explosion. Thermal explosion occurs when the released energy of the exothermic chemical reaction exceeds the external heat losses [13]. The thesis of the chemical explosion states that at first, precursor reactions run which form radicals without initial heat release. As soon as a sufficient amount of radicals is present, a chain reaction is initialized which leads to a chemical explosion [2].

Finally, energy is released by the exothermic chemical reaction of the fuel hydrocarbons and oxygen. The reaction rate is governed by chemical reaction kinetics. The fundamentals of this mechanism have been described in detail in the previous Chapter 2.1.

2.2.1 Phases of Heat Release and Emission Formation

In Diesel engines all the described processes (spray breakup, entrainment, mixing, ignition and combustion) run simultaneously. The overlapping and interaction of the mechanisms determine a characteristic rate of heat release profile. The combustion process can be characterized by 4 different phases, as schematically represented in Figure 4.

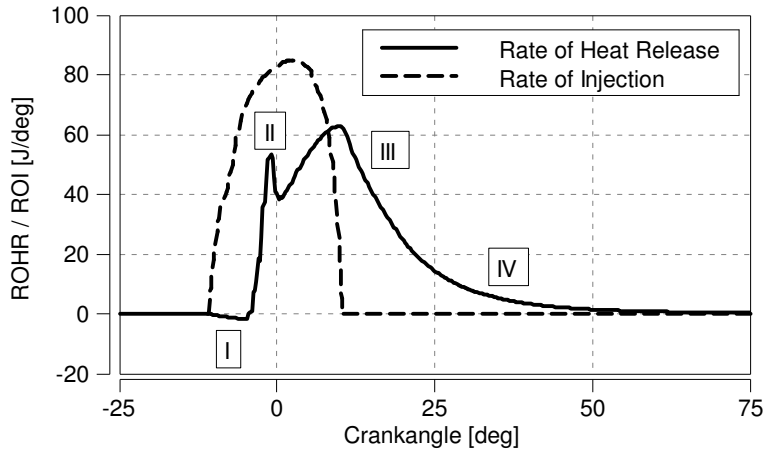

Figure 4: Phases of Combustion in Diesel Engines

Phase I is the ignition delay period from Start of Injection (SOI) to Start of Combustion (SOC) in which the initial mixture formation occurs. The energy needed for evaporation leads to a cooling of the charge which causes a negative zero crossing in the heat release curve.

Phase II: After the initial ignition the fuel which evaporates and mixes during ignition delay time, is ignited by the hot combustion gases. This causes an almost instantaneous combustion of the premixed fuel, represented by a distinct peak in the heat release curve.

In the following Phase III, the heat release is governed by the turbulent mixing process of fuel and air, driven by the momentum induced by the spray. In this phase, also known as diffusive combustion phase, all the mechanisms mentioned above (spray breakup, mixture formation and ignition delay, combustion) run simultaneously. Dec et al. [14] and Flynn et al. [15] have introduced a conceptional model for Diesel sprays under steady state conditions, which is commonly used to describe the processes during the mixture controlled combustion phase. The concept is represented in Figure 5, giving a cross section through the reacting spray. The initially liquid fuel enters the cylinder, mixes with charge and evaporates. Right after the liquid fuel core, the mixture is initially very rich. Under thermodynamic conditions typical for Diesel engines, ignition occurs at local air excess ratio of 0.25 to 0.65 [16]. Thus, the fuel can only partially oxidize and the temperatures reach approximately 1600 K. In this region precursor species are formed which are the sources for soot formation that occurs in the intermediate region of the spray. Further downstream, the air excess ratio increases which is enhanced at the spray border. At some point, stoichiometric conditions are reached. The iso-surface of stoichiometric air to fuel ratio depicts the boundary of the diffusion flame. In this area the highest temperatures of up to 2700 K can be observed which, in the presence of oxygen (lean side), leads to NO formation. When the rich combustion products pass through the diffusion flame region, a high fraction of the incompletely burned hydrocarbons, carbon monoxide, and Soot are oxidized to CO_2 and H_2O. The mechanisms of NO and soot formation are described in further detail in the following section.

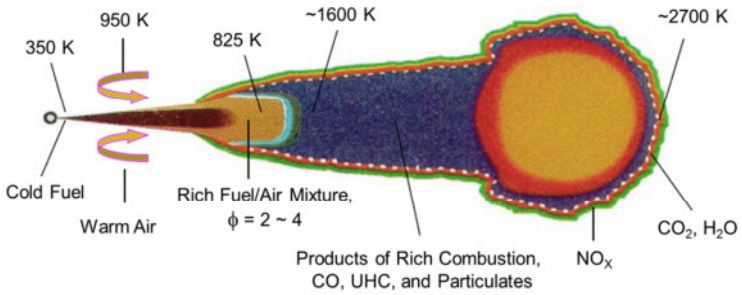

Figure 5: Conceptional Scheme of Dec [14] and Flynn [15] for Diesel Combustion

At End of Injection (EOI) the spray momentum extinguishes abruptly which leads to a sharp drop in the heat release rate. This area represents the smooth transition between combustion Phase III and Phase IV. Due to the piston expansion, the temperature in the cylinder drops. This can slow down the chemical reaction in a way that the heat release becomes reaction kinetic controlled again. Aside from the heat release, this temperature drop can also significantly affect the soot oxidation which requires temperatures above 1300 K.

2.3 Pollutant Formation

In case of a perfect combustion, the exhaust gas would only consist of the combustion products CO_2, H_2O and unburned air. While the latter two components are not harmful to health, CO_2 is seen as jointly responsible for the greenhouse effect.

As already mentioned briefly in the previous chapters, the actual, imperfect combustion process leads to the formation of several pollutant species. These are in particular products of the incomplete

combustion; unburned hydrocarbons (HC) and carbon monoxide (CO), and particulates or soot, as well as nitric oxides (NO_x). These pollutant species make only a small fraction of the overall exhaust mass. However, due to their effects on health, the emission of these components is regulated by legislation.

In gasoline engines with near-stoichiometric combustion the engine-out emissions of all relevant components can be reduced significantly by 3-way catalytic converters. Due to the lean combustion, this principle cannot be applied to diesel engines, which makes exhaust aftertreatment very demanding. This especially regards the reduction of NO_x. Inner motoric measures, which reduce NO_x, usually lead to an increase of soot emissions which causes the intrinsic diesel engine emissions trade-off. Therefore, the present work focuses on the analysis and prediction of the two pollutant emissions NO_x and soot. The present chapter describes the formation processes with regards to their basic physical and chemical principles. The models which are used to simulate these mechanisms are given in the later section 4.3: Modeling Pollutant Formation.

2.3.1 Nitrogen Oxides

Molecular nitrogen which is the major fraction of fresh air, is very stable due to its triple bond. Still, it can under specific circumstances react with oxygen to nitrogen oxides. In engine exhaust gas emissions, nitrogen oxides (NO_x) summarize nitric oxide (NO) and nitrogen dioxide (NO_2). The predominant species formed during combustion in engines is NO which oxidizes to NO_2 in the atmosphere. There are 4 different mechanisms of NO_x formation that are relevant for combustion engines.

Thermal NO

The mechanism of thermal NO formation takes place at high temperatures of above 2200K, which occur in the hot combustion gas after the flame front. The corresponding reaction mechanism was first introduced by Zeldovich in [17]. It originally involved only 2 reactions. The first one describes the reaction of N_2 and oxygen to NO and N. Due to the high activation energy required for breaking up the N_2 triple bond it is the rate determining step. The remaining atomic nitrogen from the first reaction then oxidizes and forms NO in the second step. Aside from the major influence of the temperature, the relevant factors are the availability of oxygen and the detention period at high temperatures. Due to the fast temperature drop in the expansion stroke, the reaction is frozen at some point and the NO formed in the hot combustion phase remains present until EVO. Thus, the exhaust concentrations are usually higher than depicted by chemical equilibrium. Thermal NO makes 80-95% of the overall engine-out NO_x emissions [5], [18]. For this reason, the model developed for the present work considers only thermal NO. A detailed description of the applied extended Zeldovich mechanism is given in Chapter 4.3.1.

Prompt NO

At fuel-rich conditions, hydrocarbon radicals are formed as intermediate species during combustion. These radicals react with nitrogen and form hydrogen-cyanide (HCN) and atomic nitrogen. In a subsequent oxidization step NO is formed. This process is known as Fenimore mechanism and has been introduced in [19]. Due to the low required activation energies, this mechanism already runs at relatively low temperatures of around 1000K. The overall amount of Prompt-NO makes approximately 5-20% of the overall emissions. The relative faction is higher at low temperature combustion modes, such as part load and high EGR cases. [2], [18], [20]

Fuel NO

During the combustion process the fuel bound nitrogen can react with oxygen to NO. In modern standard Diesel fuels with nitrogen mass content of below 0.01%, the contribution to overall NO emissions in negligible. [18], [20]

N_2O Mechanism

The formation of N_2O runs analogously to the first reaction step of the Zeldovich mechanism. However, there is an additional collision molecule involved which reduces the activation energy of the reaction. In a second reaction step, N_2O and oxygen form NO. Since the first reaction involves a three-body-collision, it runs predominantly at high pressure. The temperature has minor impact on the reaction rate. This mechanism gains importance at lean conditions and low temperatures, at which Thermal and Prompt NO formation are low. Such conditions occur for example during HCCI combustion. [5], [21]

2.3.2 Particulate Matter and Soot

In common speech use the terms 'soot' and 'particulate matter' or 'particulates' are often used alternately. Therefore at first a differentiation of the terms for the usage in the present work has to be made.

For vehicle homologation the limited Particulate Matter (PM) emissions are defined by the EPA (Environmental Protection Agency) as all substances, which are captured by a Teflon coated fiber-glass filter or by a Teflon membrane-filter which is perfused by diluted exhaust gas at a temperature below 52°C. [22], [23]

The particulate matter in diesel engines consists of many substances, the proportions of which depend on the engine operating conditions. It contains chain-like soot particles with accumulated hydrocarbons, ashes, sulfate particles, as well as oil, water, and fuel droplets. One can distinguish between soluble organic fractions (SOF) and insoluble components. The insoluble fraction, known as dry soot, which is responsible for the exhaust gas opacity, consists almost exclusively of carbon. It can be detracted from other particulate fractions by thermal desorption or extraction using solvents. [24], [20]

On engine test beds for steady-state measurements usually the paper-filter method is applied. A partial flow of the exhaust gas is filtered and the blackening rate of the filter paper is attributed to a certain filter smoke number. With the knowledge of the overall exhaust mass flow, this filter smoke number can be correlated to gravimetric soot emissions. [25]

In the present work, the focus deliberately lies on the analysis and modeling of 'soot', being aware that it is only a fraction of the overall particulate emissions. The reason for this is that for the engine measurements which are analyzed consistently the paper-filter method mentioned above was used. Furthermore, the applied pollutant formation models refer to the modeling of soot.

Soot Formation

The formation of soot or particles in diesel engines is governed by complex physical and reaction kinetic processes, which have still not been understood in every detail. It is widely recognized that soot is formed under fuel rich conditions with the absence of oxygen. Aside from the local composition (expressed e.g. by the lambda value), the thermodynamic conditions pressure and temperature have a significant influence on soot formation which indicates the reaction kinetic nature of the mechanism.

The heterogeneous field of thermodynamic states and composition in the spray is a consequence of the internal mixture formation. This process is characterized by turbulent heat transfer and mixing mechanisms. These are also influenced by the 3-dimensional flow field in the cylinder, which is a result of the macroscopic charge flow (swirl) and the momentum impinged by the injection spray in interaction with the combustion chamber geometry. The interaction of these mechanisms causes highly transient thermodynamic boundary conditions which makes the modeling of soot emissions a challenging task for engine simulations.

The most common theoretical conception for the description of soot formation is the mechanism of the Acetylene Pyrolysis. It is a sequence of physical and chemical sub-processes which includes the following steps, described in detail in [1] and [24].

Nucleation

During the oxidation of fuel, the more volatile hydrogen reacts first. This leads to a dehydration of the hydrocarbon molecules. Under oxygen poor conditions the thermal and oxidative pyrolysis of the high molecular weight hydrocarbon chains leads to the formation of unsaturated hydrocarbons, such as Acetylene (C_2H_2), as intermediate species (shown earlier in Figure 3). This process requires a high activation energy which makes it very temperature-sensitive. The reaction of acetylene and radicals forms polycyclic aromatic compounds. The progressing dehydration can lead to H/C ratios below 0.1. These initially formed soot nuclei make only a small fraction of the overall soot mass. However, they are the precursors for the ongoing processes so this initial step has a big influence on the total soot emissions.

Surface Growth

The nuclei formed in the first step accumulate hydrocarbons from the surrounding gas phase at progressing dehydration, which leads to a further decrease of the H/C ratio. This process causes an increase of soot mass while the number of particles stays approximately constant. In that way 95% of the overall soot mass is formed. This process of hydrogen abstraction and C_2H_2-addition is described by the so-called HACA-Mechanism, presented e.g. in [26].

Coagulation

The combination of soot nuclei due to collisions is called Coagulation. This process is superposed to the surface growth which in combination leads to the formation of bigger, nearly spherical shaped particles. Owing to this process the number of nuclei decreases at a nearly constant soot mass.

Agglomeration

Agglomeration also describes the combination of soot particles to long, chain-like structures. It is assumed that this process plays only a secondary role for Diesel engines due to the lack of time.

Oxidation

As soon as oxygen is available in the gas phase, there is an ongoing oxidation process which reduces the precursor nuclei, as well as the later formed soot particles and also the condensed hydrocarbons. Since soot particles are very stable, the soot oxidation is relatively slow in chemical terms. Thus, only a part of the soot can be oxidized in the limited time frame of the engine high pressure phase. For this process the temperature level during combustion and in the expansion phase plays an important role. As a reference value for the transition temperature of the soot oxidation reaction, a temperature level of 1300K is given.

In the late phase of diffusion combustion and during the following mixture process, the local conditions are lean and at moderate temperatures. In this phase, molecular oxygen is assumed to be the major oxidant species. This process is therefore described as low temperature oxidation. A different approach assumes that radicals such as atomic H and O or OH control the soot oxidation. This process requires high temperatures. Thus, it would be especially relevant during diffusion combustion and is therefore known as high temperature oxidation.

In addition to the reaction kinetic nature of the process, there are physical mechanisms which affect the soot oxidation. These are the turbulent mixing processes which are relevant for the supply of oxygen to the particle. This process is combined with boundary-layer- diffusion and pore-diffusion. Additionally, it has been observed that the oxidation rate depends on the particulate size, which is explained by the influence of the porosity.

As mentioned above, the composition of the particulates is affected by engine operating conditions. The ratio of dry soot to SOF highly depends on the formation (and oxidation) history of the particle. Fresh particles that can be observed, if the process is frozen shortly after the initial formation, have only a small fraction of dry soot. With increasing detention periods at high temperatures and oxygen poor

conditions the soluble fraction decreases. In general, the fraction of dry soot is dominating at full load conditions, while at part load higher fractions of SOF are common. [20]

3 Simulation of the Engine Process

The working cycle of a combustion engine is characterized by a multitude of complex and interacting thermodynamic, fluid mechanic and reaction kinetic processes. The mathematical description of these mechanisms allows a quantitative analysis and evaluation of the engine behavior based on measurements. (*Analysis*)

The validated models derived from the analysis of existing systems can be used to simulate the engine behavior beyond the measured operating conditions and for adapted engine configurations. (*Simulation*)

3.1 Simulation Models

Thermodynamic modeling of the engine process includes various components such as: pipes and plenums, turbocharger(s), cooling system, exhaust aftertreatment etc. One important part in the simulation of the engine cycle is the description of the in-cylinder processes which describes the actual conversion from chemical energy to technical work. In the course of this conversion, a major part of the emissions is formed. Thus, the description of the combustion process is essential for the prediction of engine performance, fuel consumption, and engine-out emissions.

To describe the complex mechanisms, different kinds of models are used which differ in computational time and accuracy. State-of-the-art models cover a variety of simulation approaches. Depending on the purpose, it is useful to undertake appropriate simplifications.

Empirical models describe processes by pure mathematical functions, the coefficients of which are adjusted to match a well-known operating behavior. As they do not rely on any physical mechanisms these models have no predictive capabilities outside the validated operating range. An example for this type of models is the Vibe function used to describe the rate of heat release.

Phenomenological models describe the behavior of a system by mathematical formulations that rely on the basic physical principles without directly taking into account the exact physical formulations of all relevant mechanisms. Due to this simplification, phenomenological models need to be calibrated to a specific system by empirical parameters which need to be identified from measurements. They are appropriate for variant calculations of a known system and extrapolations outside the measured operating range. The identification of model parameters and the assessment of the valid range of extrapolation is a sophisticated task in the development process.

Physical models are generally valid mathematical formulations of basic physical principles. It is assumed that a process can be described unambiguously, if all relevant physical mechanisms are considered and all boundary conditions are known. The provision of these boundary conditions for finite control volumes requires an appropriate spatial and temporal discretization of the system. Due to the high computational effort of a fully physical description of a complex system such as a combustion engine, it is necessary to find an optimal compromise between the degree of detail and computational time. Therefore, modeling approaches were introduced that partially rely on empirical and phenomenological formulations, which allows a coarser discretization of the system.

Statistical models describe the behavior of an engine or sub-systems of an engine by purely mathematical correlations. The mathematical models are based on a high number of input data which is derived either from measurements or from simulation results of validated, higher sophisticated models. Therefore, well-directed design plans such as the method of Design of Experiments (DoE) are used. Statistical models can provide global values such as performance, pollutant formation, temperatures and enthalpy flows, etc. They find their application i.a. as so-called surrogate models in the coupling with classical thermodynamic models. [27], [28]

3.1.1 Zero-Dimensional and Quasi-Dimensional Models

From thermodynamic aspects 0-dimensional modeling outlines the description of a system by means of the conservation of mass and energy. For the thermodynamic state, the only independent variable is time, or crank angle (φ) respectively. A thermodynamic system would be characterized according to the definition given in [29] and [30]. 0-dimensional models are applied to the modeling control volumes which exchange mass via valves and orifices (filling and emptying method) such as plenums, coolant reservoirs and also the cylinder. [31]

In the present work, zero-dimensional modeling especially refers to the description of the in-cylinder processes during the high pressure cycle, for which they offer an advantageous ratio of informative value to computational time. They enable an energetically correct analysis of the engine process without considering spatial phenomena that originate from the flow field in the cylinder. [30], [32]

It is without restrictions possible to subdivide a system (e.g. cylinder) into an arbitrary number of subsystems, or further 'zones'. Each of these zones is assumed to be homogeneous in composition and thermodynamic state, while the pressure is equal for all zones. This subdivision allows generating a nearly arbitrary distribution of mass, composition and energy within the system without necessarily implying spatial information. In terms of the zone discretization, 0-dimensional models are classified in single-zone and multi-zone models.

In single-zone models, the cylinder is modeled as a homogeneous zone in which an instantaneous mixing of the unburned fuel, fresh charge and combustion products is assumed. This type of model is adequate for an energetic evaluation of the engine process, if the focus lies on engine performance. As the temperature and composition field in the cylinder is averaged, it is not possible to describe local phenomena which are relevant for emissions formation.

In multi-zone models the cylinder is subdivided into an unburned and a burned domain. The energy, which is released by the combustion reaction, exclusively heats the burned domain which causes a heterogeneous distribution of temperatures in the cylinder. This heterogeneous distribution is a prerequisite for modeling the reaction kinetic processes such as the NO formation. On that account, the zones of the burned domain are also called reaction zones.

A particular and commonly used category of multi-zone models are 2-zone models. In this type of model the cylinder is divided into a burned zone and an unburned zone. The boundary between the two zones is the flame front which has no volume itself. The conversion of fresh charge and fuel in the flame front is modeled by a transfer of combustion products and the associated heat release in the burned zone. The entrained fresh charge mass is controlled by the so-called local-lambda value λ_L as given in eq. (3-1). This value can vary during the combustion process. The local-lambda characteristics determine the history of temperature and composition in the burned zone [30]. Thereby, the 2-zone approach generally allows calculating emissions and is often applied for the calculation of NO_x. Since the thermodynamic conditions that enhance the formation of NO_x and Soot are contrary, a simultaneous calculation of both pollutant species with only a single reaction zone is sophisticated.

$$\frac{dm_{ub\to b}}{d\varphi} = \frac{dm_{fb}}{d\varphi} \cdot \lambda_L(\varphi) \cdot ChF_{st} \tag{3-1}$$

Another category of models, which is used for the modeling of DI Diesel engines, are multi-zone models, which subdivide the burned domain into a high number of reaction zones each of which has an own history of temperature and composition. The discretisation of the burned domain and the modeling of the reaction zones are based on the conception of an injection spray. As a part of the sub-models rely on position dependent variables, this kind of model is often described as Quasi-Dimensional. The objective is to generate a heterogeneous field of temperature and composition which is close to reality and thus

enables the simultaneous calculation of NO_x and soot emissions. The fundamental modeling conceptions of different multi-zone approaches are discussed in detail in Chapter 4.1.

3.1.2 Computational Fluid Dynamic Models

In Computational Fluid Dynamic (CFD) models a thermodynamic system is discretized into a high number of finite volumes in multiple spatial dimensions. For each of the volumes the conservation equations of mass, energy and momentum are applied in Navier-Stokes notation as given by eq. (3-1). Here the change of a volume based value f results from the solution of the differential equation, given the internal source S_f, the external impression E_f and the flux via the boundary surface $div\ \vec{\phi}_f$. A multitude of technical processes require the modeling of reaction kinetic processes. This type of model is denoted as Computational Reactive Fluid Dynamic (CRFD) model.

$$\frac{\partial f}{\partial t} + div\,\vec{\phi}_f = S_f + E_f \tag{3-2}$$

The Navier-Stokes equations only provide a mathematically defined system of equations, if the control volumes are small and the calculation step-size is short compared to the size and timescale of the eddies in the turbulent flow. The computational effort of such a fine discretization is too high to simulate complex systems in reasonable time. Thus, for the simulation of relevant technical systems a coarser discretization is necessary. This requires a spatial and temporal averaging of the terms in the Navier-Stokes Equations. For this purpose, different turbulence models are used, out of which only the widespread k/ε model is mentioned.

1-Dimensional

If the Navier-Stokes equations are formulated in one spatial direction and the external energy source term is neglected, one receives the simplified formulations for one-dimensional (1-D) flow calculations. These models are capable of describing the unsteady and compressible flow in pipes, valves and ports in the intake and exhaust system. Therefore they are applied to simulate the gas exchange process of engines involving the gas dynamic processes caused by the pulsating flow in and out the cylinder. [5], [18] Such models are available in commercial simulation codes[2] and applied for simulating the engine gas exchange process together with thermodynamic (0-D) models for the cylinder for the layout of engine components such as the length and cross-sectional area of pipes and ports, valve lift and valve timing, turbochargers, charge-air coolers etc.

3-Dimensional

The discretization of a volume into 3 spatial directions allows the simulation of spatially resolved fluid dynamic processes in complex geometries. Of the many fields of application for 3-D CRFD simulation models, only the use for the simulation of the in-cylinder processes is mentioned. The aim is to predict the flow field in the cylinder and the interaction with the mechanisms of heat release and emission formation. A special challenge for the simulation of Diesel combustion is the description of the 2-phase regime of the initially liquid spray, including combined processes of fluid mechanics, phase transition and chemical reactions. [33]

[2] e.g. AVL BOOST, GT POWER, Ricardo WAVE

Due to the high computational effort for calculating detailed reaction kinetics mechanisms, it has so far not been possible to simulate the entire combustion process on a consistent physical basis in a reasonable calculation time. Therefore, different approaches are applied to reduce the computational effort.

The turbulent nature of the flame in combustion engines leads to a macroscopic mixing between the burned and the unburned phase. These macroscopic eddies dissipate which leads to a mixing on the microscopic scale. In the Eddy-Dissipation model approach of Magnussen [34], it is assumed that the chemical reaction is a lot faster than the microscopic mixture processes so that the latter are decisive for the heat release. This is expressed in Damköhler-Numbers $Da >> 1$. The heat release rate is calculated by means of a formulation which uses one term for the microscopic mixing (k/ε-term) combined with a term that describes the availability of reactants. As this modeling approach does not incorporate reaction kinetics processes that lead to initial combustion, the ignition delay needs to be calculated separately. [20], [24]

In Flamelet-Models it is assumed that the turbulent eddies predominantly lead to a macroscopic mixing of the reactants and to a deformation of the flame front. The combustion reaction itself is governed by mass and heat transport processes on the microscopic scale. In this model approach the combustion characteristics for the flame propagation in one spatial direction are pre-calculated from detailed reaction kinetics for given mixture properties (pressure, temperature, mixture composition and flame front deformation). The 3-D flow simulation delivers these mixture properties which are used for the interpolation in the pre-calculated array. [20], [24] The approach, which was originally intended for classical flame-front combustion in perfectly or partially mixed zones, has been adapted to the Extended Coherent Flame Model in [35] to also account for unmixed combustion in Diesel engines.

3.2 Fundamentals of Zero-Dimensional Modeling

The analysis and simulation of the combustion process with 0-dimensional models concentrates on the high pressure part of the engine process from Intake Valve Closing (IVC) to Exhaust Valve Opening (EVO). Therefore the model requires the thermodynamic conditions at start of high pressure (SHP) and appropriate fuel injection characteristics as an input. The thermodynamic state at IVC takes the relevant engine parameters turbocharging, exhaust gas recirculation (EGR), charge air and EGR cooling, valve timing, etc. into account. Depending on the application (Analysis / Simulation) it is derived either from one-dimensional gas exchange simulation or it needs to be estimated from measurements, which requires certain assumptions on the gas exchange process.

The model developed for present work is predominantly used for analysis purposes, so most calculations are done on the basis of steady-state testbed measurement data. The boundary conditions for the simulation are calculated from these measurements as described below.

3.2.1 Quasi-Stationary Description of the Engine Process

The thermodynamic conditions of the working gas at IVC are defined by state and composition. To unambiguously define the thermodynamic state for a mixture of ideal gases, two out of three intensive state variables pressure, temperature and density are required.

Estimation of Boundary Conditions from Measurements at Steady-State Conditions

If measurement data is available, the pressure at IVC can be estimated from high pressure indication p_{cyl}, which defines the first one of the two required state variables. In-Cylinder temperature measurement is usually not available and estimating it from the inlet temperature implies uncertainties because of the heat transfer in the inlet system. The second variable that defines the state at IVC is the cylinder mass which is directly proportional to density, as the cylinder volume at IVC is known from geometrical relations. Usually, intake air massflow m_{air} is measured and external EGR is estimated from the CO_2

concentration in the intake manifold. Out of these values it is possible to estimate the in-cylinder mass at IVC. This obviously implies a certain degree of uncertainty due to unknown influences from the gas exchange process, such as internal residual gases and scavenging.

Figure 6 shows a schematic representation of an engine with an external EGR system on the high pressure side of the turbocharger. The figure involves the measured and estimated mass flows out of which the trapped total cylinder mass is calculated according to the considerations below.

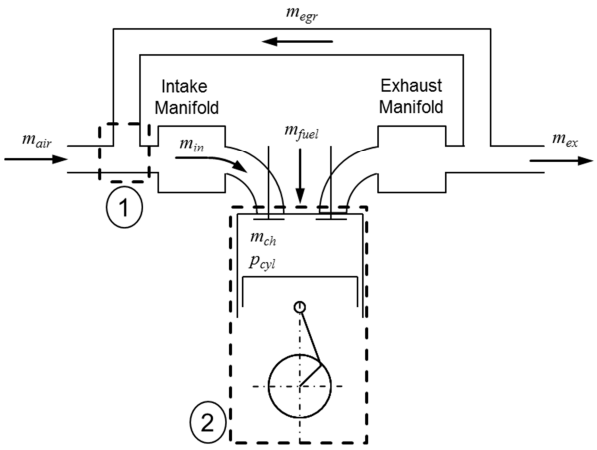

Figure 6: Quasi-Stationary representation of the Engine Process

The intake massflow consists of fresh air and recirculated residual gases and is defined by the mass balance of system 1, eq (3-3). Scavenging to the exhaust reduces the trapped intake mass $m_{in}^{\ t}$ which results from the mass balance of system 2, eq. (3-4). The residual gas mass m_{rg}, hich remains in the cylinder, from the gas exchange does not occur in the mass balance; however, it is crucial for the estimation of charge mass m_{ch} and species composition at IVC. Therefore, it needs to be estimated using 1-D gas exchange simulation or estimated from experience data of similar engines. The fractions of EGR X_{egr} and residual gases X_{rg} are defined by equations (3-6) and (3-7).

Mass Balance System 1

$$\dot{m}_{in} = \dot{m}_{air} + \dot{m}_{egr} \tag{3-3}$$

Mass Balance System 2

$$\dot{m}_{ex} - \dot{m}_{egr} - \dot{m}_{fuel} = \dot{m}_{in} = \dot{m}_{in}^{t} + \dot{m}_{sc} \tag{3-4}$$

$$m_{ch} = m_{in}^{t} + m_{rg} \tag{3-5}$$

$$X_{egr} = \frac{\dot{m}_{egr}}{\dot{m}_{air} + \dot{m}_{egr}} \tag{3-6}$$

$$X_{rg} = \frac{m_{rg}}{m_{ch}} \tag{3-7}$$

The underlying assumption of the present work is that scavenging of charge to the exhaust is negligible, so $m_{sc}=0$. By means of some reformulations, it is possible to express the charge massflow as a function of air massflow and residual gas fractions. The mass flows are converted to cyclic values using the cycle frequency N_{cyc} which is a function of engine speed and the number of strokes.

$$X_{ch/air} = \frac{\dot{m}_{ch}}{\dot{m}_{air}} = \frac{1}{\left(1 - X_{egr}\right) \cdot \left(1 - X_{rg}\right)} \tag{3-8}$$

$$m_{ch} = \dot{m}_{air} \cdot \frac{X_{ch/air}}{N_{cyc}} \tag{3-9}$$

Estimation of Charge Concentration at Intake Closing

Analogously to the balance of mass it is possible to calculate the charge concentration at IVC from the balance of species (3-10). In the following equations x_j denotes the concentration of an arbitrary species Y_j, which is one of the products and educts of the complete combustion O_2, N_2, CO_2, H_2O and unburned fuel in the present case. Due to mass conservation, the composition of the recirculated combustion products is a function of the global lambda value. It can be calculated from eq. (2-12) in Chapter 2.1.2.

Species Balance:
$$m_{ch} \cdot x_j^{ch} = m_{air} \cdot x_j^{air} + \left(m_{egr} + m_{rg}\right) \cdot x_j^{cp} \tag{3-10}$$

Solving for Concentration:
$$x_{Y_j}^{ch} = \frac{1}{X_{ch/air}} \cdot \left[x_j^{air} + x_j^{cp} \cdot \left(X_{ch/air} - 1\right)\right] \tag{3-11}$$

3.2.2 Mathematical description of a 0-Dimensional Thermodynamic System

For engine cycle simulation, the thermodynamic systems - which are in the modeling context described as zones - are considered to be open and unsteady, containing mixtures of ideal gases. The thermodynamic properties of the ideal gas depend on temperature, pressure and composition - represented by the mass fractions of the species x_j, see equations (3-12) - (3-14). The balance equations for the zones species (and the minimum number of independent variables required to unambiguously define them) are discussed in Chapter 2.1.2 (Figure 2).

$$\vec{W} = \left[x_1 \ldots x_k\right]^T \tag{3-12}$$

$$R = R\left(T, p, x_1 \ldots x_k\right) \tag{3-13}$$

$$u = u\left(T, p, x_1 \ldots x_k\right) \tag{3-14}$$

As the independent variable it is common practice to use crank angle instead of time. While for engine cycle simulation the use of crank angle is more descriptive, it also determines a better numerical accuracy for the simulation of different engine operating conditions [36]. For one individual zone the conservation equations and the equation of state in differential form, considering the total derivative of the gas properties, are given by eq. (3-15) to (3-19). Here, the index *i* indicates the zone-number and the index *j* stands for the different species.

Energy:

$$\begin{aligned} &\sum \frac{dQ_i}{d\varphi} + \sum \frac{dH_i}{d\varphi} - p \cdot \frac{dV_i}{d\varphi} = \\ &u \cdot \frac{dm_i}{d\varphi} + m_i \cdot \left(\frac{\partial u}{\partial T} \cdot \frac{dT_i}{d\varphi} + \frac{\partial u}{\partial p} \cdot \frac{dp}{d\varphi} + \sum_j \frac{\partial u}{\partial x_j} \cdot \frac{dx_j}{d\varphi} \right) \end{aligned} \tag{3-15}$$

State:

$$\begin{aligned} &p \cdot \frac{dV_i}{d\varphi} + V_i \cdot \frac{dp}{d\varphi} = R_i \cdot T_i \cdot \frac{dm_i}{d\varphi} + m_i \cdot R_i \cdot \frac{dT_i}{d\varphi} \\ &+ m_i \cdot T_i \cdot \left(\frac{\partial R}{\partial T} \cdot \frac{dT_i}{d\varphi} + \frac{\partial R}{\partial p} \cdot \frac{dp}{d\varphi} + \sum_j \frac{\partial R}{\partial x_j} \cdot \frac{dx_j}{d\varphi} \right) \end{aligned} \tag{3-16}$$

Mass:

$$\frac{dm_i}{d\varphi} = \sum \frac{dm_{i,in} - dm_{i,out}}{d\varphi} \tag{3-17}$$

Species:

$$\frac{dm_j}{d\varphi} = \sum \frac{dm_j^{in} - dm_j^{out}}{d\varphi} + S_{m_j} \tag{3-18}$$

$$\frac{dx_j}{d\varphi} = \frac{d}{d\varphi}\left(\frac{m_j}{m}\right) = \frac{1}{m^2} \cdot \left(m \cdot \frac{dm_j}{d\varphi} - m_j \cdot \frac{dm}{d\varphi} \right) \tag{3-19}$$

In the species balance (3-18) S_{mj} represents a source term that considers the transformation of one species into another during chemical reactions.

For the calculation of the thermodynamic state of each zone, the unknown derivatives of temperature, pressure, and volume are required. Assuming a system consisting of n zones with uniform pressure, $2n+1$ state values are unknown. Applying eq. (3-15) and (3-16) for each zone, $2n$ equations are available. The required final criterion states that the entity of all zone volumes equals the cylinder volume. Hence, one derives the $n+1^{st}$ equation that can be expressed in differential form:

$$\frac{dV_{cyl}}{d\varphi} = \sum \frac{dV_i}{d\varphi} \tag{3-20}$$

One sophisticated solution for solving this problem in an arbitrary number of zones has been introduced by Grill in [29]. In the present work, a different formulation is used. Since in the present work the mass balance is calculated separately, it is not necessary to calculate the volume derivative as well. Furthermore an over-determination of the system shall be prevented. This is accomplished by eliminating the volume derivative in eq. (3-15) and (3-16). After algebraic reformulations one obtains the following formulation (3-21), which is reduced to the derivatives of temperature and pressure. In the resulting equation the variables are separated and combined to terms, which are known or constant (f_{Ti} and f_{pi}) on the left hand side. The right hand side (RHS_i) represents the source terms, which are given externally by the user-defined models.

$$\begin{aligned} &\frac{dT_i}{d\varphi} \cdot \underbrace{\left[m_i \cdot \left(\frac{\partial u}{\partial T} + R_i + T_i \cdot \frac{\partial R}{\partial T} \right) \right]}_{=f_{T_i}} + \frac{dp}{d\varphi} \cdot \underbrace{\left[m_i \cdot \left(\frac{\partial u}{\partial p} - \frac{R_i \cdot T_i}{p} + T_i \cdot \frac{\partial R}{\partial p} \right) \right]}_{=f_{p_i}} = \\ &\underbrace{\sum \frac{dQ_i}{d\varphi} + \sum \frac{dH_i}{d\varphi} - \frac{dm_i}{d\varphi} \cdot \left(R_i \cdot T_i + u_i \right) - m_i \cdot \sum \frac{dw^j}{d\varphi} \cdot \left(T_i \cdot \frac{\partial R}{\partial w^j} + \frac{\partial u}{\partial w^j} \right)}_{=RHS_i} \end{aligned} \tag{3-21}$$

In the final criterion, the equation of state is applied to the volume derivative. Therefore, eq. (3-15) is algebraically reformulated to be explicit in volume. Using (3-20) and (3-22) one obtains the formulation (3-23) for the final criterion.

$$\frac{dV_i}{d\varphi} = \underbrace{\frac{T_i}{p}\cdot\left(R_i\cdot\frac{dm_i}{d\varphi} + m_i\cdot\sum\frac{\partial R}{\partial w^j}\cdot\frac{dw^j}{d\varphi}\right)}_{=FV_i} + \frac{dT_i}{d\varphi}\cdot\underbrace{\left[\frac{m_i}{p}\cdot\left(R_i + T_i\cdot\frac{\partial R}{\partial T}\right)\right]}_{=V_{T_i}} + \frac{dp}{d\varphi}\cdot\underbrace{\left[\frac{m_i}{p}\cdot\left(T_i\cdot\frac{\partial R}{\partial p} - \frac{R_i\cdot T_i}{p}\right)\right]}_{=V_{p_i}} \tag{3-22}$$

$$\frac{dV_{cyl}}{d\varphi} = \sum V_{T_i}\cdot\frac{dT_i}{d\varphi} + \frac{dp}{d\varphi}\cdot\sum V_{p_i} + \sum FV_i \tag{3-23}$$

Using (3-21) and (3-23), a system of *n+1* equations can be formulated for *n+1* state variables. The resulting set of equations can be expressed as a system of coupled ordinary differential equations. In matrix-notation we obtain (3-24). The solution for this system of linear equations is applied by use of the Gaussian elimination.

Hence, the derivatives of pressure and individual temperatures are derived explicitly. For the numerical integration, a 4-step Runge-Kutta-Method is used which involves an advantageous ratio of numerical accuracy and computational time for 0-D thermodynamic simulations [36].

$$\begin{bmatrix} f_{T_1} & 0 & 0 & \dots & 0 & f_{p_1} \\ 0 & f_{T_2} & 0 & & \vdots & f_{p_2} \\ 0 & 0 & \ddots & 0 & & \vdots \\ \vdots & & 0 & & 0 & \\ 0 & \dots & & 0 & f_{T_n} & f_{p_n} \\ V_{T_1} & V_{T_2} & \dots & & V_{T_n} & \sum V_{p_i} \end{bmatrix} \cdot \begin{bmatrix} dT_1/d\varphi \\ dT_2/d\varphi \\ \vdots \\ \\ dT_n/d\varphi \\ dp/d\varphi \end{bmatrix} = \begin{bmatrix} RHS_1 \\ RHS_2 \\ \vdots \\ \\ RHS_n \\ dV_{zyl}/d\varphi - \sum FV_i \end{bmatrix} \tag{3-24}$$

3.2.3 Universal Calculation Platform

The previous formulations provide the thermodynamic framework for a universal calculation platform based on which different modeling approaches can be implemented and investigated. Table 1 summarizes the capabilities of the platform. In terms of the zone discretization, the platform provides three different calculation approaches: Single-zone, 2-zone, and multi-zone.

Each of these models distinguishes between two different calculation modes:

- In the Pressure Trace Analysis (PTA), the combustion process is analyzed accounting for all relevant physical mechanism. The heat release is calculated on the basis of the measured cylinder pressure trace.
- In the Working Process Calculation (WPC), the cylinder pressure is predicted from a given heat release. The heat release can derive from calculation models, the mechanisms and parameters of which are identified and validated by measurements.

Within the single-zone and 2-zone modeling approaches it is possible to calculate the heat release directly from the cylinder pressure curve by applying of the first law of thermodynamics. Therefore, the 2-zone model requires certain assumptions for the entrainment of unburned charge to the burned zone, which is represented by the local lambda value, as discussed in Chapter 3.1.1. For reasons of consistency, the identification of the heat release in the PTA is done iteratively in each time-step and therefore uses exactly the same routines as the WPC.

The direct identification of the heat release is no more possible for the multi-zone approach because, due to the higher sophisticated models, the distribution of states (= zones) is not known a priori [29].

Therefore a special procedure is required which screens the combustion process on the basis of the spray model approach and identifies the mechanisms in an iterative procedure. This method will be described in further detail in Chapter 6.3.2.

Table 1: Overview of the Capabilities of the Thermodynamic Platform

Simulation approach	**WPC** **Work Process Calculation** (Prediction of combustion stroke)	**PTA** **Pressure Trace Analysis** (Heat release calculated from pressure curve)	**Prerequisites for PTA** (assumptions and strategies for the analysis of heat release and emissions)
Single-zone	**Heat release estimated** by Vibe functions or phenomenological models	**Analytical solution** for heat release calculated from cylinder pressure curve	**No assumptions** for heat release Emissions cannot be identified
2-zone	**Heat release estimated** by Vibe functions or phenomenological models	**Analytical solution** for heat release calculated from cylinder pressure curve	**Assumptions for the Local lambda** Special procedure for emissions
Multi-zone (MZCM)	**Higher sophisticated models** for spray, fuel evaporation and charge entrainment, heat release by chemical reaction model	**Numerical identification** of fuel evaporation, charge entrainment and chemical reaction kinetics	**Special procedure** for heat release, Special procedure for emissions (identical to 2-zone approach)

3.2.4 Thermodynamic Fit of the Pressure Curve for the Motored Engine

The compression curve is calculated for a given thermodynamic state at IVC in the cylinder (T, p, mass, composition) and geometrical values of the engines such as the compression ratio and the exact position of top dead center (TDC). Usually, the raw data of the indicated cylinder pressure curves do not match the calculated compression curves due to uncertainties in the thermodynamic and geometrical boundary conditions, as well as model assumptions for heat losses and blow-by. Thus, they require thermodynamic adaption. This is preferably done for motored engine conditions.

The applied matching procedure is described in detail in [37]. Finally, it has to be emphasized that the fine tuning of the absolute pressure at IVC is carried out at each individual engine operating point.

3.3 Calculation of the Injection Rate Profile

As an input for the simulation of the combustion in diesel engines the crank angle resolved characteristic of the fuel injection is required. On engine testbed the injection rate profile cannot be measured directly during operation. However, it is possible to estimate it from other characteristic physical values which can be measured. Figure 7 shows a schematic picture of the injection system with measurement positions and relevant values for the calculation. The measured values are the injector needle lift l_n and injector pipe pressure p_{Pipe}.

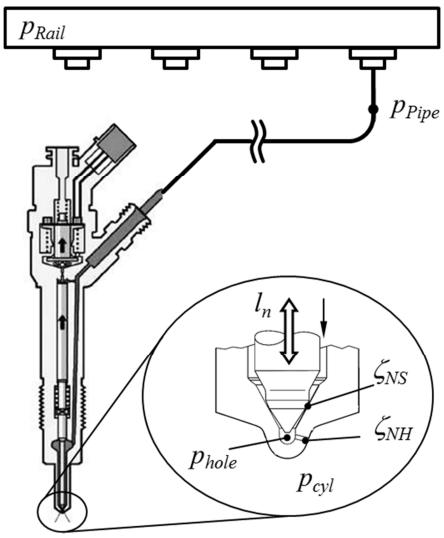

Figure 7: Injection System Rail, Pipe and Injector with Positions of Pressure Signals

A commonly used approach (applied i.a. in [30], [38], [39]) is to calculate the injection rate from the nozzle hole area and the injection velocity. The velocity is calculated from the Bernoulli equation for viscous flows. The resulting equation (3-25) involves the fuel density and the discharge coefficient c_D. This discharge coefficient represents the friction losses in the entire injection system, from the pipe pressure measurement position via the injection pipe and injector flow (involving needle seat gap) and the injector nozzle hole. The characteristics of the discharge coefficient are measured as a function of the needle lift on an injector test rig.

$$\frac{dm_{inj}}{dt} = A_{NH} \cdot c_D \cdot \sqrt{2 \cdot \rho_{fuel} \cdot \left(p_{Pipe} - p_{cyl}\right)} \tag{3-25}$$

In the present work, a slightly different approach is used. Here, the friction losses in the injection system are represented by two flow restrictions: (1) the injector nozzle hole with constant area and flow coefficient ζ_{NH}, which separates the injector blind hole from the cylinder and (2) the restriction between the pipe pressure measurement position and the blind hole, which includes the needle seat gap with flow coefficient ζ_{NS}. For both restrictions, constant flow coefficients are assumed. The needle seat throttling expresses by a variable flow area as a function of needle lift. This system is schematically shown in Figure 8.

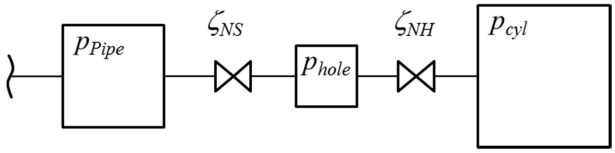

Figure 8: Simplified Modeling Approach for the Estimation of the Injection Rate Profile

For both restrictions, the Bernoulli principle is applied. By eliminating the unknown blind hole pressure, the injection massflow can be calculated from the measured pressures, which is summarized in eq. (3-26). The flow coefficients ζ_{NS} and ζ_{NH} need to be specified for a specific injection system.

$$\frac{dm_{inj}}{dt} = \sqrt{2 \cdot \rho_{fuel} \cdot \left(p_{Pipe} - p_{cyl}\right) \cdot \frac{1}{\left(\frac{\zeta_{NS}}{A_{NS}^{\ 2}} + \frac{\zeta_{NH}}{A_{NH}^{\ 2}}\right)}} \tag{3-26}$$

The flow coefficient of the nozzle hole ζ_{NH} can be estimated from the steady state nozzle flow measurement at fully opened needle position, which is usually specified by the injector manufacturer. Therefore it is assumed that the needle throttling is negligible at fully opened position.

Furthermore, from eq. (3-26) the injector flow can be calculated as a function of needle lift. This curve can be compared to the corresponding measurement data - if available - and used to correlate ζ_{NS}. Otherwise, it is possible to qualitatively fit the curve to the characteristics of a known injector of a similar type. Therefore, it is assumed e.g. in [38] and [40] that injectors with similar design show comparable injection characteristics vs. needle lift.

The injection characteristics of one of the systems used in the present work (Engine 3 of Table 2) are shown in Figure 9 for a variation of the value ζ_{NS}. The steady state nozzle flow at maximum needle lift is specified with 353 to 367 cm^3 per 30 sec at 100 bar. This range is also sketched in the figure.

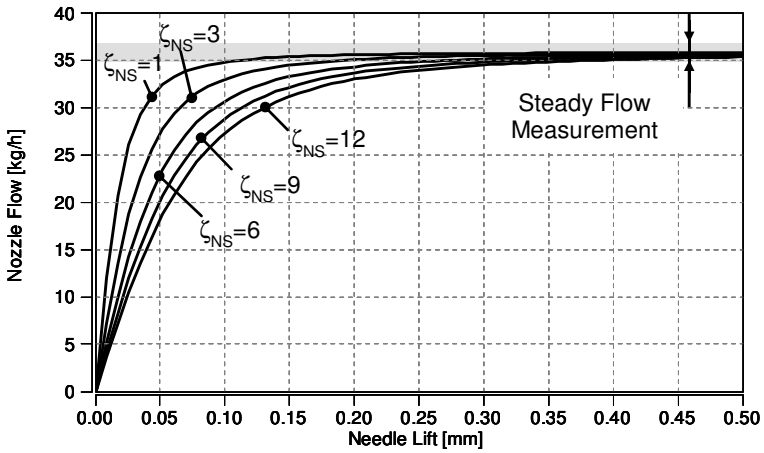

Figure 9: Calculated Nozzle Flow for Injector of Engine 3

By applying the measured signals of needle lift, pipe pressure and cylinder pressure to eq. (3-26), the crank angle resolved injection rate profile is derived. It needs to be considered, that the pipe pressure signal requires an adaption due to the runtime of the pressure wave between measurement position and the nozzle hole. A commonly applied approach to account for the effect of pressure waves was presented by Woschni and Anisitis in [41].

Figure 10 shows crank angle resolved characteristics of measurements and the resulting calculated values for one operating point. In the present work, the pressure signal is shifted by a constant crank angle delay to account for the pressure wave runtime. The shift time is estimated from the characteristic drop of the pipe pressure signal. This is done for each operating point. In the present example the injector needle does not have a mechanical stop which leads to a ballistic movement, even at full load operation. There is a clear offset between the start of the injector current signal to the starting of the needle lift. This offset is known as injection delay which in the present case is about 3 deg CA. Right after the beginning of needle lift, the injection rate shows a sharp increase, as the needle seat throttling is omitted already at a small needle opening positions.

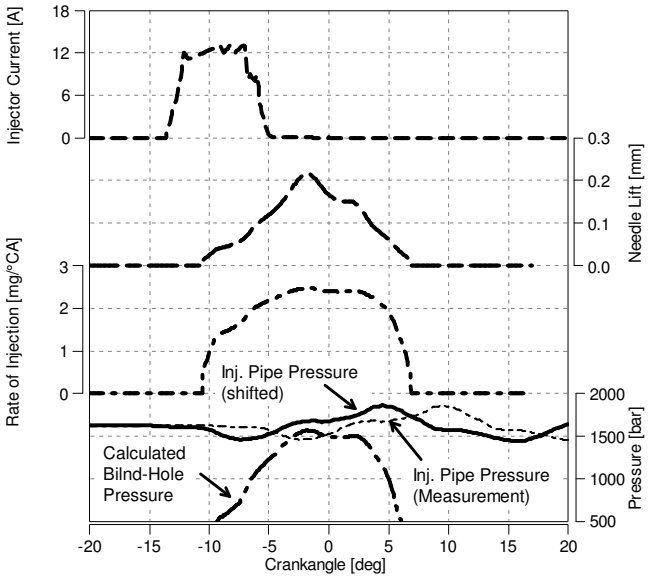

Figure 10: Injection Rate calculated from Needle Lift and Pipe Pressure

4 Modeling Diesel Combustion on the Basis of the Injection Spray

4.1 Quasi-Dimensional Combustion Models for Diesel Engines and State of the Art

In direct-injection Diesel engines there is a close interrelation between the injection rate profile and the heat release due to the momentum impinged by the injection spray. Therefore, the injection rate is usually the basis for the modeling of heat release and pollutant formation. In transient fuel jets the mechanisms of atomization, spray motion, evaporation, air entrainment, fuel air mixing, ignition and combustion run simultaneously. From a modeling point of view, there are different approaches to account for these mechanisms and their limiting impact on the heat release.

Empirical Spray Models

Austen and Lyn presented an empirical approach for estimating the heat release from the injection rate in [42]. Their approach is based on the comparison of heat release and injection rate diagrams. In their empirical model the injected fuel is subdivided into a finite number of sub-quantities. There is no thermodynamic balancing of these fuel quantities in the sense of reaction zones, so the model is intended for the estimation of heat release only. Each of the fuel quantities has a triangular heat release profile. The fuel injected during ignition delay burns instantaneously. The peak combustion rate decreases for the later injected fuel. The overall heat release is a result of summing up the heat release of all fuel quantities. This model assumes that the combustion is mainly governed by the turbulent flow field in the cylinder and mixing processes. Fuel evaporation is not considered.

Another approach to be mentioned is the one of Constien [43], which is referenced in [30] and [32]. This model is similar to the above one in terms of the discretization, but contrary in the emphasizing of the individual mechanisms. The injected fuel is also divided into sub-quantities, without a thermodynamic discretization into zones. It is assumed that the heat release is mainly governed by the ignition delay and evaporation. For each quantity the Sauter diameter is calculated. The evaporation process is modeled by a diffusion type mechanism on the basis of the concentration gradient at the droplet surface. The Wolfer approach [44] is used to calculate the ignition delay for each fuel quantity. As soon as ignition occurs in the individual element, the fuel that is evaporated by then burns instantaneously. Further on the heat release is governed by the evaporation process. The global heat release results from the summation of all elements.

Mixing Controlled Combustion

Chmela and Orthaber [45] present a global formulation for the estimation of the heat release from the injection rate which is based on the approach of Magnussen and Hjertager [46]. They assume that the heat release rate is mainly driven by the mixing process of fuel and air which allows avoiding a detailed description of the mixture formation and oxidation processes. In the related Mixing Controlled Combustion (MCC) model, the heat release is controlled by two function terms: The first one is the available fuel mass which results from the difference of injected and burned fuel, so evaporation is assumed to be fast. The second term is a function of the instantaneous density of turbulent kinetic energy. The approach relies on a k-ε formulation which is adapted for 0-dimensional modeling by introducing a Taylor-Approximation for the dissipation rate [30]. From an analysis of different sources for in-cylinder turbulence, namely swirl and squish flow and injection, they conclude that the turbulence impinged by the injection spray has by far the highest contribution. The resulting set of differential equations, which consists of the balance equation for the turbulent kinetic energy and available fuel mass, allows calculating the heat release directly from the injection rate profile.

An adapted version of the MCC modeling approach is used in [47]. Therein, the model is extended by an evaporation mechanism based on Varde et al. [48] and Sitkei [49]. The ignition delay is calculated separately using the model of Andree and Pachernegg [50]. This model considers a special treatment for the premixed combustion, assuming a Vibe function shaped heat release for the fuel, which evaporates during ignition delay.

Pirker [32] introduces a heat release model on the basis of the MCC approach. The model uses a combined Arrhenius and Magnussen approach for the calculation of the ignition delay to account for both chemical and physical mechanisms that govern the ignition process. For the calculation of the heat release, the injected fuel is subdivided into several pools e.g. a premixed and a diffusion fraction. The heat release of the premixed fuel is modeled by an Arrhenius approach. For the diffusive combustion, a refined Magnussen model is introduced on the basis of a detailed spray model. In that way, the model accounts for effects of mixture dilution and wall interaction.

Turbulent Gas Jet Models

There is a number of models which are based on the theory of the turbulent gas jet. The basic approach was presented by Abramovich in [51]. Among others, the conception was then followed by Hohlbaum [52] and Shahed [53]. In the model, the injection is represented as a stationary gas jet. The tip penetration velocity and the velocity profile in radial direction are calculated from empirical relations. Additionally, the model considers corrections to account for changes in tip penetration and tangential displacement of the spray due to swirl motion. The model assumes a specific profile for the distribution of the fuel concentration in the spray. The integration of these formulations defines the spray geometry and the resulting continuous distribution of fuel and air. The ignition delay is calculated separately. For the description of the combustion and pollutant formation, the continuous spray profile is discretized into a number of (m) combustion zones within the lean and rich flammability limits, a rich core ($m+1$) and the surrounding fresh air zone ($m+2$). During combustion, additional fuel zones are added adjacent to the rich core due to ongoing injection and vaporization. Outer zones are diluted with air from the surrounding fresh gas zone. The heat release in the individual zones is calculated with a reaction kinetic approach. The zones are balanced thermodynamically, which gives the heterogeneous temperature distribution. As the turbulent gas jet model does not consider an evaporation mechanism, the heat release is limited mainly by the mixing process.

Multi-Zone Package Models

Another category of models are so-called package or n-zone models which rely on the long-established approach of Hiroyasu et al. [54]. In these models, a high number of reaction zones is defined. At each time-step during injection, the injected fuel generates one new parcel of zones. Each parcel is subdivided into a number of radial zones (nr). This leads to a discretization of the spray in axial and radial direction. Consequently, the number of zones, which is generated during the combustion process, depends on the duration of injection (DOI), the calculation time-step $\Delta\varphi$ and the radial zone number (nr). The overall number of spray-zones is given by $n = (DOI \cdot nr) / \Delta\varphi$. Each of these reaction zones is balanced thermodynamically and has its own history of temperature and composition, while the pressure is equal for all zones. The model assumes that there is no transfer of heat and mass between the spray zones.

Initially each zone consists of pure liquid fuel. The amount of fuel in each zone remains constant during the calculation. In the moment of break-up, which is calculated from empirical relations, the dense liquid fuel disintegrates to single droplets. The droplet size distribution is represented by a Sauer Mean Diameter (SMD) which is constant within one zone but changes between the zones and during runtime. The liquid droplets heat up from the surrounding hot charge and evaporate. At the same time, the zones are decelerated by the interaction with the surrounding cylinder charge. The penetration velocity of the spray zones is modeled by a phenomenological approach. The formulation considers injection system parameters and operating conditions. The mixing of fuel with the surrounding cylinder charge finds its model-representation in the entrainment of charge into the zones. The amount of charge entrained into

the zone is calculated on the basis of momentum conservation, so the deceleration reflects in a gain of mass. It is assumed that the outer radial zones of the spray decelerate faster, thus having higher entrainment rates than the zones on the spray centerline. Additionally, the model considers simplified mechanisms for wall-interaction and swirl. Therefore, the penetration length of each zone is integrated and as soon as it reaches a notional combustion chamber wall, the entrainment is increased by a constant factor. These mixing processes generate a heterogeneous distribution of fuel and charge in the zones which should represent the conditions in the injection spray. Once a combustible mixture is formed, chemical ignition delay is calculated by a Wolfer approach. This is done separately for each zone. After ignition, the fuel/air mixture burns immediately. The heat release is limited either by the evaporated fuel or by the available air (oxygen) in the zone. The overall rate of heat release is calculated by summing up all zones. This genuine modeling conception of Hiroyasu has been followed up and adapted by a number of researchers.

Rakopoulos and Hountalas [55] perform a discretization of the spray in 3 spatial dimensions. Thus, each parcel is additionally subdivided in angular direction. A major extension of the genuine Hiroyasu approach is the consideration of an Arrhenius type reaction kinetic approach as a limiting factor for the heat release. In their model, the heat release in each zone is limited by the minimum value out of available fuel, available air, and the chemical reaction.

Merker and Stiesch [5], [56] also introduce a package model based on the Hiroyasu approach with consideration of reaction kinetics. One innovation in their proposed model is the consideration of a so-called slipstream effect in the spray. It is assumed that momentum of the spray changes the in-cylinder flow field in a way that later injected packages are less decelerated by the cylinder charge. Therefore, the charge entrainment is highest at the spray tip and decreases for the later packages. Together with the radial velocity profile, this generates a more descriptive distribution of states in the spray.

Reinhart [57] has reviewed the Multi-Zone package approach from a very interesting point of view. In his work, the model is in particular intended for the analysis and simulation of the ignition delay in direct-injection diesel engines. The precursor processes of spray break-up, air entrainment, heat-up and evaporation of the droplets, which lead to the formation of a combustible mixture, are regarded as physical ignition delay. The chemical part of ignition delay is treated separately, modeled by a reaction kinetic approach. From the theoretical point of view, this modeling conception takes a similar line as the approach of Pirker to model the ignition delay with a combined Magnussen and Arrhenius approach.

4.1.1 Considerations for the Model Development

Regardless of the differences in the described modeling approaches there are certainly several allegories among them. The described models partially emphasize different mechanisms that govern the combustion process. Most of them regard the mixing process as limiting for the heat release; others additionally consider the fuel evaporation and/or the chemical reaction. Another distinguishing feature is the number of zones used for the discretization of the cylinder volume. This affects the model complexity and the computational effort, but also the accuracy of results.

Subject of the present work is the development of a 0-dimensional model that simulates the combustion process of direct-injection Diesel engines. The model is developed for the application in 1-dimentional full cycle simulation codes. The modeling approach is supposed to describe the rate of heat release on a physical basis as generally valid as possible. Additionally, the model is intended for the prediction of engine out emissions with focus on NO_x and soot. In this field, especially the hard-to-predict soot emissions present a sophisticated task for a 0-D model. With regard to this, the model needs to qualitatively predict the trends for changing operating conditions. By tuning a minimum number of model parameters to one specific engine configuration, it should further be possible to quantitatively describe the engine behavior. The calculation time is supposed to be in the order of magnitude of present 1-D/0-D codes.

For the modeling of pollutant formation, especially the simultaneous calculation of NO_x and soot, it is seen as a prerequisite to consider a heterogeneous distribution of states and composition in the injection spray. Both the turbulent gas jet model and the multi-zone package model consider such a heterogeneous distribution. From the proposed models, the package approach of Hiroyasu offers the highest modeling depth, as it considers all relevant physical mechanisms: fuel evaporation, fuel/air mixing (entrainment) and the chemical reaction. All these mechanisms are modeled as integrated, continuous processes. Which one of them is dominating in a local reaction zone, is left to the model. Thus the model provides a high degree of general validity. This makes it possible to get along without the necessity of introducing case distinctions for the individual processes or combustion phases, which would indicate constraints to the underlying physical assumptions.

For these reasons, the package approach is seen as the most adequate for the modeling activities in the present work. As a starting point for the development, the basic multi-zone package model is implemented to the thermodynamic calculation platform. The mathematical formulations of the individual sub-models are taken from state-of-the-art models in the literature, as described in Chapter 4.2.

The model is reviewed by a continuous comparison and validation of the results with engine testbed measurement data. The findings of this permanent development and validation process provide the basis for the modeling extensions proposed in Chapter 4.4, which supplement the current state-of-the-art models. These extensions are introduced only if absolutely necessary and when the hypothesis of the new approach is confirmed by the physical principles of the combustion process.

4.2 Modeling the Reaction Zone in a Multi-Zone Spray Model

In the multi-zone model the processes of mixture formation and combustion are expressed by different sub-models. Mathematically speaking, they provide the source terms for the thermodynamic solution described by the system of coupled differential equations given in Chapter 3.2.2. In the following chapter, the mathematical formulations of these sub-models are outlined and the physical background of the phenomenological approaches is discussed.

The relevant mechanisms of the combustion process in the MZCM discussed in the section above are graphically represented for a single zone in Figure 11. A set of zones is generated at the very time-step a fuel parcel is injected into the combustion chamber. Each zone initially consists of pure liquid fuel. Due to the mechanisms of primary and secondary breakup, the liquid core disintegrates into single droplets. After that breakup point, the continuous processes of mixture formation commence. The mixing of fuel with the surrounding cylinder charge finds its model-representation in the entrainment of charge into the zones. Simultaneously, the liquid droplets heat up from the surrounding hot charge and evaporate. Once a combustible mixture is generated, chemical ignition delay elapses. The combustion itself is described by an Arrhenius type reaction kinetic approach. After combustion has been completed, the individual spray zones are summarized to a 'Burned-Gas' zone. These combustion products are then recycled together with the fresh charge back into the reaction zones (Chapter 4.4.1).

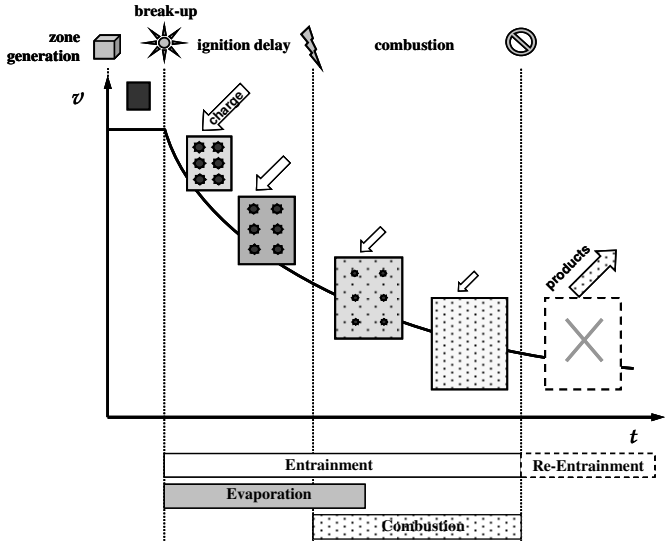

Figure 11: Mechanisms of Mixture Formation and Combustion in the MZCM

4.2.1 Fuel Injection and Charge Entrainment to Zones

The entrainment of the cylinder charge into the spray zones is calculated by applying the conservation of the overall package momentum. The deceleration of a package due to the interaction with the cylinder surrounding charge is reflected in an increase of mass, eq. (4-1). The model parameter $C_{Entrain}$ is introduced to account for inaccuracies in the empirical correlations, as well as for phenomena that are not implied in the current model (e.g. combustion chamber geometry, injection system, swirl). A method for the identification of this parameter, based on the physical impact, is presented in Chapter 6.

$$m_i = m_{inj} \cdot \left[1 + \left(\frac{v_{inj}}{v_{tip}} - 1 \right) \cdot C_{Entrain} \right] \tag{4-1}$$

We assume that the flow through the injector nozzle is quasi-steady and incompressible. The correlation for the injection velocity at nozzle exit v_{inj} is derived from the Bernoulli's principle, represented in eq. (4-2). Herein, the pressure difference Δp stands for the pressure drop over the injector nozzle. It is approximated from pressure before the nozzle and the backpressure of the combustion chamber (i.e. cylinder pressure in the case of an internal combustion engine). Rail pressure is usually one order of magnitude higher than chamber pressure, so it is the main engine parameter that defines the injection velocity.

$$v_{inj} = c_D \sqrt{\frac{2 \cdot \Delta p}{\rho_{fuel}}} \quad \text{for} \quad t < t_b \tag{4-2}$$

The fuel package enters the cylinder with its initial velocity until breakup occurs. Breakup time is calculated according to eq. (4-3) which is derived from equating eq. (4-2) and eq. (4-4) to assure a steady progression of velocity.

$$t_b = \frac{2.95^2}{8} \cdot \frac{\rho_{fuel} \cdot d_{inj}}{{c_D}^2 \sqrt{\Delta p \cdot \rho_{ch}}} \tag{4-3}$$

Hiroyasu et al. [54] have introduced a semi-empirical correlation for the velocity of the spray tip $v_{tip,c}$ penetrating the combustion chamber given by eq. (4-4). Herein, the tip penetration velocity decreases

reciprocal with time, assuming $t^{-0.5}$ dependency. The only parameters in this equation that depend on engine operating conditions are the injection pressure difference Δp and charge density ρ_{ch}.

$$v_{tip,c} = \frac{2.95}{2} \cdot \left(\frac{\Delta p}{\rho_{ch}} \right)^{0.25} \cdot d_{inj}^{0.5} \cdot t^{-0.5} \quad \text{for} \quad t \geq t_b \tag{4-4}$$

Based on the tip penetration velocity expressed by eq. (4-4), the spray model additionally considers correction functions to account for the axial (f_{ax}) and radial (f_{rad}) position of the zones in the spray which leads to eq. (4-5).

$$v_{tip,i} = v_{tip,c} \cdot f_{rad} \cdot f_{ax} \tag{4-5}$$

The velocity profile of the spray packages decreases from the spray centerline to the spray border, since there is a stronger interaction between the fuel package and the cylinder charge at the spray periphery. This leads to higher entrainment. An exponential decrease in radial direction is assumed in [54], [56], [57], expressed by the correction function (4-6). Here i_{rad} represents the radial position of the package in the spray. The velocity of the outer radial zones has half the value of the zones on the spray centerline. Hence, one can estimate the model constant C_{rad} from eq. (4-7) as discussed i.a. in [5].

$$f_{rad} = e^{\left[C_{rad} \cdot (i_{rad}-1)^2\right]} \tag{4-6}$$

$$C_{rad} = \frac{\ln(0.5)}{(nr-1)^2} \tag{4-7}$$

During fuel injection, the flow field in the combustion chamber is affected by the momentum of the spray. This leads to a slipstream effect for the later injected packages which are less decelerated and have lower entrainment. This effect is considered by a correction function depending on the axial position of the zone i_{ax}, represented by eq. (4-8) that is given in [56] and [57]. The model parameters C_1, C_2 and C_3 in (4-8) are kept constant, while the actual injection duration Δt_{inj} and the actual number of axial packages $i_{ax,max}$ increase during the injection. Reference Values for parameters C_1 - C_3 are given in [56].

$$f_{ax} = C_1 \cdot \left[1 + \left(\frac{i_{ax} - 1}{i_{ax,\max} - 1} \right)^{C_2} \cdot \frac{\Delta t_{inj}}{C_3} \right] \tag{4-8}$$

4.2.2 Droplet Breakup and Evaporation

Due to mechanisms that can be characterized as primary and secondary breakup, the condensed liquid package disintegrates to separate droplets [6], [7]. These mechanisms find their model representation in an instantaneous transition from a condensed liquid spray to separate droplets in the moment of breakup. The droplet size distribution is represented by the Sauter Mean Diameter (SMD). In the present model, the initial value of the SMD after breakup SMD_{tb} is calculated using the correlation of Varde et al. [48], see eq. (4-9). It is assumed that this diameter (which is calculated at spray breakup) is constant within the zone, but it should be noted that different zones have different *SMD* (caused by the changing injection pressure difference $\Delta pinj$ and charge density ρ_{ch}). It is assumed that all droplets have spherical shape. The SMD and the liquid fuel mass define the number of droplets. During evaporation, the decrease of liquid mass is reflected by a decrease of the SMD at constant droplet number.

$$SMD_{tb} = \frac{12.392 \cdot d_{inj}^{0.44} \cdot \rho_{fuel}^{0.42} \cdot \left(\sigma_{fuel} \cdot \upsilon_{fuel}\right)^{0.28}}{\Delta p_{inj}^{0.42} \cdot \rho_{ch}^{0.28}} \tag{4-9}$$

The evaporation model that is used for the present work is a droplet evaporation model, which is introduced in [58]. A refined version of the model is presented in [57]. The application of the evaporation model in multi-zone approaches is shown in [57] and [59].

The model considers two different mechanisms for the evaporation, depending on the liquid temperature as introduced in [57]. If the local temperature is lower than the critical fuel temperature, the governing mechanism for vaporization is the diffusive mass transport of vapor away from the droplet, represented by eq. (4-10). Therefore, Sherwood-number proportionality is assumed. The relevant concentration gradient is concealed by the relation between the temperature dependent saturation pressure and the absolute pressure. If the temperature exceeds the critical temperature, the evaporation rate is exclusively controlled by diffusion, expressed by eq. (4-11). The dependency on liquid temperature cancels.

In the following equations, subscript '*i*' refers to zone gas-phase conditions, '*l*' to the liquid droplet and '*m*' denotes the mean values from liquid and gas-phase.

$$\frac{dm_{fv}}{dt} = C_{Evap} \cdot \pi \cdot SMD \cdot D_v \cdot Sh \cdot \frac{p}{R \cdot T_m} \cdot \ln\left(\frac{p}{p - p_s}\right) \tag{4-10}$$

$$\frac{dm_{fv}}{dt} = C_{Evap} \cdot C_1 \cdot \pi \cdot SMD \cdot \left(\frac{p}{6}\right)^{C_2} \tag{4-11}$$

The heating up of the droplets is modeled by calculating the convective heat transfer from the hot gas to the droplet which is proportional to the Nusselt-number (4-12). For the resulting change of the droplet temperature, the heat of vaporization is taken into account. In eq. (4-12) the function $z/(e^z-1)$ corrects the effect of boundary layer thickening due to mass transfer. The resulting change of liquid temperature is expressed by eq. (4-13), considering latent heat of vaporization. The overall heat transfer q is considered as energy sink in the thermodynamic solution.

$$q = C_{eht} \cdot \pi \cdot SMD \cdot \lambda_m \cdot (T_i - T_l) \cdot Nu \cdot \left(\frac{z}{e^z - 1}\right) \quad \text{with} \quad z = \frac{c_{p,v} \cdot \frac{dm_{fv}}{dt}}{\pi \cdot SMD \cdot \lambda_m \cdot Nu} \tag{4-12}$$

$$\frac{dT_l}{dt} = \frac{1}{m_l \cdot c_{p,l}} \cdot \left(q - dh_v \cdot \frac{dm_{fv}}{dt}\right) \tag{4-13}$$

The model constants C_1 and C_2 in (4-11) are given in the literature [57]. A correction parameter C_{Evap} is foreseen that is used to calibrate the overall evaporation rate, which has the same value for the formulations below and above the critical temperature. In addition to that, it is possible to calibrate the heat transfer to the droplet by the parameter C_{eht} in eq. (4-12).

4.2.3 Ignition Delay

Once fuel vapour and air (oxygen) are available within a zone, the pre-reactions for self-ignition immediately start [56]. The time until combustion starts, denoted as chemical ignition delay, substantially depends on temperature and pressure and is approximated by the Arrhenius type correlation (4-14). This correlation is based on the approach of Wolfer [44] which was followed up i.a. in [59] and [57]. The latter publications also suggest reference values for the model parameters. The ignition delay time is calculated by integration of the reciprocal of 'τ' from start of injection (*inj*) until a threshold value of 1 is reached; see equation (4-15).

$$\tau = C_{IgnDel} \cdot p_{cyl}^{-1.02} \cdot e^{\frac{C_2}{T_{IgnDel}}} \tag{4-14}$$

$$\int_{inj}^{inj+\bar{\tau}} \frac{1}{\tau} \cdot dt \geq 1 \tag{4-15}$$

If equation (4-14) uses the actual temperature of the individual zone (T_{IgnDel}), the ignition delay stays approximately constant during the whole injection period. Thus, later injected fuel packages show unrealistically long ignition delays. For this reason, the average spray temperature (mean value of all existing zones) is used for T_{IgnDel} in eq. (4-14). This reflects the increase of temperature in the cylinder after initial ignition which caused the distinct premixed combustion peak.

The present formulation does not consider any impact of the fuel or charge composition on ignition delay. The effect of fuel composition, which in real engine operation is expressed by the Cetane number, must be correlated in the model by the parameters C_{IgnDel} and C_2, as shown in [60]. In real engine operation, the charge composition also has a significant impact on ignition delay. This effect is for example in alternative combustion concepts (HCCI), deliberately used to control the start of combustion by means of extremely high EGR rates (70% and higher). For the present work, the use of a simple model is not seen as a delimitation as it is primarily applied to conventional combustion concepts with relatively short ignition delays (< DOI) and moderate EGR rates (< 50%). For the simulation of alternative combustion concepts, the use of higher sophisticated models or the application of detailed chemistry calculations can contribute to improving the prediction of ignition delay.

4.2.4 Combustion Reaction

The energy release in the zone is calculated by a simplified 1-step reaction mechanism. Such a mechanism is commonly used for 0-dimensional multi-zone models, e.g. by [59], [56] and [61]. All these published approaches have in common that the reaction educts are the fuel vapor and oxygen concentrations and the temperature dependency is modeled by an Arrhenius-type formulation. In eq. (4-16) the heat release expression is given in the most general form, which can be modified by its model parameters and exponents. A discussion of the impact of different parameter settings on the characteristics of the reaction is given in Appendix 10.1.

$$\frac{dx_{fb}}{dt} = K_b \cdot \rho_{ch}^{a_{rho}} \cdot p^{b_p} \cdot x_{fv} \cdot x_{o_2}^{c_{O_2}} \cdot e^{\frac{-E_a / R_m}{T_i}} \tag{4-16}$$

4.2.5 Sub-models for Heat Loss and Blow-by

The platform incorporates different sub-models for wall heat losses by Woschni [62], [63], Hohenberg [64], Bargende [65] or Wimmer et al. [66], which can be arbitrarily chosen. For the calculations in the present work the modified Woschni model from 1990 [63] is used. The partitioning of the wall heat loss to the individual zones is reached by a weighting function, considering zone mass and temperature.

Blow-by is calculated by the orifice flow equation which is a function of the pressure difference between cylinder and crank-case [18]. An annular-gap with constant width is assumed.

4.3 Modeling Pollutant Formation

4.3.1 Nitric Oxide

The physical mechanisms that govern NO formation in combustion engines are discussed in chapter 2.3.1. Here, the formulations that are used for the modeling of NO formation are given. The present model considers only the mechanism of Thermal-NO formation as it represents the major fraction of the overall emissions.

The formation of Thermal NO is modeled by the extended Zeldovich mechanism which is given below. Zeldovich [17] denoted the importance of the first two reactions and Lavoie et al. [67] added reaction three to account for under-stoichiometric conditions. The first reaction has, due to the involved N_2 triple bond, the highest activation energy and is thus rate determining. The squared brackets indicate molar concentrations in mol/cm^3 and the subscript e denotes the concentrations at chemical equilibrium. The reaction rate constants were taken from [18].

$$N_2 + O \xleftrightarrow{k_1} NO + N \tag{4-17}$$

$$N + O_2 \xleftrightarrow{k_2} NO + O \tag{4-18}$$

$$N + OH \xleftrightarrow{k_3} NO + H \tag{4-19}$$

With reaction rates of the forward reactions:

$$R_1 = k_1 \cdot [NO]_e \cdot [N]_e \tag{4-20}$$

$$R_2 = k_2 \cdot [NO]_e \cdot [O]_e \tag{4-21}$$

$$R_3 = k_3 \cdot [N]_e \cdot [OH]_e \tag{4-22}$$

Using the auxiliary variables:

$$AK = \frac{R_1}{R_2 + R_3} \tag{4-23}$$

$$\alpha = \frac{[NO]}{[NO]_e} \tag{4-24}$$

One derives the net change of NO concentration in Mole per volume and time:

$$\frac{d[NO]}{dt} = C_{NO,kin} \cdot \frac{2 \cdot R_1 \cdot \left(1 - \alpha^2\right)}{\left(1 + \alpha \cdot AK\right)} \tag{4-25}$$

The parameter $C_{NO,kin}$ is used adjust the model to measurements. For the comparison with measured NO_x emissions, the calculated mass of NO at the end of combustion has to be scaled with a constant factor of 46/30, representing the ratio of molar masses of NO_2 to NO. Additionally, the final result can be scaled with a pure multiplicative parameter $C_{NO,fac}$. The effect of these parameters and a procedure to identify them systematically are discussed in later Chapter 6.4.

4.3.2 Soot

According to the model concept of Dec [14] the spray after the nozzle exit primarily consists of liquid fuel, followed by a premixed area which is very rich of fuel vapor. Under these conditions, the initial soot formation occurs. Further, this is followed by a soot-filled central region which is surrounded by a diffusion flame. The soot oxidation takes place in the outside of the diffusion flame under near-stoichiometric conditions.

For zero-dimensional combustion simulation empirical two-step models are commonly used. In the present work, the model introduced by Hiroyasu et al. in [54] is applied. Since therein soot calculation is based on local information about composition and state, it is predestined for the application in MZCM and CFD Codes [59], [55], [68]. The model considers two reactions: One for the soot formation and one for the soot oxidation. Both mechanism are governed by Arrhenius type correlations. The net soot mass rate is the difference between soot formation rate and soot oxidation rate.

In the Hiroyasu model, the soot formation is directly attributed to the presence of fuel vapor (4-26). The oxidation reaction is governed by the net soot mass and the available oxygen in the reaction zone (4-27). These two reactions take place simultaneously as soon as ignition occurs, thus the temperature increases. At this point, the mass fractions of the reactants have already been established by the fuel-air mixing which happens between nozzle exit and the point of ignition. Right after ignition the reactant concentrations of the soot reaction (fuel favor and oxygen) drop significantly. The subsequent evolution of the reactants establishes according to the relevant transport mechanisms (charge entrainment, evaporation) and the chemical reaction rate. A fast evaporation leads to fuel-(vapor)-rich areas in which soot formation is enhanced, whereas a higher charge entrainment (high rail pressure) or higher charge oxygen concentration (low EGR) enhances soot oxidation.

$$\frac{dm_{s,f}}{dt} = C_{s,f} \cdot m_{fv} \cdot p^{0.5} \cdot e^{-\frac{E_{sf}}{R_m \cdot T}} \tag{4-26}$$

$$\frac{dm_{s,o}}{dt} = C_{s,o} \cdot m_{soot} \cdot \frac{p_{O_2}}{p} \cdot p^{1.8} \cdot e^{-\frac{E_{sc}}{R_m \cdot T}} \tag{4-27}$$

Net Soot mass rate:

$$\frac{dm_{soot}}{dt} = \frac{dm_{s,f}}{dt} - \frac{dm_{s,o}}{dt} \tag{4-28}$$

The activation energy representatives E_{sf} , E_{so} are taken from the literature [61]. The parameters $C_{s,f}$ and $C_{s,o}$ respectively are used adjust the model to measurements. The effect of these parameters and a procedure to identify them systematically are discussed in Chapter 6.4.

For 2-zone approaches which do not imply local information on composition and state within the spray, a global formulation is used for the soot formation mechanism. As the 2-zone approach in comparison to the MZCM is assessed in the later chapters, the widely used soot model of Schubiger et al. [69] is implemented to the calculation platform for the 2-zone calculation mode. This model also considers two reactions for the soot formation mechanism that are governed by Arrhenius type correlations.

In the 2-zone soot model, the formation reaction is attributed to the combustion rate of the diffusion combustion (4-29). The oxidation reaction depends on the existing soot and the oxygen availability in the reaction zone, with an additional mixing term τ_{char} which is related to the global heat release rate.

$$\frac{dm_{s,f}}{dt} = A_{s,f} \cdot \frac{dm_{fb,diff}}{dt} \cdot \left(\frac{p}{p_{ref}} \right)^{n1} \cdot e^{\frac{T_{A,f}}{T_m}} \tag{4-29}$$

$$\frac{dm_{s,o}}{dt} = A_{s,o} \cdot \frac{1}{\tau_{char}} \cdot (m_{soot})^{n2} \cdot \left(\frac{p_{O_2}}{p_{O_2,ref}} \right)^{n3} \cdot e^{\frac{T_{A,o}}{T_m}} \tag{4-30}$$

4.4 Discussion of the Multi-Zone approach and Useful Modeling Extensions

A major advantage of the multi-zone approach is its simplicity. As an aspect of this, the original Hiroyasu model does not consider heat and mass exchange between the reaction zones. The only actual mass transfer is the unidirectional entrainment of the cylinder charge into the reaction zones.

The following chapter will discuss, if these modeling assumptions are still valid in the scope of modern combustion concepts and the required accuracy of results. If considered necessary, modeling extensions are introduced.

4.4.1 Re-Entrainment of burned mass

In the original model approach (Figure 12, left), the unidirectional entrainment of fresh charge to the spray may cause the problem that all oxygen of the cylinder charge is used up before the end of combustion. In these cases, the combustion process stops prematurely, even though there is an oxygen surplus in some of the elder spray zones. Due to the lack of mass transfer, this oxygen is not available for the subsequent combustion.

This indicates that the fundamental modeling assumption for the mass transfer leads to a discrepancy in the model in specific operating conditions, especially at high load points with low global lambda values and high injection pressure. These specific operating conditions were probably not a constraint when the original modeling approach was developed, as such low lambda values can only be realized with acceptable soot emissions by means of the high injection pressures of modern injection systems.

In order to solve this problem, a 'Burned-Gas' zone was introduced which continuously absorbs all the completely burned reaction zones. Part of them is recycled together with the fresh charge back into the later generated reaction zones by the entrainment mechanism. The dosage of burned re-entrainment mass into the fresh charge is controlled by one parameter. The mechanism is schematically represented in Figure 12, right.

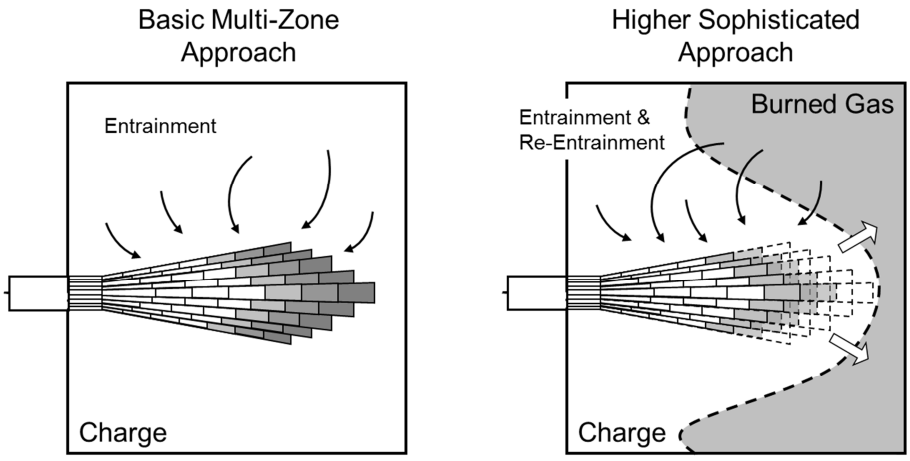

Figure 12: Comparison of Model Conceptions for Entrainment and Re-Entrainment

Figure 13 demonstrates the effect of the Re-Entrainment mechanism on the calculation process. It shows a comparison between the two calculation modes in one operating point (point 12 of engine 2 in Figure 36). In the basic entrainment calculation mode (left), the charge mass is entirely entrained into the spray and therefore consumed at ~52deg, which leads to a premature termination of the combustion. In the Re-Entrainment calculation mode, the later injected zones obtain their entrainment mass from both the fresh charge zone and the burned zone. This has two consequences: (1) the charge zone is no more entirely consumed and (2) since combustion products in the burned zone hardly contain oxygen, the mean oxygen concentration of the entrained mass drops (shown in the traces 'O2 Entrained Gas' in Figure 13).

This second effect of the suppressed oxygen supply on the later injected zones has special relevance for the calculated soot emissions, as demonstrated by the comparison of the 'Net Soot Mass' traces in Figure 13. In the initial phase of combustion, the net soot mass in the cylinder shows a similar progress in both calculation modes. However, with consideration of Re-Entrainment the oxidation is suppressed in the later phase (starting from ~30°) due to the lower oxygen supply, which obviously reduces soot oxidation. This effect is more pronounced at high load points with low global air excess ratios which in general produce more soot. This is the reason why the Re-Entrainment strongly effects the calculation of soot emissions; in fact, it is required to predict its characteristics versus engine load.

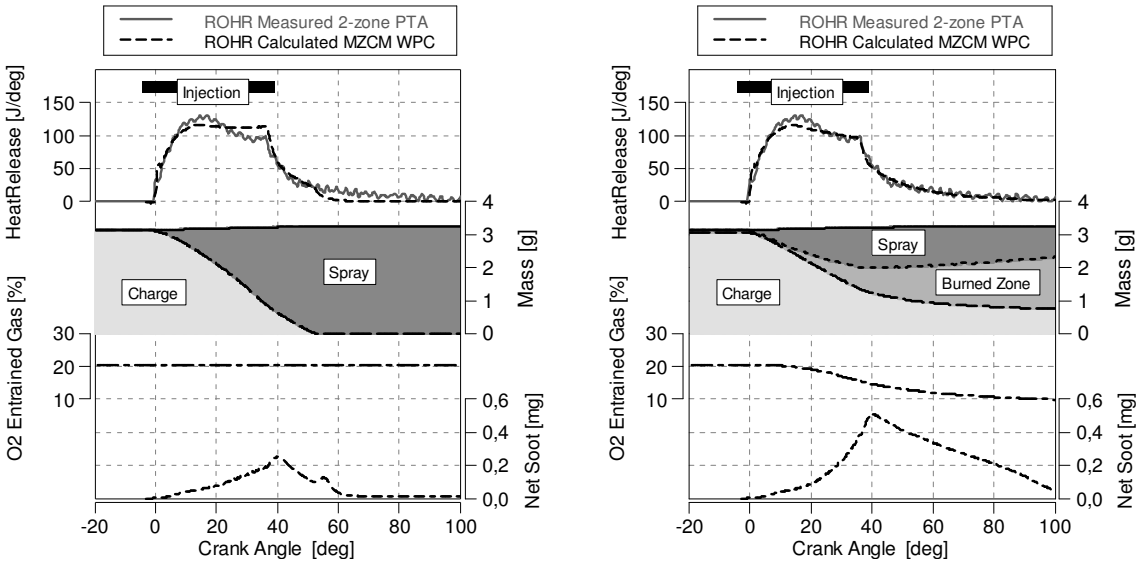

Figure 13: Comparison of calculation results with two different Entrainment mechanisms (left) Basic Entrainment Model (right) Extended Model with Re-Entrainment

In literature, there are different approaches for considering the interactions between fuel spray(s) and burned combustion products by mixing. Thoma et al. [70] have suggested an extension of the multi-zone approach to account for pre-injection events. In this approach, all zones of the first spray are combined to one single pre-injection zone. When the zones of the main injection penetrate the pre-injection zone, the entrainment is taken from this zone instead of the fresh charge zone, which reduces the ignition delay of the main injection. Hountalas et al. [61] also introduce a mixing mechanism which aims at improving the model for predicting the combustion process for multiple injections. This especially regards the accounting for post-injection by partial mixing of the main injection combustion products into the post injection spray. After post injection a progressive mixing of all zones is assumed.

All approaches have in common that they reduce oxygen availability and increase temperature for the later spray zones, thus affecting heat release and pollutant formation. Details of the above mentioned mechanisms are not described in the referenced literature, so assets and drawbacks of the individual approaches can hardly be assessed.

However, one advantage of the approach presented in this work is seen in the fact that the zone mixing is a continuous process which does not distinguish individual injection events. Therefore, it is supposed to be more generally applicable for the simulation of arbitrary injection strategies.

4.4.2 In-Cylinder Temperature Profile and Resulting Heat Transfer

A common ground for all multi-zone approaches is to divide the cylinder into an unburned and a burned domain. In the case of the MZCM, the burned domain summarizes all spray zones and the re-entrainment zone. The energy, which is released by the combustion reaction exclusively heats the burned domain which causes a heterogeneous distribution of temperatures in the cylinder.

While this heterogeneous distribution is a prerequisite for modeling reaction kinetic processes such as the NO formation, it also has consequences for the calculated pressure gradient of the high pressure cycle. Therefore, calculated heat release and pressure curves cannot be compared in-between different single- and multi-zone modeling approaches. The differences result from the thermodynamic properties of the working gas which show a progressive increase of specific heat at high temperatures. Above 2000K, the energy required for dissociation leads to a non-linear increase in internal energy. If, as in the case of multi-zone models, a part of the cylinder mass reaches this temperature region, a higher energy release is necessary to reach the same mean-temperature and pressure level. This accumulated internal energy is retrieved when the temperature falls below the dissociation region. [29]

In reality, continuous heat and mass transport processes, fanned by the turbulence of the injection, naturally lead to a homogenization of the temperature and concentration field in the cylinder. If this is not considered in a multi-zone model, it can lead to an improper calculation of the indicated work. For a correct treatment it is important that a homogenization of the temperature profile occurs within the high pressure cycle. Otherwise, the calculated energy balance of the cylinder is deferred in a way that the exhaust enthalpy is overestimated at the expense of a lower volumetric work of the process.

In 2-zone models it is common practice to assume a well-directed development of the entrainment from the unburned to the burned zone in a way that the entire cylinder mass is homogenized in the burned domain until EVO. [30]

In the MZCM usually a part of the cylinder mass remains in the unburned domain (i.e. charge zone) until EVO, as exemplarily shown in Figure 13 (right), causing a heterogeneous temperature field. From a physical aspect there are two different ways to realize the required temperature homogenization in the model. These are the consideration of (1) mass transfer or (2) heat transfer.

Ad (1): If the homogenization is realized by mass transfer, it would require successively entraining the charge zone into the burned domain, similar to the approach in 2-zone models. The entrainment to the spray zones must not be altered as it is defined by the spray model. However, it would be possible to

consider a continuous mixing of the fresh charge into the 'Burned Gas' zone which also consumes all the spray zones after they have been completely burned (compare Figure 12). In that case, the entire cylinder mass is accumulated in the Burned Gas zone until EVO.

The drawback of this approach is that it would interfere with the Re-Entrainment mechanism, as the rich Burned Gas zone would be diluted with lean fresh charge. This dilution would be a constraint to the control of the composition of the entrained mass. It would not be possible anymore to constitute very rich conditions for the entrainment which can be crucial e.g. for post injections.

Ad (2): In the second approach the temperature homogenization is accomplished by means of a heat transfer between the high temperature zone(s) of the burned domain and the unburned charge zone. Therefore, a convective heat transfer model is attached to the MZCM. The heat transfer is modeled using a Newton's law formulation, see eq. (4-31). The driving temperature difference can directly be calculated from the zone temperatures. The surface area is calculated from the zone volume, assuming a spherical shape while the heat transfer coefficient α_{ht} is an input parameter to the model. The heat transfer only occurs in-between the zones, thus not affecting the external heat losses to the cylinder walls.

$$\frac{dq_{i\rightarrow ch}}{dt} = \alpha_{ht} \cdot A_i \cdot (T_i - T_{ch}) \qquad (4\text{-}31)$$

Figure 14 demonstrates the effect of this inter-zone heat transfer on the thermodynamic characteristics of the high pressure cycle by comparing calculated results for two different (constant) values of the heat transfer coefficient α_{ht}: 0 and 2500 W/m²/K.

The effect of the heat transfer is clearly reflected in the temperature histories of the burned and the unburned domains. Without consideration of the heat transfer (α_{ht}=*0 W/m²/K*), the temperature of the unburned zone almost follows the temperature of the motored cylinder, while the mean temperature of the burned domain remains high until EVO. In contrary to that, the temperatures of the burned and unburned domain approach the mean cylinder temperature and an equalization is reached by ~ 80 degCA in the second case (α_{ht}=*2500 W/m²/K*).

Another important aspect of the heat transfer mechanisms is the impact on calculated emissions. Since the temperatures in the burned domain are lowered, the chemical reaction driven mechanisms of emissions formation are clearly affected.

Calculated NO_x emissions show a decline with increasing heat transfer. However, the highest temperatures during the initial phase of combustion are hardly affected by the heat transfer mechanism and are still representative for NO_x calculation. In terms of soot, it shows that the formation histories in the initial phase are similar. However, the temperatures in the later phase of combustion are now significantly lower and so the soot oxidation is considerably suppressed. Therefore, calculated engine-out soot emissions are very sensitive to the heat transfer mechanism. For both NO_x and soot, the model still predicts the correct trends of emission characteristics for changing engine parameters. Different heat transfer coefficients require different settings for the emission model parameters.

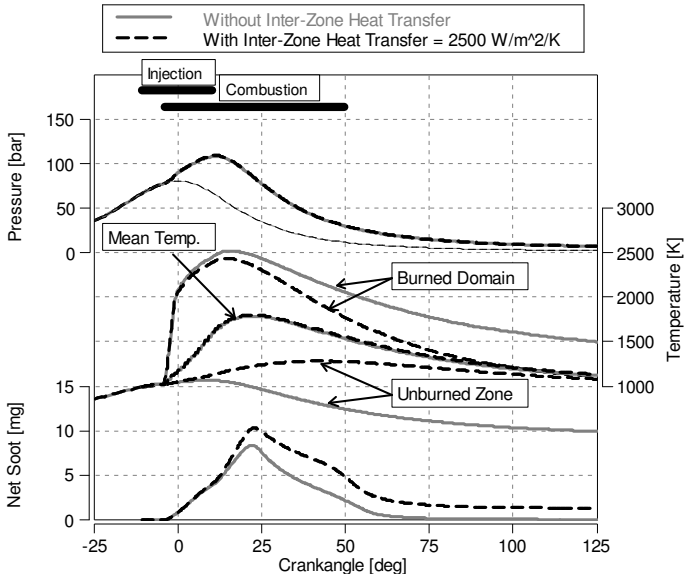

Figure 14: Effect of Inter-Zone Heat Transfer on Characteristics of the high pressure cycle

In Figure 15, the performance and emission relevant results of the high pressure cycle are plotted for a variation of the heat transfer coefficient. It shows the opposite trend of volumetric work (represented by IMEP_HP) and the exhaust enthalpy (represented by the internal energy at EVO). In the present example, indicated fuel consumption (ISFC_HP) is affected by up to 2%. Calculated engine performance characteristics are most sensitive at small parameter values and then approach a certain value asymptotically.

The figure also shows the impact on calculated emissions described above. As already mentioned above, the heat transfer mechanism does not detract the predictive quality of the model. The characteristics at changing engine settings (speed, load, EGR, rail pressure, etc.) can still be predicted correctly, but different heat transfer coefficients require different settings for the emission model parameters.

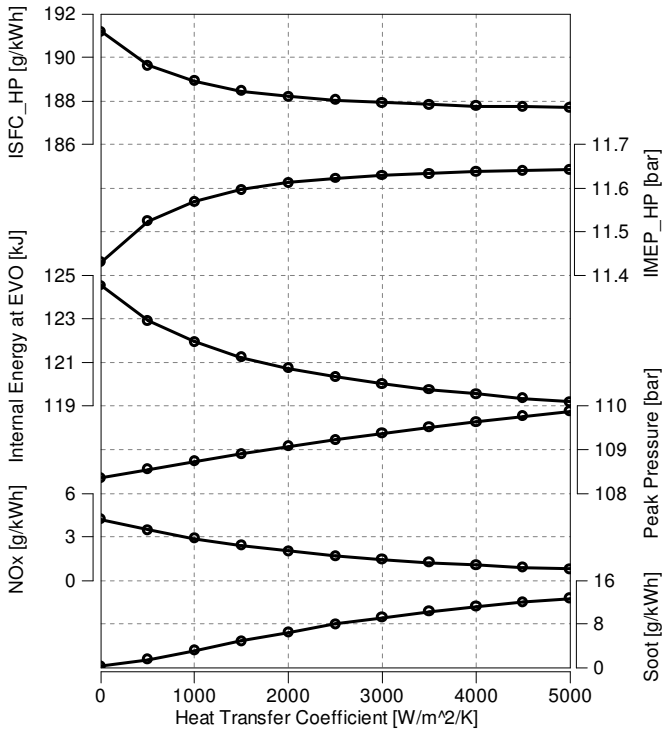

Figure 15: Engine Performance and Emission for Variation of Inter-Zone Heat Transfer

5 Effect of Engine Operating Conditions on the Fundamental Mechanisms in the Reaction Zone

In the multi-zone model heat release and emission formation are calculated in each of the individual reaction zones by reaction kinetic approaches. The reaction kinetic processes however stand at the end of a long chain of precursor mechanisms that describe the supply of reactants to the reaction zones. What is expressed as supply mechanisms in modeling terms is thought of as mixture formation in the understanding of the combustion process.

Figure 16 demonstrates the interrelations of mixture formation and combustion on the basis of a single reaction zone. As described before, there are mainly three mechanisms which limit the heat release in the MZCM. The first two mechanisms summarize the mixture formation process, as they describe the external supply of fuel and oxygen to the reaction zone. The third one is the chemical reaction of these reactants. This approach of clustering sub-models is continued in the later chapters when global heat release and emission are analyzed under real engine operating conditions.

1. Supply of Oxygen by the Entrainment
2. Supply of Fuel Vapor by Evaporation
3. Chemical Reaction of Fuel Vapor and Oxygen

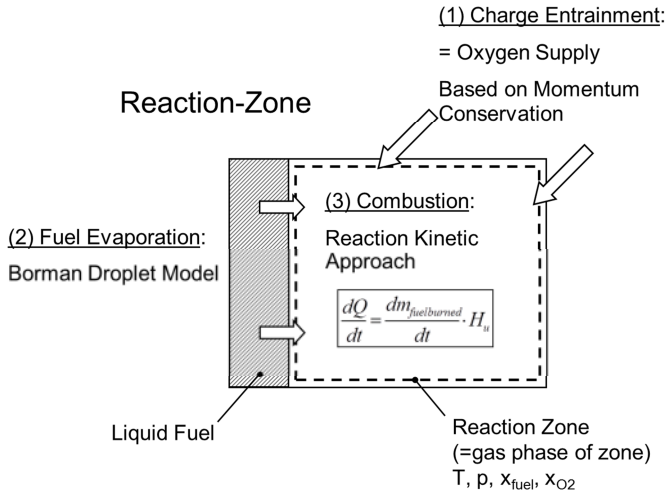

Figure 16: Basic Mechanisms that govern the Combustion of a Single Reaction Zone

Different physical boundary conditions caused by changing engine operating parameters impinge in the phenomenological sub-models. The present chapter analyzes the individual models with the scope of the processes in a single zone. Finally, the interaction between these mechanisms and the resulting global processes which determine the heat release are demonstrated by an example.

5.1 Effect of Engine Settings on Mixture Formation

5.1.1 Entrainment

The charge entrainment is calculated from the assumption of momentum conservation in the zone. Thus, it is directly related to the injection velocity and penetration velocity expressed by eq. (4-1). According to the governing equations (4-2) and (4-4), the main relevant parameters for entrainment that are affected by engine operating conditions are injection pressure difference and charge density. The injection pressure is a direct input to the model. The charge density is defined by the cylinder pressure and temperature at IVC and the crank angle position of the injection. The cylinder pressure level during

injection covers a wide range in turbocharged engines, while the IVC temperature is controlled by charge air cooling.

In order to demonstrate the effect of the individual parameters in the entrainment model a computational study is conducted. For this purpose, the boundary conditions for the package entrainment are defined externally and varied in range that covers reasonable operating conditions for modern diesel engines. The baseline point for the variations is defined by: $p_{Inj} = 1000\ bar$, ρ_{ch} calculated from $T_{ch} = 1000K$, $p = 100bar$. The variation range of the boundary conditions is derived from assuming intake valve closing conditions of $p_{IVC} = 1 - 3\ bar$, which represents around $\varepsilon^{\kappa} \sim 18^{1.35} \sim 50 \cdot p_{IVC}\ bar$ at firing TDC and $T_{IVC} = 360K$. The extension of the chamber pressure range towards lower values is done to account for early or late injection timings.

Railpressure: 500 – 1500 bar

Chamber Pressure: 25 – 150 bar

Chamber Temperature: 1000 K (constant)

Figure 17 shows the characteristics of package velocity and package mass at a variation of rail pressure (left) and chamber pressure (right) in a steady-state environment. For the calculations,all other relevant parameters are kept constant.

An increase of the rail pressure results in higher injection velocity and higher tip velocity. So the effect would partially compensate in the momentum equation. However, as the impact of injection pressure is more pronounced in injection velocity (exponent = 0.5 instead of 0.25), an increase of rail pressure ultimately results in a higher entrainment mass gain.

In contrary to that, a variation of chamber pressure hardly affects the initial injection velocity since the injection pressure is usually an order of magnitude higher than chamber pressure. However, the chamber density (and thus pressure) has a big impact on the penetration velocity. Thus, an increase in boost pressure results in a higher deceleration of the package which leads to a higher entrainment mass gain.

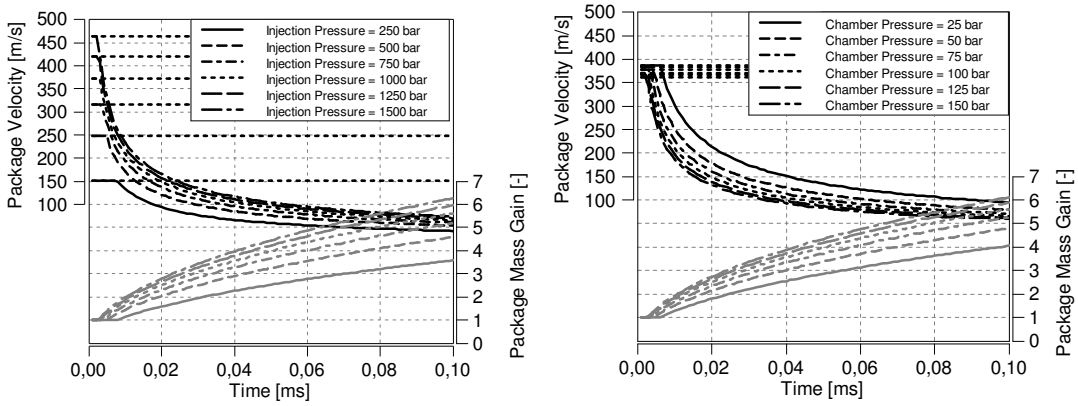

Figure 17: Characteristics of Package Velocity and Package Mass Gain (left) at Variation of Rail Pressure T_{ch}=1000K, p=100bar (right) at Variation of Chamber Pressure T_{ch}=1000K, p_{inj}=1000bar

The individual measures do have a completely different impact on the velocity characteristics. Rail pressure mainly affects initial velocity while chamber pressure is relevant for the deceleration of the package. Nevertheless, they result in similar characteristics of the overall entrainment mass gain as shown in the lower axis of Figure 17 (grey lines). In fact, the temporal evolution of the entrainment distinguishes only by a constant factor of $\Delta p^{0.25}\ \rho_{ch}^{-0.25}$ between different engine operating conditions despite the different injection- and tip-velocity characteristics.

5.1.2 Evaporation

Effect of Engine Operating Conditions on Droplet Size Distribution

According to eq. (4-9), the main relevant engine parameters for the calculation of the initial SMD are injection pressure difference and charge density. Figure 18 shows calculated values for the initial Sauter Diameter for different engine operation settings. The computational study covers the same operating conditions as outlined in the previous chapter. The nozzle hole diameter has a constant value of $d_{inj}=0.125mm$.

The calculated droplet size varies from 4 to 10 µm. It decreases with higher injection pressure and with higher chamber pressure.

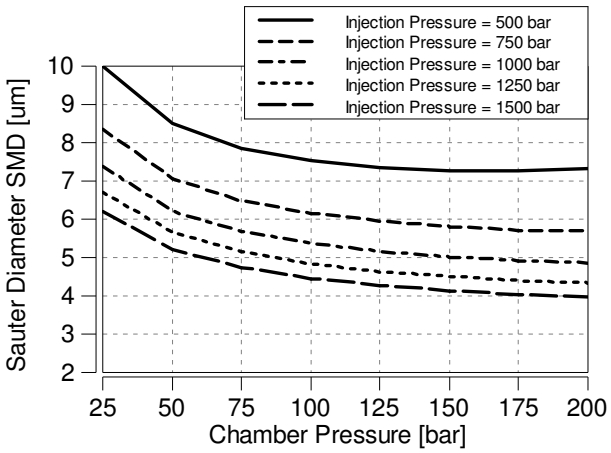

Figure 18: Sauter Diameter as Function of Chamber Pressure for different Injection Pressures Correlation of Varde et al.

In literature [6], measurement data of droplet size distributions under real engine conditions show the same qualitative trends as given by the applied correlation. The quantitative values are also in the same order of magnitude. In another citation [7], results of CFD calculations for droplet size distributions show higher values in the order of magnitude of 10 to 25 µm. The referenced works refer to Diesel engines with modern injection equipment. However, as there is in both cases no detailed information on the boundary conditions and nozzle design available, a direct comparison of the quantitative values (or even a calibration of the applied correlation) is not possible.

Effect of Engine Operating Conditions on Evaporation Duration

In real engine cycle calculations the boundary conditions for the individual phenomenological models do not vary independently from each other, as it was so far assumed for the computational study. Especially for the evaporation mechanism there are systematic relations between engine settings (such as rail pressure or chamber pressure), that that can affect the progress in different ways. For example, rail pressure is not directly implied in the mathematical formulations of the evaporation model, but it affects evaporation due to the impact on the initial SMD (acc. to Figure 18) and the droplet velocity (acc. to Figure 17).

To demonstrate these effects, the calculated duration for droplet heat up (when critical temperature is reached) and the duration to total evaporation (99% mass fraction evaporated) are examined.

Figure 19 (left) shows calculated results for heat-up and evaporation duration at a variation of chamber pressure. The grey dashed lines show the characteristics for different (artificially specified) initial SMDs. As expected, the time to reach the critical temperature decreases with higher pressures due to the better heat transfer. The evaporation rate below the critical temperature decreases with increasing ambient

pressure according to eq. (4-10). Thus evaporation duration shows a minimum at 75 - 100bar, which results from the opposing effect of faster heat up and lower evaporation rate.

However, it needs to be considered that a variation of chamber pressure has a direct impact on the calculated SMD. If we intersect the lines of constant SMD at the corresponding chamber pressure and connect these points, we obtain the actual trend of evaporation duration vs. chamber pressure plotted in the continuous lines. In the present example, higher pressures would in any way enhance evaporation.

In Figure 19 (right) the dashed lines show the heat-up and evaporation durations for different initial SMDs as a function of droplet velocity. Evaporation rate increases with higher velocity and smaller initial SMD. The SMDs have deliberately been calculated from even numbered chosen values of injection pressures. Hence, one can intersect the iso-lines of SMD at the corresponding values of droplet velocity for the given injection pressures (assuming that droplet velocity equals injection velocity during the entire evaporation). A higher injection pressure leads to smaller droplets and a higher velocity, both enhancing evaporation. The resulting line shows that an increase of injection pressure leads to a dramatic reduction of evaporation duration.

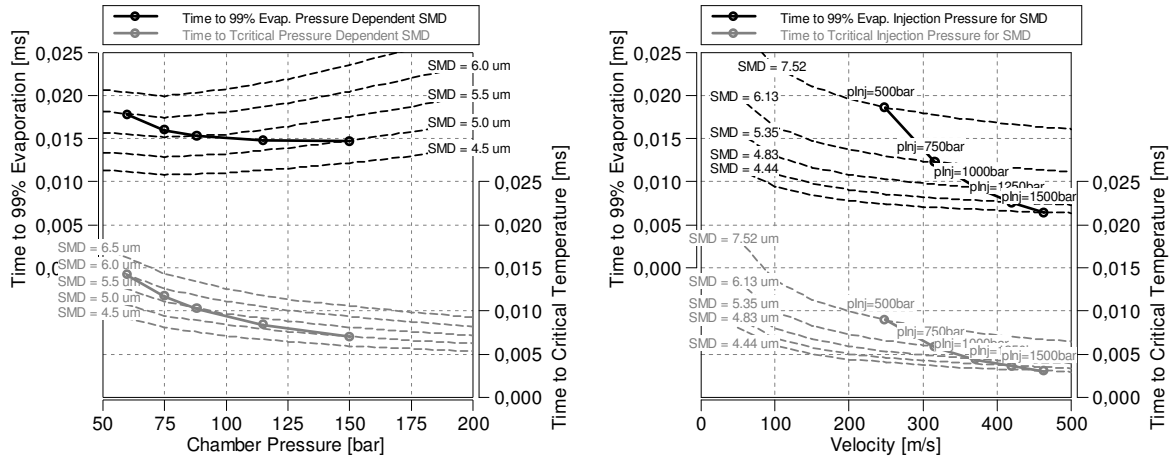

Figure 19: Duration of Heat-up and Evaporation
(left) Effect of Chamber Pressure (right) Effect of Injection Pressure

5.2 Fundamental Effects of Thermodynamics and Reaction Kinetics

The following considerations concentrate on the thermodynamic change of state of the reaction zones in the multi-zone model. The main relevant change of state occurs during combustion, when fuel and oxygen react and the temperature rises up to a region that is relevant for emission formation.

Of course on the one hand, this process depends on the composition and state of the zones in the moment of ignition, which defines the theoretical combustion temperature. The other important aspect is the actual course of the combustion process determined by the chemical reaction and the superposed piston movement.

5.2.1 Effect of the Zone Composition on the Adiabatic Flame Temperature

Due to the heterogeneous nature of the (conventional) diesel engine combustion, global values such as the global lambda value or EGR Rate are not directly relevant for the processes that take place locally in different areas of the spray. The thermodynamic processes are rather determined by the local mixture ratio of fuel and charge and the species concentrations. In the MZCM, the heterogeneous concentration field is represented by the distribution of fuel and charge within the different reaction zones of the spray. This is schematically represented in Figure 20. In terms of composition, the zone is divided into a fuel

vapor mass m_{fv} and a zone charge mass m_{ch}. The ratio of fuel mass to charge mass results from the interaction between the mixture formation mechanisms: entrainment and evaporation. The composition of the zone charge mass however is equal to the cylinder charge up until the moment of ignition[3].

As discussed in Chapter 2.1.2, two independent values are required in order to unambiguously define the composition of a zone in the moment of ignition ($x_b=0$). These are the oxygen concentration of the zone x_{O2}^{zone} and the zone lambda value λ^{zone}.

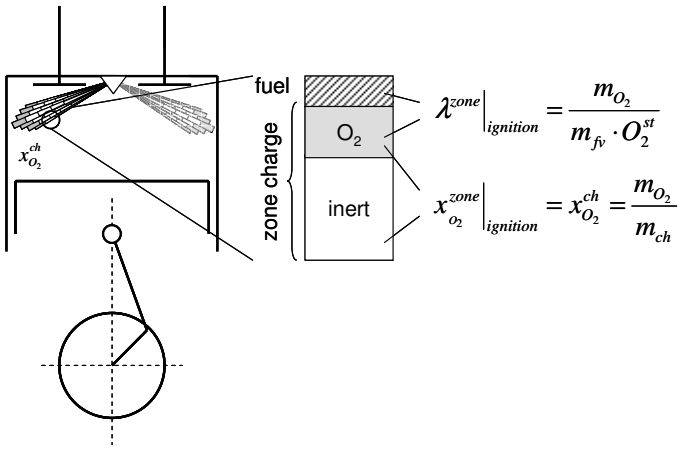

Figure 20: Schematic Representation Definition of Zone Composition and Effect of Charge Dilution

A first approximation for the temperatures that occur during the process is the Adiabatic Isobaric Flame Temperature (AIFT). It represents the theoretical temperature of a zone at an instantaneous and complete combustion under isobaric conditions.

The AIFT is calculated from the fuel energy that is released by the reaction and the mass or heat capacity respectively that needs to be heated up. In the case of lambda > 1 a complete combustion of the fuel is assumed. At higher lambda values the overall mass that needs to be heated up increases, which reduces the AIFT. For lambda values < 1 the lack of oxygen limits the amount of fuel that can take part in the reaction. In this case, it is assumed that only that part of the fuel reacts which is given by the stoichiometric ratio. Intermediate species of the reaction, which occur with incomplete combustion such as CO, are not considered. As part of the fuel remains unburned, the released energy is reduced. Therefore, the AIFT has its highest value at near stoichiometric conditions which is a result of the highest ratio of induced energy to thermal inertia.

With increasing charge dilution the same amount of oxygen involves a higher fraction of inert species. The inert species increase the thermal inertia without participating in the reaction. Hence, at the same lambda value the mass of the package increases for a constant amount of oxygen.

Figure 21 plots the calculated values for the AIFT as a function of zone lambda for different initial oxygen concentrations. The initial boundary conditions are chosen with $T_0 = 1000\ K$, $p = 100\ bar$. A charge oxygen concentration of $x_{O2}^{ch}=0.233$ corresponds to pure air.

[3] If the Re-Entrainment mechanism (Chapter 4.4.1) is considered, the composition assembles from the concentrations of the fresh charge zone and the burned zone with respect to the ratio of fresh charge entrainment to burned gas entrainment.

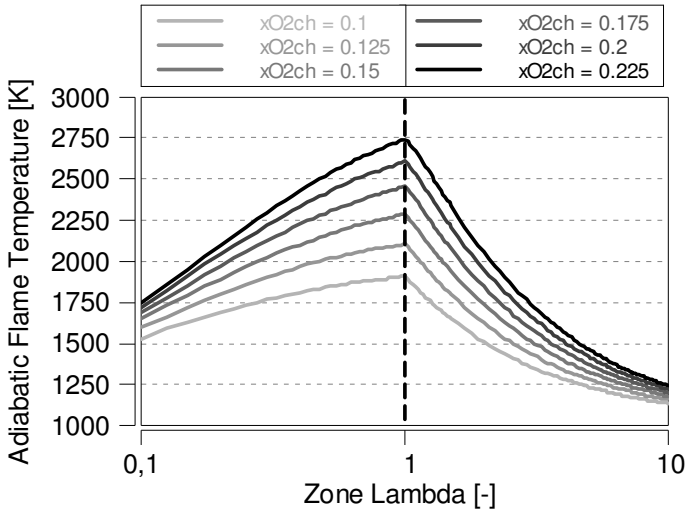

Figure 21: Adiabatic Isobaric Flame Temperature
For different Oxygen Concentrations as a Function of Lambda

5.2.2 Effect of the Non-Isobaric Combustion Process on Peak Temperature

It is a well-accepted fact, that an increase of the peak combustion pressure e.g. at an advanced combustion timing leads to higher peak temperatures which enhances NO formation. In this context, it is important to note that the AIFT discussed in the previous chapter is nearly independent from the absolute pressure level of the process. This is demonstrated in Figure 22, showing the thermodynamic change of state for an isobaric combustion at two different pressure levels (100bar and 200bar) in a Temperature-Entropy Diagram. Both processes have the same initial Temperature.

This indicates that the simplification of an isobaric combustion, which is made for the approximation of the theoretical combustion temperature does not entirely describe the actual process in a reciprocating engine. Here, combustion takes a certain time and consequently the pressure changes due to the heat release and the piston movement. Thus, for the peak temperatures not only the absolute pressure level is relevant, but also the course of the process.

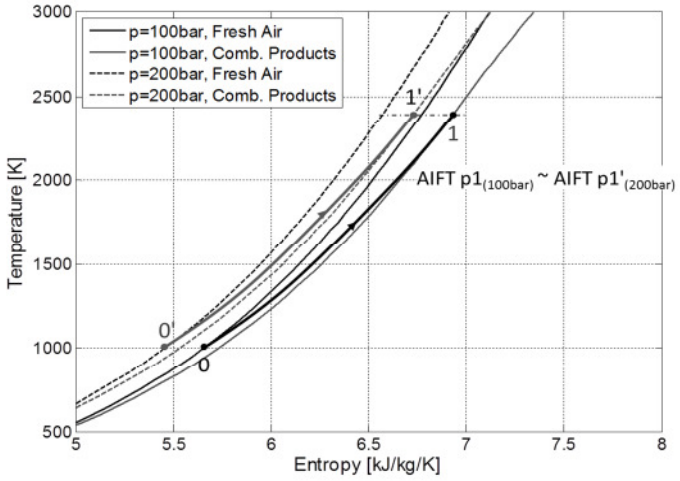

Figure 22: Isobaric Combustion at two Different Pressures in the T-s Diagram
Initial State: T=1000K, Lambda=1.25, xO2=0.2

In order to demonstrate the influence of pressure change during combustion, a more realistic process is defined. We assume an initial state of 1000K and 100bar which shall represent the conditions at start of combustion (at an arbitrary point in the compression or expansion stroke). Then we apply 2

fundamental thermodynamic changes of state: (1) an isobaric heat release and (2) an isentropic compression from 100 to 200bar. These two changes of state are carried out as given and in reverse order.

Figure 23 shows the changes of state in the Temperature-Entropy Diagram. The first process (plotted in grey) starts with the isentropic compression (State 0 to 1) which is followed by the isobaric combustion (State 1 to 2). The second process (plotted in black line) applies these changes of state in reverse order. The isobaric combustion occurs at 100bar (State 0 to 1') and is followed by the isentropic compression (State 1' to 2'). One can clearly see that the second process ends at a higher temperature. In reality, the change of state would be located somewhere between these two special cases.

From this example, we can conclude that the process cycle influences the peak temperature of combustion in a way that an early heat release with subsequent compression leads to the highest temperatures. This is an important finding as the cylinder state is always exposed to the compression / expansion due to the piston movement and the pressure rise due to combustion. This characteristic especially applies to the discretized zones of the MZCM which burn at different phases of the combustion process. This is discussed in more detail in the analysis of changes in engine settings in Chapter 7.

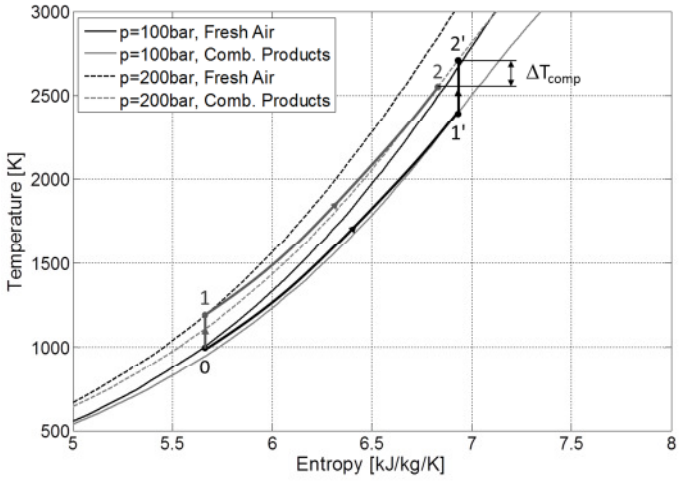

Figure 23: Combined Combustion / Compression Process of a Reaction Zone in the T-s Diagram
Initial State: T=1000K, p=100bar, Lambda=1.25, xO2=0.2

5.2.3 Effect of Composition and Zone State on Combustion of a Single Package

The combustion reaction determines the history of temperature and species concentrations in the individual zones which are relevant for the formation of NO_x and soot. The following considerations concentrate on the impact of the chemical reaction on the evolution of zone temperature and species concentration during the combustion process. Therefore, we assume a closed system with given initial state and species concentrations. This demonstration example represents one imaginary zone at start of combustion. It assumes that the entire fuel is available as vapor and that there is no heat and mass transfer to / from the surrounding charge zone. The composition of the combustion zone is defined by its fuel-air excess ratio (lambda) and by the oxygen concentration which initially corresponds to that of the cylinder charge, as given by the considerations to Figure 20. During combustion, the pressure is assumed to be constant.

Under these conditions the interrelations of stoichiometry and reaction kinetics (heat release acc. to eq. (4-16)) determine the evolution of temperature and species concentrations. The progression of species conversion during combustion is characterized by the mass fraction of fuel burned x_b, which is defined as $x_b = m_{fuel}^{burned} / m_{fuel}^{total}$.

Figure 24 shows the characteristics of combustion in an Arrhenius-type plot (see Appendix 10.1) for the given initial conditions: *T=1000K*, *p=100bar* (remaining constant), $x_{O2}^{ch} = 0.2$ for different lambda values.

The zone lambda value defines the concentrations of fuel vapor and oxygen in the zone, so it has the most significant influence on the reaction rate and its evolution. Figure 24 compares the characteristics of the combustion reaction for three zones with different lambda values. The initial reaction rates are in a similar order of magnitude. However, it can be observed that the reaction rate drops faster at small lambda values. This becomes apparent focusing on the lines of 50% fuel burned ($x_b = 0.5$), which are highlighted. In the case of lambda < 1, x_b can only reach values up to the lambda value, so part of the fuel remains unburned. The case of lambda = 1.25 has the highest reaction rates throughout the combustion. At lambda = 1 both educt concentrations approach zero towards the end of combustion. Therefore the concentrations term in the reaction equation takes very small values, which expresses itself in a severe drop of the reaction rate at $x_b = 0.95$ *to* 0.99.

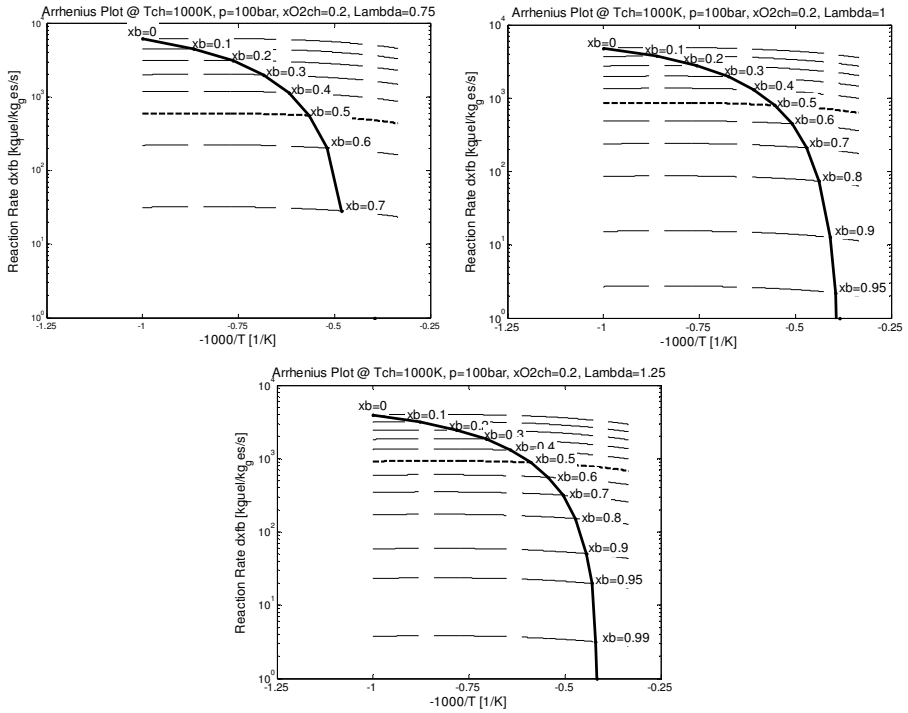

Figure 24: Theoretical Evolution of Combustion Rate of a Spray Package
Arrhenius-Type Plot Comparison of lambda=0.75 vs. Lamda=1 vs. lambda=1.25

Under most conditions the combustion reaction is fast compared to the mixture formation processes. Hence, the characteristics from Figure 24 cannot be transferred to the global heat release rate in the cylinder. The global heat release rate results from the sum of heat release in all zones and is to a great extend determined by the transport processes of the reactants to the zones as discussed in the Chapter 5.3.

5.2.4 Effect of Thermodynamic Boundary Conditions on NO Formation

The main relevant inputs to the Zeldovich mechanisms are the temperature and equilibrium concentrations of the participating species. Figure 25 shows the molar fractions of O and O_2 calculated from chemical equilibrium as a function of zone lambda for different initial zone oxygen concentrations. For these calculations, the temperature equals the AIFT shown in Figure 21. The availability of O_2 increases dramatically when lambda becomes > 1 which is a result of the combustion stoichiometry. Atomic oxygen predominantly occurs first, when there is plenty of oxygen available and second, when

temperatures are in addition high enough for dissociation. This is the case in the area right above stoichiometric conditions.

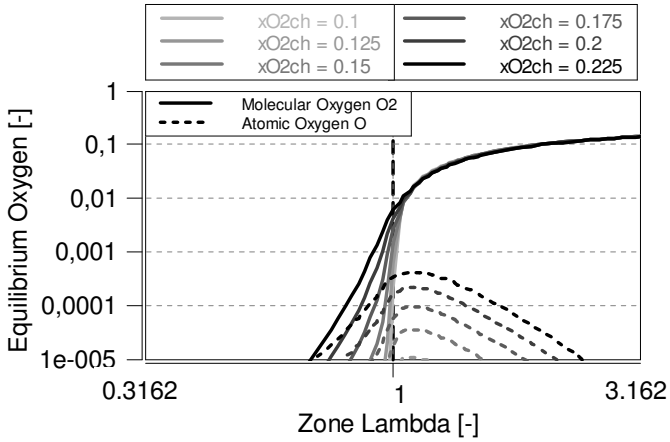

Figure 25: Equilibrium Concentrations of O and O_2 as a Function of Lambda Different Initial Zone Charge Oxygen Concentrations at corresponding AIFT

Figure 26 shows the NO formation rates calculated with the extended Zeldovich mechanism. For the calculation of these instantaneous reaction rates, the alpha value (defined by eq. (4-24)) is chosen with $\alpha=0.5$. The boundary conditions temperature, pressure and composition are the same as for the results above. The maximum NO formation rate is right above stoichiometric conditions at lambda = 1 to 1.1. This results from the combination of high temperatures along with availability of oxygen. The NO formation dramatically drops at lower oxygen concentrations which is a result of the lower combustion temperature.

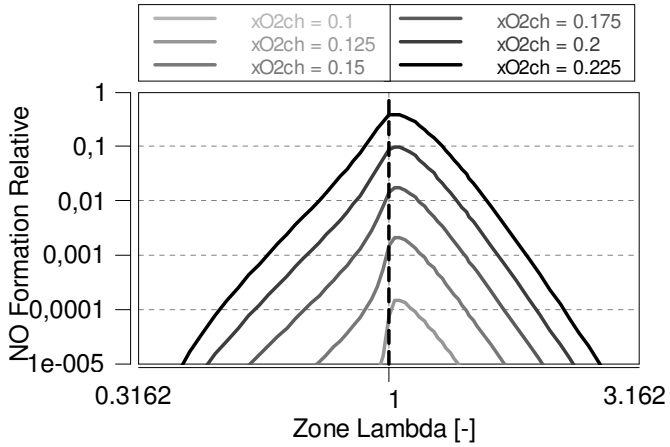

Figure 26: NO Formation as a function of Zone Lambda and Oxygen concentration Acc. to the Zeldovich mechanism

Figure 27 summarizes the previous results. It shows the NO formation rate as a function of adiabatic flame temperature. In the plot, oxygen concentration (full lines) and lambda values (dashed lines) are represented as iso-lines.

A characteristic of diffusion combustion is that part of the heat release is limited by the mixing process of oxygen and fuel. Thus, it has to be assumed that in most cases there are areas within the spray that burn at stoichiometric conditions and therefore have such high rates of NO formation. The only practical way to reduce the theoretical stoichiometric combustion temperatures is to limit them by means of charge dilution, causing a reduction of the oxygen content.

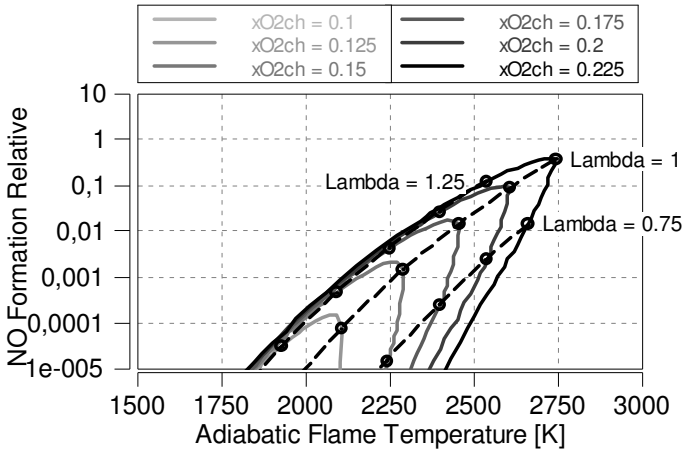

Figure 27: NO Formation as a Function of Temperature for different Zone Compositions

5.3 Temporal development of Spray Zones during Combustion

5.3.1 Development of the Reaction Zone States

To demonstrate the evolution of the spray combustion in the MZCM the evolution of all reaction zones in the field of temperature and lambda have to be observed. This is shown in Figure 28 for one specific case at different crank angle positions. On top of each of these diagrams the line of the adiabatic flame temperature is again shown as a function of lambda, though in a clockwise rotated view of Figure 21. The underlying state for the calculation of the AIFT is the instantaneous charge zone state (temperature, pressure and oxygen concentration). The intermediate graph in each crank angle plot shows the crank angle position relative to the injection rate and heat release, while the lowest graph shows the in-cylinder NO_x and soot mass.

For the demonstration we focus on 3 zones which are highlighted in Figure 10. The position in the spray is defined by the axial position '*a*' and radial position '*r*'. These three zones are injected at the same time step (defined by the axial position $a = 3$, which means 3 deg after start of injection), but at different radial positions of the spray which are denoted as $r = 1, 3$ and 5. Accordingly, the spray zone numbering (Zone Nr = a/r) means that the axial position $a = 3$ corresponds to the package of zones which are injected 3 deg after the start of injection, and the radial position $r = 1$ refers to the spray centerline, $r = 5$ to the spray periphery.

Heat Release

The first diagram in Figure 28 shows the spray zone distribution at phi = -3 degCA, which is the first time step after ignition. As expected, the zones at the spray periphery (e.g. Zone Nr. 3/5) have the highest lambda values due to the enhanced entrainment. Within the first 1 to 2 degCA after ignition 30 to 40 % of the fuel was already burned in the highlighted zones. The fraction of fuel burned is highest at the spray periphery (Zone Nr 3/5: $x_b = 0.4$) and decreases towards the spray centerline. This fast combustion is a result of the high availability of both fuel vapor and oxygen, which have been transported to the zones during the ignition delay period. After this first fast 'premixed' part of combustion, heat release is governed by the transport processes of fuel and oxygen to the zones. These are significantly slower compared to the chemical reaction. For example, Zone Nr. 3/1 at the centerline of the spray does not exceed stoichiometric conditions until phi ~15 degCA, which is ~24deg after it has entered the cylinder. Finally, it can be concluded that the transport processes determine the global heat release rate to a great extent, which is demonstrated in the following Chapter 5.3.2.

Emissions

As shown in Figure 28, in the phase up to 20° CA there is still a high number of zones at low lambda values, indicated by the grey shadowed regions reaching into the low lambda-zone. This is accompanied by a high amount of fuel vapor and a lack of oxygen in these zones, while their temperatures are already high. These conditions clearly enhance soot formation and suppress soot oxidation, which can be observed by the in-cylinder soot trace shown in the lower part of the diagrams of Figure 28.

The NO_x formation is driven by temperature, so the actual rate depends on the number and size of zones that pass the lambda ~ 1 area. On the other hand, the temperature that occurs in this area is a function of the charge concentration and is therefore determined by charge dilution.

… Field of all Spray Zones in the Temperature / Lambda Diagram at the given phi-angle

… Zones which refer to the Spray Package 'a=3' injected at -9 degCA (see picture on the right)

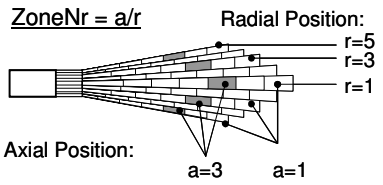

phi = -3 deg CA

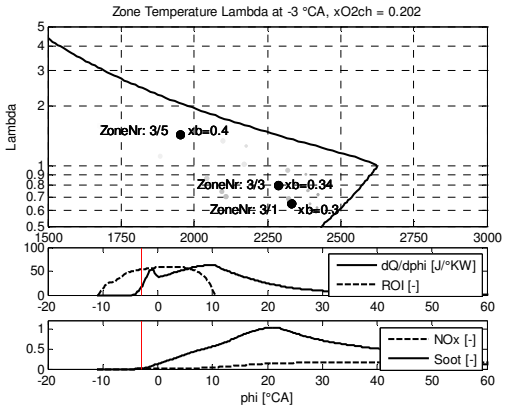

phi = 10 deg CA

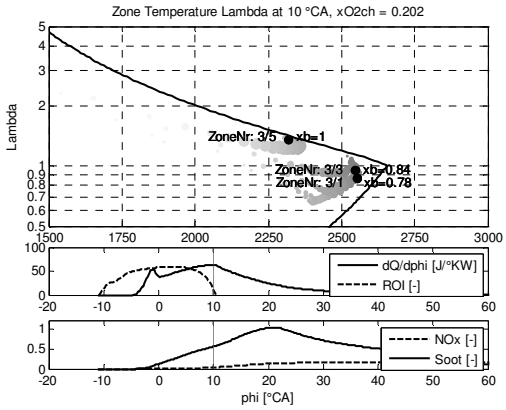

phi = 0 deg CA

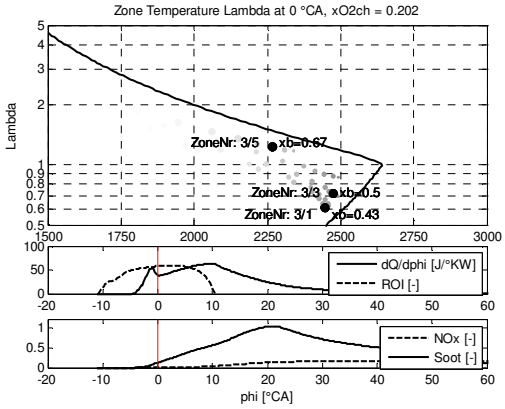

phi = 15 deg CA

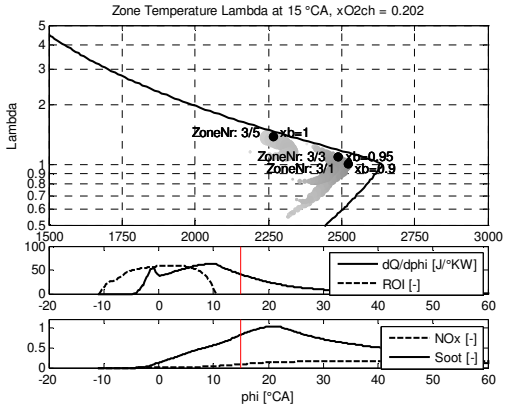

phi = 5 deg CA

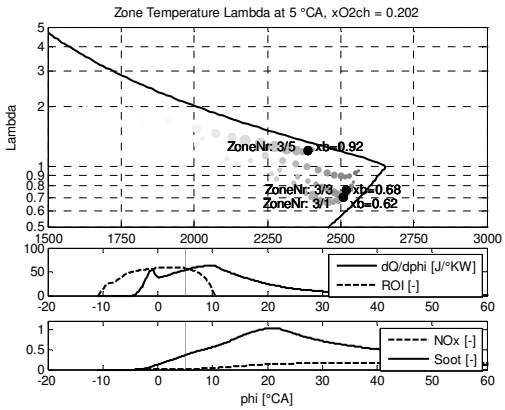

phi = 20 deg CA

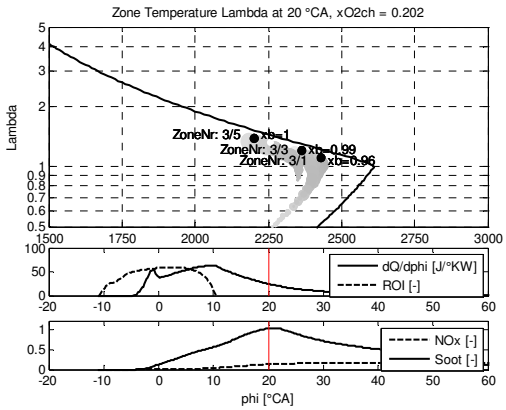

Figure 28: Temporal Evolution of the Spray in the Temperature and Lambda Field Comparison of 3 Zones (highlighted) injected at the same Time at different radial positions in the spray

5.3.2 Description of the Combustion Process by Global Mechanisms in the Spray

As stated in advance, the limiting factor for the reaction (on the basis of a single zone) is either the availability of fuel or oxygen, or the chemical reaction. The derived global combustion process, which is observed as heat release, adds up from all reaction zones. Thus, a global consideration of the main limiting processes (entrainment / evaporation) provides important information on the development of the combustion process.

Each of the mechanisms in the multi-zone approach is modeled as an independent and continuous process. However, due to the different temporal evolution of the individual processes and their interactions, it is possible to clearly distinguish phases in which individual mechanisms come to the fore. These different phases determine the characteristic heat release profile of diesel engines, as demonstrated in the theoretical considerations to Figure 4.

The spray averaged characteristics of the individual processes are shown for one example in Figure 28. The diagram shows the available liquid and vaporized fuel, the supply of oxygen and the heat release both in an integral view and by their time derivatives. These are derived from summing up all spray zones. In order to compare the available oxygen to the fuel quantities it is converted by the stoichiometric ratio and limited at lambda=1. In the integral view, the values are normalized to the overall injected fuel quantity.

Liquid fuel is provided to the cylinder by the injection which is an input to the model. As shown in the upper axis of Figure 28, entrainment starts immediately at the beginning of the injection, represented by an immediate increase of available oxygen. Other than that, the break-up of the liquid fuel, the heat up and evaporation initially take a certain time which delays the evaporation. This time period represents the physical ignition delay. At a certain point, chemical ignition delay is elapsed and the combustion process starts. In the early phase, a main part of the fuel which vaporizes during ignition delay burns fast which leads to the characteristic premixed combustion peak. As shown on the lower axis of Figure 28, the available oxygen exceeds the available fuel in the early phase of combustion. Therefore, in this phase the global heat release is governed by the evaporation mechanism.

At the end of injection, the momentum impinged by the spray stops abruptly. This leads to a decay of the entrainment and the global heat release becomes more and more controlled by the available oxygen. This phase denotes the diffusion combustion domain.

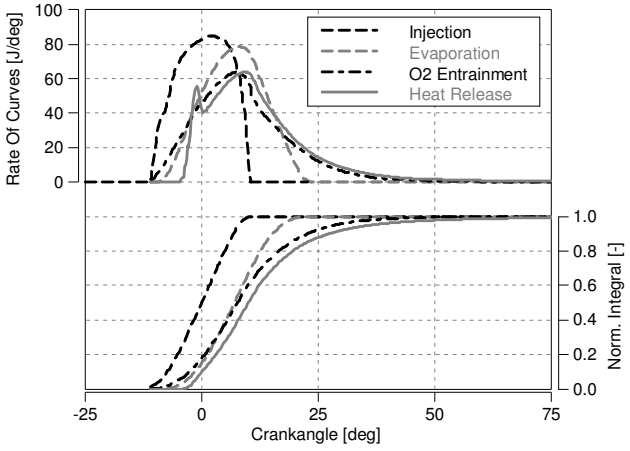

Figure 29: Heat Release governing Processes in the Multi-Zone Model

During this entire process, the heat release rate does not identically follow the curves of the mechanism which is limiting at a time. This offset is caused by two circumstances: (1) The heterogeneous spreading of fuel and air in the spray. Thus, there is always a part of the zones which is limited by entrainment (lambda < 1) and a part which is limited by evaporation (lambda > 1), as demonstrated in Figure 28. (2) The influence of the chemical reaction.

6 Methodology for Model Calibration and Validation

In this chapter the model is validated and assessed by the comparison of calculated results with experimental data. For this purpose an appropriate number of engine performance and emission data is selected. To assure a certain degree of general applicability, but also to ensure the usability of the model it is necessary to reduce the number of parameters to a minimum. The aim of this step is to develop a systematic procedure for automatic parameter identification which delivers unambiguous solutions for one set of model parameters.

It is postulated in advance that the quality of combustion modeling is founded primarily on a correct prediction of interrelationships between the various processes, which control combustion of a Diesel engine. Therefore, the dataset for the model validation must cover various operating points (speed / load) and variations of engine settings in these points (injection timing, injection pressure, boost pressure and EGR). In the present investigation, three different engines were considered (see Table 2).

The model parameters are identified with the objective to reach optimal matches with all measured values. Finally, the spreading of the identified parameters allows an assessment of the modeling sophistication.

6.1 Measurements

Experimental data from 3 different research engines were selected. As stated above, the data include various engine operating points (engine speeds and loads) and cover reasonable ranges for the engine settings such as EGR rate, lambda, injection pressure, injection timing and boost pressure. For reasons of simplicity, only data with single injection were chosen.

Table 2: Test engines and operating conditions

	Engine 1	**Engine 2**	**Engine 3**
Displacement /cyl	0.9 lit/cyl	1.3 lit/cyl	0.5 lit/cyl
EGR Rate	15 - 25 %	10 - 20 %	5 - 25 %
Lambda Global	1.3 - 2.5	1.3 - 3	1.3 - 2.5
Swirl (AVL nomenclature)	1.3	≈ 0	2.2
Injection System	Common Rail	Common Rail	Common Rail
Injection Pressure	800 - 1600 bar	600 - 1500 bar	800 - 1500 bar
Timing Variation Range	+/- 5 deg	+/- 7 deg	+/- 5 deg
Turbocharging	0 - 2 bar rel.	0 - 2 bar rel.	0.4-1.4 bar rel.

For the basic model calibration data of Engine 1 and 2 were used and 12 different speed and load points were selected for each of the two engines. The following values were available for each individual point:

- Engine speed and torque
- Mass rates of air, fuel and recirculated exhaust gas
- Indicated cylinder pressure curve (measured by quartz pressure transducer)
- NO_x emissions (measured by heated chemi-luminescence analyzer)
- Soot emissions (approximated from measured Filter Smoke Number by AVL correlation formula given in [25])

It has to be mentioned that most of the measurements originate from automated test runs, which are usually performed with the purpose of engine calibration by the method of Design of Experiment [71]. In contrast to exact scientific measurements, such tests e.g. allow shorter stabilization times. However, individual points were randomly repeated (they were repeatedly approached from different other operating points) in order to evaluate the scatter band of the measured values. These measurements were deliberately chosen in order to include a certain degree of measuring inaccuracy in this assessment. This mainly refers to the measurements of soot which show a very high relative scattering especially at operating points with low absolute soot levels such as low engine loads.

6.2 Basic procedure of Model calibration

The process of model calibration on the basis of the indicated pressure curves and the measured emissions is performed by a systematic procedure of two chronological steps. In advance, the pressure curve under motored conditions needs to be calibrated as described in Chapter 3.2.3.

The first step of the parameter identification is the systematic identification of the combustion process to match the measured pressure curve during combustion. In the second step, the parameters for the emissions formation models are identified. Since the combustion process defines the thermodynamic boundary conditions for the emission models, it is absolutely necessary to proceed in the given way.

6.3 Step 1: Identification of the Combustion Process with Multi-Zone Model

The combustion process characterizes the engine performance and provides the thermodynamic change of state in the zones. The latter defines the boundary conditions for the calculation of NO_x and soot emissions.

Within the single-zone and 2-zone modeling approaches, it is possible to calculate the heat release directly from the cylinder pressure curve by the application of the first law of thermodynamics. So the PTAs with single and 2-zone models result in exact analytical solutions for the heat release and the change of thermodynamic state throughout the combustion process. This is an optimum prerequisite for the calibration of emission models and therefore the 2-zone approach was included in this work. As no predictive combustion model was considered for the single and 2-zone approaches, the PTA does not provide any information on the mechanisms behind the heat release characteristics which could be applied to future WPCs of similar engines.

In the multi-zone approach WPC, combustion is calculated from continuous processes on the basis of the spray model. In the case of a PTA the distribution of the heat release to the individual zones is not known a priori. Consequently, the identification of states at one arbitrary time step within the combustion process requires information on the histories of all zones from their initial formation. For this reason, the model parameters cannot be identified time step by time step, but only by an integral consideration of the total combustion process. A new method for the PTA on the basis of the multi-zone model is discussed in the following Chapter 6.3.2.

6.3.1 Interrelations of Sub-Models for the Identification of Cylinder Pressure Curve

The present task started with the application of different optimization approaches, including sensitivity analyses and general purpose minimum search algorithms on the basis of the measured pressure trace. From the variety of studies the knowledge was obtained that the identification of the combustion parameters can only be successful, if it considers the physical impact and interrelations of the different

mechanisms. The reason for this is that in the MZCM the heat release process cannot be seen independent from the evolution of thermodynamic states in the spray zones. This is due to the strong physical interrelations between the individual sub-models for fuel evaporation, mixture preparation and chemical reactions. Thus, a purely mathematical identification of the heat release, e.g. on the basis of the measured pressure trace (which is a global observation), does not necessarily lead to a correct prediction of the distribution of the local states in the spray zones. This leads to unreasonable boundary conditions for the pollutant formation processes.

The evaluation of the mechanisms in the previous chapters and the sensitivity study gave a clear conception on how to cluster the sub-models and their associated parameters. The combustion process can be broken down to three governing mechanisms: the supply of oxygen and the supply of fuel vapor to the chemical reaction zones and the conversion rate of the chemical reaction. This was already shown in Figure 16. From a physical point of view this clustering of sub-models clearly represents the basic understanding of the combustion process.

Each of the sub-models has one characteristic model parameter which is kept constant for the entire combustion cycle. The relevant dependencies are summarized in Table 3. The physical impact of the parameters and a procedure to identify them automatically is discussed in the following chapter.

Table 3: Sub Models and Parameters for Model Calibration

Mechanism	Relevance	Equations	Parameter
Charge Entrainment	Oxygen Supply	(4-1) to (4-8)	$C_{Entrain}$
Fuel Evaporation	Fuel Supply	(4-9) to (4-13)	C_{Evap}
Heat Release	Chemical Reaction	(4-16)	K_b

6.3.2 Model Based Pressure Trace Analysis with the Multi-Zone Approach

Pressure Trace Analysis with the MZCM

As described above, there is no straight-forward approach for the pressure trace analysis with the multi-zone model. The reason for this is, that even if the heat release is known, e.g. from a single- or two-zone analysis, there is no information on the distribution of this global heat release to the individual spray zones. Thus, for the present work a new method for the pressure trace analysis with the multi-zone model has been developed.

In this PTA approach, the mixture formation processes entrainment and evaporation as well as ignition delay are calculated just as in the WPC mode. Therefore the PTA uses exactly the same routines as the WPC which ensures a consistent treatment of the spray model and the thermodynamic solution. The particularity of the PTA is that during calculation the reaction parameter K_b is varied iteratively at each time step to match the measured pressure trace. All other parameters of the spray model are kept constant. This calibration of the parameter K_b leads to a weighted distribution of the overall heat release to the individual zones according to the reaction mechanism (eq. (4-16)), which considers the availability of fuel and oxygen and the zone state. Therefore, it must be assured that sufficient reactants are available within the zones, otherwise the heat release is limited by one of the mixture formation processes. In the latter case, the lack of either of the reactants (fuel or oxygen) cannot be compensated for by an increase of the reaction rate. Thus, the parameter K_b approaches infinity.

Since the zone generation and their history always rely on the same spray principle, the PTA requires the same inputs as the WPC: nozzle specification, injection rate, and predefined model parameters. As underlying mixture formation models partly originate form phenomenological modeling assumptions,

the multi-zone PTA always remains an approximation of the real conditions. However, the information derived by the PTA can be used to identify the model parameters for the WPC.

A similar approach for a multi-zone PTA was presented by Haas in [72]. He also calculates the spray and mixture formation processes on the basis of phenomenological models. The difference to the present work is that in [72] the heat release is drawn directly from a single-zone analysis and then distributed to the individual zones, weighted by the fuel mass. Aside from the problematic comparability between single-zone and multi-zone heat release due to thermodynamic inconsistencies (compare Chapter 4.4.2), the weighting only according to the fuel mass cannot assure that there is plenty of oxygen available in all zones. This issue is mentioned in [72] by the fact that in the case of locally rich combustion the released energy is too high, compared to a reaction kinetic approach, which leads to an overestimation of temperatures.

Identification of Mechanisms by PTA

The present example screens the combustion process and evaluates the phases in which alternately the charge entrainment and the fuel evaporation mechanisms come to the fore. This is done by successively suppressing individual mechanisms (setting the associated parameters $C_{Entrain}$ or C_{Evap} to low values). The development of the parameter K_b versus time finally provides the desired information on the relevant mechanisms.

First, the charge entrainment is suppressed ($C_{Entrain}$ = 'low') and C_{Evap} is given a 'high' value. These parameters are deliberately specified in relative terms ('low' and 'high') because their absolute values depend on the boundary conditions. From the temporal development of the identified parameter K_b we obtain the information whether it is possible to meet the objective function (measured pressure trace) with the given parameter values.

This is demonstrated in Figure 30, which shows the measured and calculated cylinder pressure curves, the objective function (difference between measured and calculated cylinder pressure) and the evolution of the identified combustion parameter K_b. The bars on top indicate the phases of fuel injection and combustion. It is obvious that within a certain phase no agreement is achieved between measured and calculated cylinder pressures. This cannot even be compensated for by the combustion parameter K_b which tends to unrealistic high values (approaches infinity) in this phase. Consequently, this is exactly the phase at which the dominance of the charge entrainment mechanism comes to the fore.

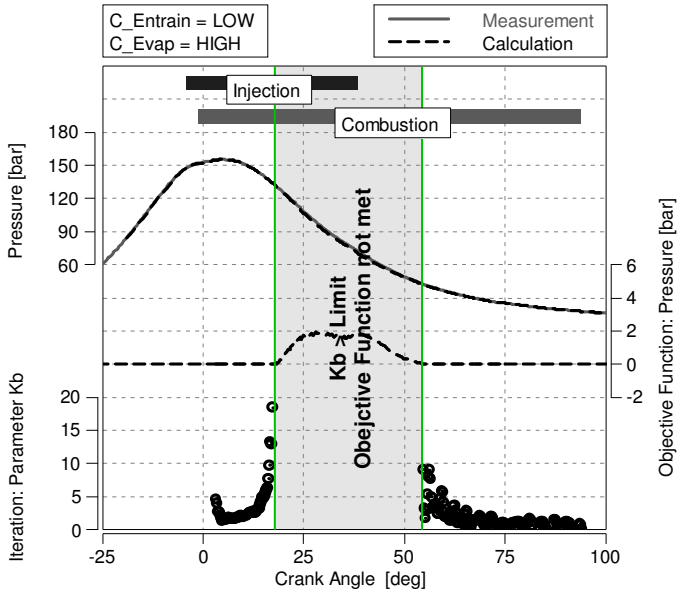

Figure 30: Pressure trace analysis with multi-zone model: suppressed entrainment parameter

Analogously, Figure 31 shows the process for vice versa parameter settings ($C_{Entrain}$ = 'high' and C_{Evap} = 'low'). This example demonstrates in which way the fuel evaporation influences the heat release characteristics. Here, the mismatch clearly occurs in an earlier phase of the combustion.

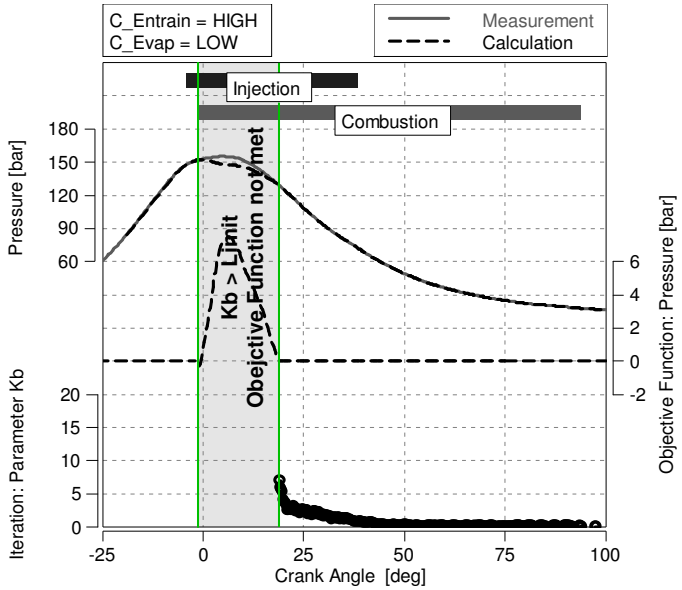

Figure 31: Pressure trace analysis with multi-zone model: suppressed evaporation parameter

Finally, both parameters are set to 'high' values, see Figure 32. In this case, the match of measured and calculated cylinder pressures is successful and the combustion parameter K_b is identified to reasonable values.

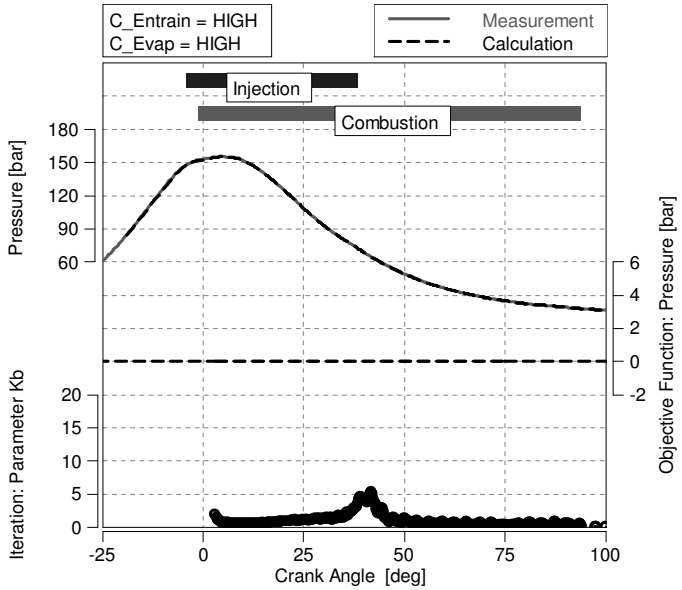

Figure 32: Pressure trace analysis with multi-zone model and preset parameters for charge entrainment and fuel evaporation

The result of these three examples is again explainable from a physical point of view. In the initial phase and during injection, a high amount of charge is entrained into the spray due to the high spray momentum and the fast decrease of velocity of the spray front. For this reason, it is likely that sufficient oxygen (or even a surplus) is supplied to the reaction zones, even if the entrainment is damped by a low value for $C_{Entrain}$. In a later phase, entrainment affects combustion much more sensitively because of the fast decrease of spray momentum after the end of injection and due to the lower oxygen content in the charge (re-entrainment mechanism).

On the other hand the liquid fuel first needs to heat up and evaporate at the beginning of the process, thus the evaporation rate (influenced by C_{Evap}) controls the process. At a certain point, the entire fuel has evaporated, which is enhanced by the temperature increase during combustion. Then the evaporation is no longer a limitation to the process.

6.3.3 Algorithm for Parameter Identification Based on Physical Principles

The knowledge drawn from the theoretical study above is applied to develop a generally applicable algorithm for an automatic identification of the two combustion parameters ($C_{Entrain}$ and C_{Evap}) for one operating point. The algorithm varies the combustion parameters for entrainment and evaporation from cycle to cycle and conducts a PTA. The idea behind the algorithm is to successively suppress the supply of individual reactants and therefore deliberately generate deficits of fuel or oxygen. These areas can be recognized in the algorithm by the characteristics of the parameter K_b which is used to identify valid parameter combinations. The course of the combustion parameter settings during one optimization is shown in Figure 33.

Since the evaporation predominantly affects the initial phase of combustion, it is necessary to calibrate the evaporation parameter first. Therefore the initial value for the entrainment is set to the maximum value of 1 to ensure that it is fast enough. At the same time evaporation starts at a very low value which causes a behavior as shown in Figure 31. In the first optimization step 1, evaporation is stepwise increased. As soon as the evaporation parameter is high enough, the pressure trace can be met during the entire combustion phase with reasonable values for the reaction parameter K_b. At this point, step 1 is finished and the parameter C_{Evap} is set 'valid' and kept constant. Since there certainly is an interrelation between the entrainment and the evaporation mechanism, the use of a very high entrainment parameter for the first step leads to the estimation of an evaporation parameter which is by trend too low. This is a systematic error which is explainable by the nature of this algorithm.

In the next step 2, entrainment is identified in a similar way. The parameter is set to a low value (step 2) and then gradually increased in step 3. The entrainment parameter $C_{Entrain}$ is set to 'valid' as soon as the abort criterion is again met. As the entrainment is identified at a relatively low evaporation (systematic error from step 1), it can be assumed that the entrainment rate is by trend too high.

Due to these systematic errors, the whole procedure is repeated in several loops, each one with a better guess for the initial parameter values. After several loops the parameters approach their final values. The evaporation parameter steadily increases and the entrainment decreases which compensates the systematic errors.

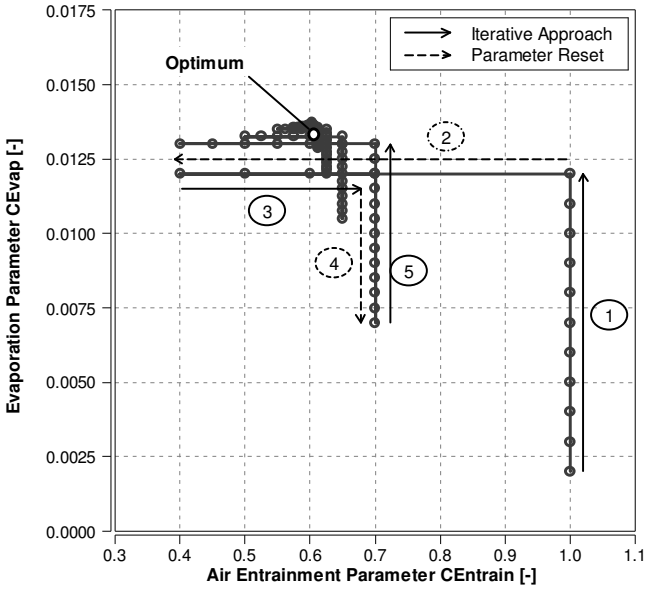

Figure 33: Variation of Parameters during Optimization using automatic Algorithm

As a validation that the parameter combination found by the automatic algorithm in fact represents an optimum, the whole observation area is screened in a full factorial grid in WPC calculation mode. As a criterion for the agreement of measurement and calculation the heat release curves are compared. Therefore, the square deviation of the two curves is integrated and normalized (NSD) which represents the target function of the optimization.

$$NSD_{ROHR} = \left[\int_{SOI}^{EOC} \left(dq_{meas} - dq_{\mathrm{calc}} \right)^2 \cdot d\varphi \right]_{norm} \tag{6-1}$$

This value is plotted in Figure 34, which also includes the optimum point of the optimization algorithm. This example shows that the solution of the automatic algorithm is indeed positioned in the optimum (minimum) area of the target function.

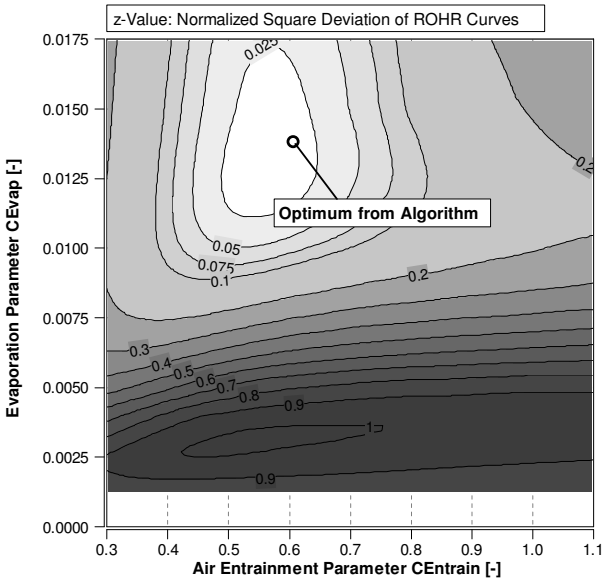

Figure 34: Full Factorial screening of combustion parameters for Evaluation of the automatic Algorithm result

6.3.4 Identified Combustion Parameters for each Operating Point of Engine 1 and 2

For the engines 1 and 2 the measured data refer to the operating points of the European Stationary test Cycle (ESC), excluding low idle. Thus, the points cover 3 speeds and 4 loads for each engine. As stated above, the engine settings such as injection timing, injection pressure, EGR rate and boost pressure vary at the individual points within the ranges given in Table 1.

The combustion model was identified and checked with the described algorithm for every individual engine operating point. Finally, one common set of constant parameters for $C_{Entrain}$, C_{Evap} and K_b was determined for engines 1 and 2. At this point it has to be emphasized that the introduced 0-dimensional modeling approach does not consider for any effects from the combustion chamber geometry and the cylinder charge motion (e.g. swirl and squish). It is expected that these boundary conditions specifically influence the air entrainment. Therefore, it is likely that the identified air entrainment parameters differ for different engines and also for different engine operation conditions.

This effect can significantly be observed in the characteristics of the identified charge entrainment parameter $C_{Entrain}$ which is shown as a function of speed and load for both engine 1 and 2 in Figure 35. There is a clear increase of $C_{Entrain}$ versus increasing speed that can be attributed to the increasing turbulence level due to charge motion (swirl, squish, …).

Furthermore, there is also a dependency of $C_{Entrain}$ versus engine load, primarily at engine 2. However, the trends are less clear, which deduces that there are obviously some opposing mechanisms which overlap. It is likely that these mechanisms refer to modeling simplifications of the spray (such as e.g. the phenomenological modeling assumptions, geometrical effects, uncertainties in the injection rate, …).

Very unusual is the load characteristic of engine 2 at speed A. If the entrainment parameter falls below 0.5, the measurement must be questioned. Figure 36 below demonstrates that the operating point at speed A, 75% load, is always outside of the general trends.

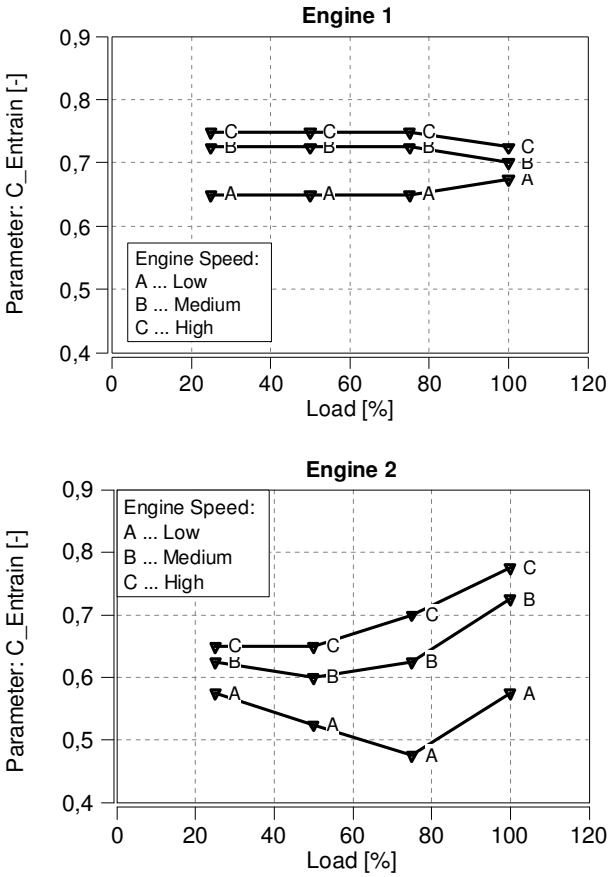

Figure 35: Identified entrainment parameter $C_{Entrain}$ in ESC operating points (top) Engine 1 (bottom) Engine 2

The identified parameters of the evaporation model hardly vary at the individual operating points, thus one common parameter could be used even for both engines. The identified value is C_{Evap}=*7.5e-3*. For the chemical reaction, as mentioned in the previous section it is reasonable to keep the value for K_b close to 1, since engine specific parameters that influence the fuel-air mixing process should not affect the combustion reaction itself. This constant value can be applied for all engines and operating points in the present work.

This example demonstrates that the individually identified results at all operating points depict very interesting information on interrelations which can be explained from physical aspects. In order to produce optimum boundary conditions for the calculation of emissions, the individually identified values for $C_{Entrain}$, as given in Figure 35, were used for the following evaluations of the emission models.

6.3.5 Assessment of Working Process Calculations with Identified Model Parameters

The assessment compares calculated and measured results. These are in particular the Indicated Mean Effective Pressure of the high pressure cycle (IMEP_HP), the peak cylinder pressure (p_{max}) and the rate of heat release. The experimental heat release (as the objective function to be compared to the multi-zone heat release) was calculated from a 2-zone PTA (see above). In order to avoid a comparison of heat release curves - a comparison of curves for 24 operating points is definitely confusing - three characteristic values were extracted thereof. These are the crank angle positions with 10%, 50% and 80% of the fuel Mass Fraction Burned (MFB10, MFB50, MFB80).

Figure 36 shows the results with the individually identified parameters of Figure 35. Additionally, the calculations were repeated with one constant parameter $C_{Entrain}$ for each engine, in order to provide information on the sensitivity of the model on the parameter, which is shown in the thinner lines ($C_{Entrain}$=*0.7* for Engine 1, $C_{Entrain}$=*0.65* for Engine 2). In both cases, good agreement is still achieved.

Engine 2 shows two larger deviations at speed A, 75% and 100% load. These points have already been addressed in the previous chapter because they also showed peculiarities during the identification of the charge entrainment parameter. Now, Figure 36 gives some more details. The deviations at these points exclusively refer to the end of the combustion process (MFB80). The measured heat release curves seem to be extremely distorted in this phase. Consequently, it is likely that the measurement at this point is incorrect.

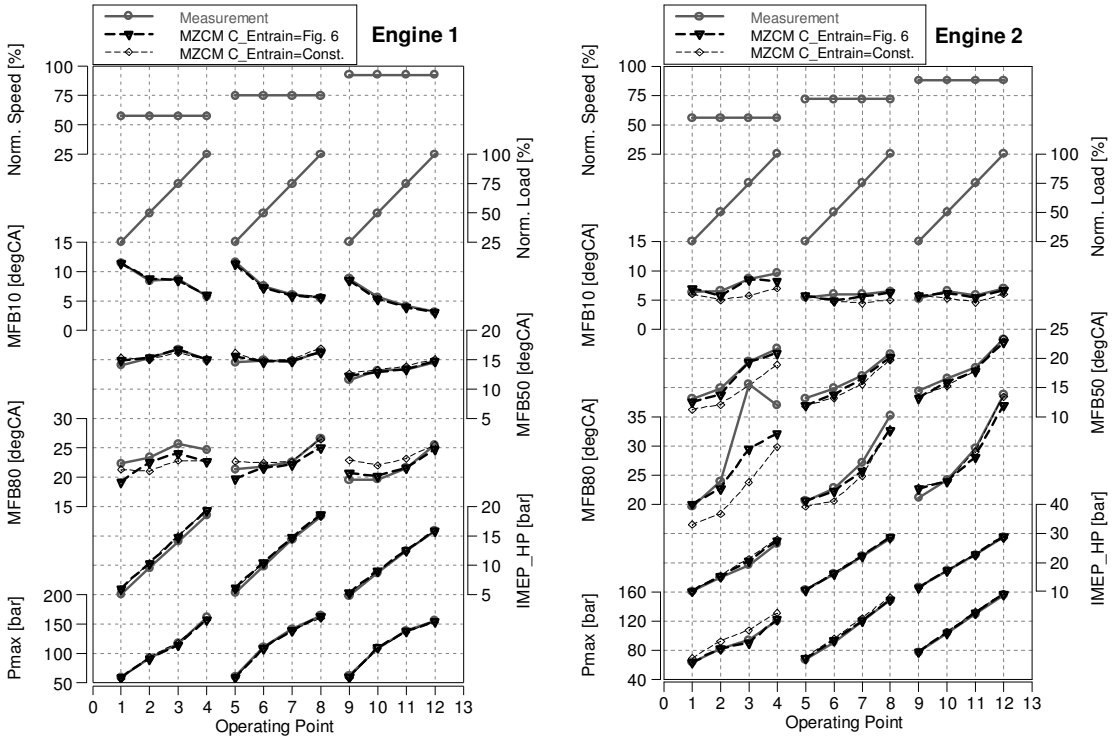

Figure 36: Results of working process calculations with identified combustion parameters Comparison with measured data: (left) Engine 1 (right) Engine 2

6.4 Step 2: Identification of the Parameters for NO and Soot Emissions

A systematic method is introduced for the identification of the emission model parameters for NO eq. (4-25) and Soot eq. (4-26) - (4-30). As stated above, the prerequisite for this procedure is the identified combustion process, which defines the thermodynamic conditions during the combustion processes. For each of these emission models two parameters are kept variable for the identification procedure. These are $C_{NO,kin}$ and $C_{NO,fac}$ for NO_x and $C_{s,f}$ and $C_{s,o}$ for soot. An automatic algorithm estimates if any target values (pair of measurements) provide unambiguous mathematical solutions. As mentioned before, the present work deliberately uses measured data which include a certain degree of inaccuracy due to the measurement principles. For this reason, statistical evaluation of the identified results allows to account for inaccuracies of the measurements. Therefore, the method is applicable to depict obvious measurement outliers, which should be sorted out as they distort the mathematical result. Finally, the method allows emphasizing certain engine operating conditions (e.g. full load) by attributing individual groups of measured values a higher weight.

The procedure is applied to the 2-zone and the multi-zone modeling approach, thus their comparison demonstrates the effects of the MZCM modeling sophistication. Furthermore, it is discussed whether the results from the individual approaches (2-zone and multi-zone) are interchangeable among each other.

6.4.1 Procedure for the Identification of NO and Soot

The procedure follows the basic principle: As both emission models keep two parameters variable for the identification procedure, at least two measurements are required to identify them. Furthermore, each model contains one parameter which controls its nonlinear characteristic and a second parameter which has a pure scaling character.

Based on this principle the following procedure is derived:

The amount of NO, which is formed during the entire combustion process, is calculated by equation (4-25). In this equation the variable 'α' is a function of the NO concentration (see equation (4-24)), which is the driving concentration gradient for the chemical reaction. Equation (4-25) is schematically repeated in eq. (6-2).

$$\frac{d[NO]}{dt} = f\left(C_{NO,kin}, [NO], State\right) \tag{6-2}$$

Since the concentration of NO appears on the right side of this equation, it represents an ordinary differential equation which cannot be solved by separating the variable [NO]. Consequently, the parameter $C_{NO,kin}$ cannot be taken out of the function f. Within the thermodynamic calculation platform it is solved numerically by a 4th order Runge-Kutta algorithm.

In equation (6-3) the function F schematically represents the solution of the differential equation (6-2) within the integration limits from start to end of combustion. The parameter $C_{NO,fac}$ is used as a scaling factor for the function F. Thus, the absolute NO emissions per engine cycle are represented by:

$$[NO]\big|_{\text{Point}} = C_{NO,fac} \cdot F\left(C_{NO,kin}, [NO], State\right)\Big|_{start\ of\ combustion}^{end\ of\ combustion} \tag{6-3}$$

In the next step the function (6-3) is applied to two measured engine operating points (A, B). The result is represented by the ratio of NO emissions between points A and B. By means of this procedure, the scaling factor $C_{NO,fac}$ cancels and one gets a characteristic function of the single parameter $C_{NO,kin}$.

$$\frac{[NO]\big|_{\text{Point A}}}{[NO]\big|_{\text{Point B}}} = \frac{F\left(C_{NO,kin}, [NO], State\right)\big|_{\text{Point A}}}{F\left(C_{NO,kin}, [NO], State\right)\big|_{\text{Point B}}} \tag{6-4}$$

From the measurements, the NO ratio between points A and B is known and constant. Consequently, equation (6-4) represents one equation for the variable $C_{NO,kin}$ which thus can be determined. Finally, the scaling factor is calculated from the absolute NO emissions in either point A or B on the basis of the previously identified parameter $C_{NO,kin}$.

An analogous procedure is applied for soot, see eq. (6-5). Herein the function 'p' represents the soot formation rate defined by either eq. (4-26) or eq. (4-29) and the function 'q' represents the soot oxidation rate, as calculated by eq. (4-27) or eq. (4-30). Due to the presence of m_{soot} on the right side of the equation for soot oxidation, it also represents an ordinary differential equation which cannot be solved by separation of the variable m_{soot}. However, this is not the case in the equation for soot formation. Consequently, the model parameter $C_{s,f}$ plays the role of the scaling factor and the parameter $C_{s,o}$ depicts the nonlinear characteristic.

$$\frac{dm_{soot}}{dt} = p\left(C_{s,f}, State\right) - q\left(C_{s,o}, m_{soot}, State\right) \tag{6-5}$$

The rest of the procedure is analogous to the calculation of NO. In eq. (6-6) the function '*S*' schematically represents the solution of equation (6-5).

$$m_{soot}\big|_{Po\,\mathrm{int}} = C_{s,f} \cdot S\left(C_{s,o}, m_{soot}, State, t\right)\Big|_{start\ of\ combustion}^{end\ of\ combustion} \tag{6-6}$$

Again, the ratio between Soot at points A and B is formed, thus the scaling factor cancels and one gets one characteristic function for the single parameter $C_{s,o}$.

$$\frac{m_{soot}\big|_{Po\,\mathrm{int}\,A}}{m_{soot}\big|_{Po\,\mathrm{int}\,B}} = \frac{\left[S\left(C_{s,o}, m_{soot}, State, t\right)\right]\big|_{Po\,\mathrm{int}\,A}}{\left[S\left(C_{s,o}, m_{soot}, State, t\right)\right]\big|_{Po\,\mathrm{int}\,B}} \tag{6-7}$$

Finally, the scaling factor $C_{s,f}$ is calculated from the absolute m_{soot} emissions in either point A or B on the basis of the previously identified parameter $C_{s,o}$.

6.4.2 Discussion of Solutions for Parameters of Emission models

Based on the principles outlined above, the exact mathematical solutions for the NO and soot model parameters at two arbitrary engine load points (A and B) can be graphically represented. This is schematically shown in Figure 37 which plots the calculated ratios [Soot Point A / Soot Point B] for three different pairs of engine load points as functions of the nonlinear model parameter $C_{s,o}$. Furthermore, the ratios of the measured soot values [Soot Point A / Soot Point B] are also introduced to these diagrams as constant lines.

In the upper diagram, the ratio of the measured soot values clearly crosses the function of the calculated soot ratio. Consequently, the intersection represents the exact solution of the model parameter $C_{s,o}$ for the given pair of engine load points. The scaling parameter $C_{s,f}$ for soot formation can be directly derived from an identification of (absolute) soot for the identified parameter $C_{s,o}$.

In contrast to that, the center diagram does not show any intersection. Thus, no mathematical solution exists. The model definitely cannot match both objective values at these specific operating points. However, this example provides us with the important information that the identification procedure can only provide a best approximation for the aggregate of operating points.

The lower diagram depicts the unpleasant situation of multiple solutions. From these the most obvious result must be chosen due to the statistics of solutions from other pairs of measured engine operating points.

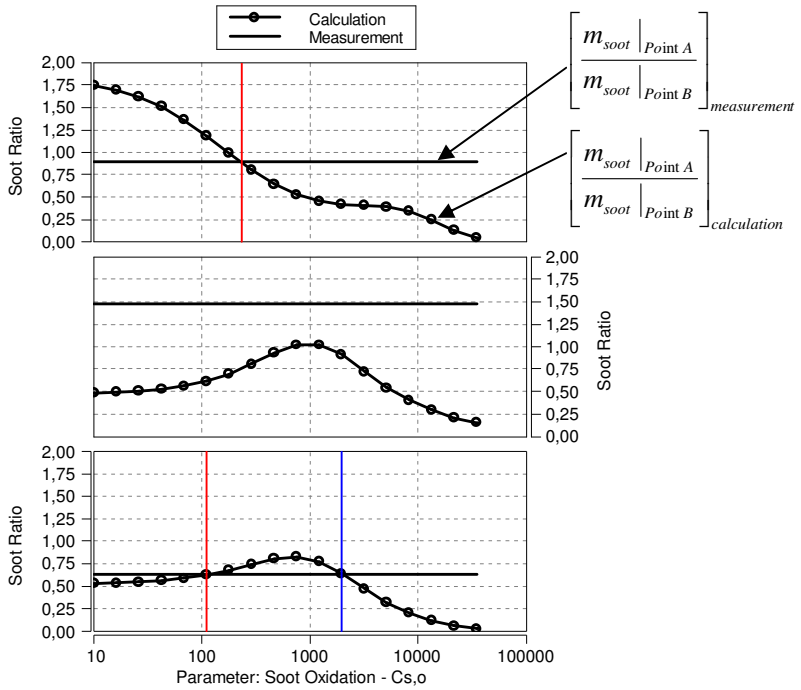

Figure 37: Possible cases of mathematical solutions for parameters of Soot model to fit objective values to three different pairs of chosen engine operating points

6.4.3 Statistical Evaluation of Identified Parameters from NO and Soot Models

The procedure, which was exemplarily demonstrated for two engine operating points, was extended to a higher number of experimental data. Thus, all possible combinations of pairs were formed and the procedure was applied to each of these pairs. According to the Gaussian summation formula, a number of n measurements results in $(n-1)\cdot n/2$ possible pairs.

The individual combinations may result in either one exact solution, no solution, or multiple solutions (according to Figure 37). The solution set of the statistical analysis allows all exact solutions and all feasible results from multiple solutions. In general, the latter can be easily selected because in most cases only one or two solutions have a reasonable order of magnitude, and the others are orders of magnitude away.

This statistical evaluation provides two important results:

- The percentage of exact solutions based on the total number of all possible pair combinations
- The frequency distribution of solutions

Considering the experimental data under discussion, e.g. 12 engine operating points (ESC) result in 66 possible pair combinations. The solution set for the soot oxidation parameter is illustrated in Figure 38 (bottom) for the data of Engine 2. Each result is on the one hand allocated to one operating point at the abscissa and on the other hand to the second operating point by marking its number. Consequently, in Figure 12 each solution appears twice. Out of the 66 possible pair combinations, 52 pairs provided solutions, which is a percentage of 79%. The statistical information of this result is 12 (79%), indicating that 12 measurements were used and 79% of the pair combinations provided solutions in the sense of Figure 37. Figure 38 (bottom) gives an impression of the frequency distribution. It can be seen that the values for the identified soot oxidation parameter spread over three orders of magnitude, thus the results have to be analyzed in greater detail.

As already mentioned in the previous sections, the soot measurements show high relative inaccuracies at low absolute values. The error introduced by these measurement inaccuracies distorts the distribution of the identified parameters when all pairs of operating points are given the same weighting factor. Therefore, it is advantageous to perform a weighting within the data set. With respect to the 12 ESC points under discussion, it is obvious to give the high load points, which result in high absolute soot emissions and better measurement accuracy, a higher weight.

This is done for the top graph of Figure 38. Here, the points with 25% load are suppressed (points 1, 5, 9). Furthermore, point 3 (75% load at engine speed A) was suppressed because it already indicated a measurement error, as discussed in the considerations to Figure 36. Now, the statistical information of the remaining 8 measurements becomes 8 (82%), and the frequency distribution has considerably advanced. If only considering the 3 full load points (4, 8, 12), the statistical information becomes 3 (100%), which is also shown in Figure 38 (top).

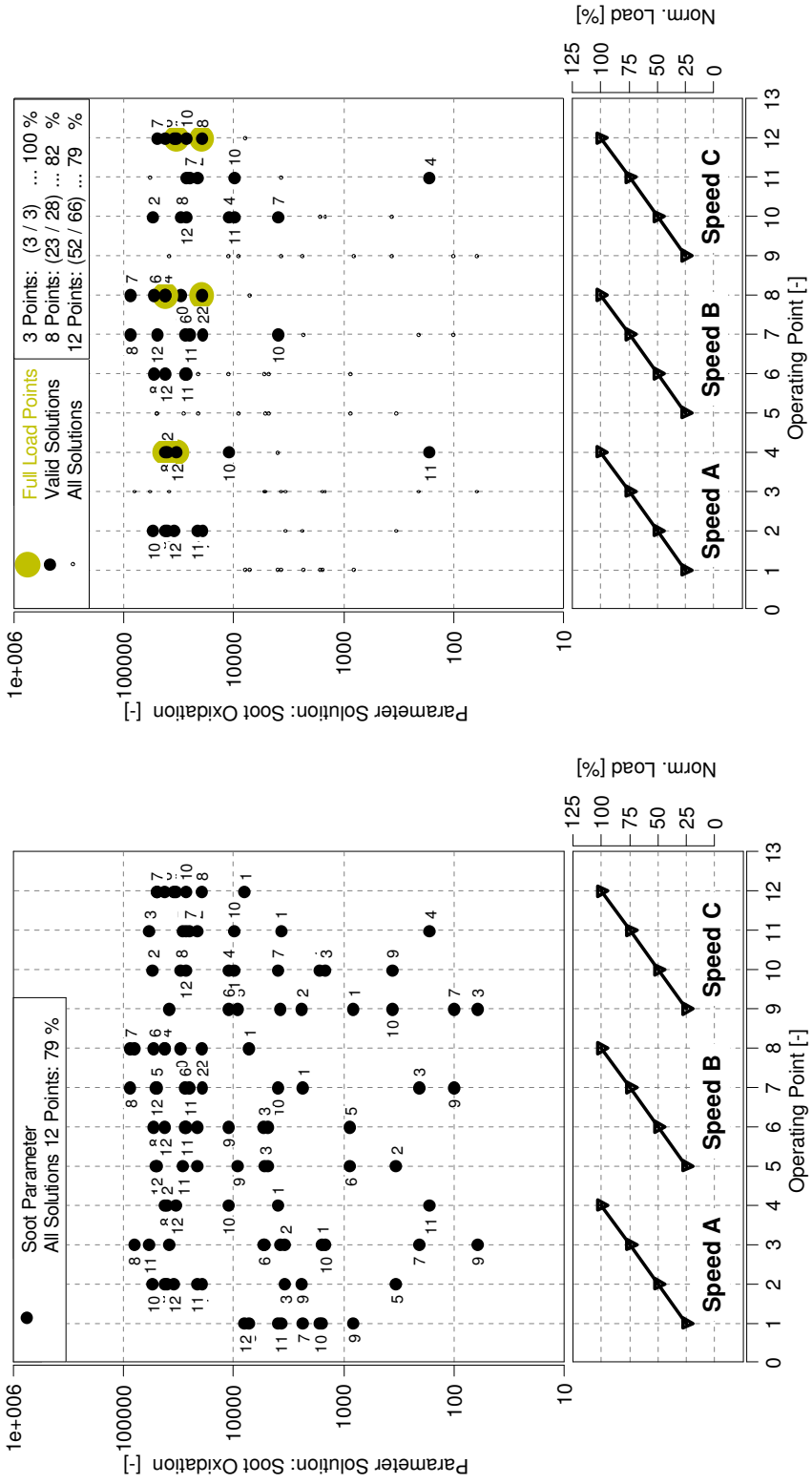

Figure 38: Identified Soot Oxidation Parameter Allocated to Measured Operating Points Engine 2 (bottom) All Solutions, (top) Measurements with Low Absolute Soot Values and Incorrect Measurements Being Suppressed

6.4.4 Frequency Distributions of the Nonlinear NO Parameter

The frequency distributions of $C_{NO,kin}$ are calculated for the measurements of Engines 1 and 2. For Engine 3 only five measurement points were available, thus its statistical analysis is not as significant as for the other engines. Therefore, the detailed discussion of the results is left out. However, the quality of simulated results is also given for Engine 3 in Chapter 7 (Figure 44). In order to demonstrate the influence of the different modeling approaches, the procedure was carried out with the 2-zone model (in PTA mode) and the multi-zone model (in WPC mode).

Figure 39 shows the frequency distributions for the two modeling approaches. These diagrams are derived from rotated views of Figure 38, as now the model parameter appears on the abscissa and the ordinate shows the frequency of solutions for the identified model parameters. Figure 39 shows all individual pair solutions twice (in the same way as Figure 38). However, this representation was kept, for Figure 39, as this assumption only affects the scaling of the ordinate axis. The shapes of the functions would remain the same if the solutions were taken only once. The statistical information is also given in the diagrams (number of experimental data and percentage of pair solutions). The individual curves show the results for Engine 1 and 2 (bold lines) and the sum of frequencies for both engines (thin line).

With the 2-zone model, the data of Engine 1 show a clear frequency peak at $C_{NO,kin}=0.8$; however, the data of Engine 2 do not show any characteristic optimum. In contrast to that, the results of the multi-zone model are more consistent for both engines, as both frequency distributions show optima at approximately $C_{NO,kin}=8$. For both modeling approaches, the variety of solutions spreads over three orders of magnitude.

The results of the multi-zone approach may first appear as an improvement towards modeling generalization. However, these results are not clear enough to argue this improvement as a general conclusion. In fact, it shows that the 2-zone approach is already reasonably good for the simulation of NO_x emissions. One important result is that the results from the 2-zone model can certainly not be transferred to the multi-zone approach.

When going into greater detail, the presented results point out obvious differences coming from the physical background of the modeling approaches. The 2-zone model calculates the NO formation in only one combustion zone with one fixed (local) air excess ratio, which is in the region of lambda ~ 1. Consequently, the entire burned domain is present at a high temperature and conditions which clearly enhance NO formation. In contrast to that, the multi-zone model estimates a distribution of the temperature and lambda field. Thus, at each crank angle only a part of the spray is present around stoichiometric conditions and at the related high temperatures and NO formation rates (compare Figure 26 and Figure 28). Due to these fundamental differences in the thermodynamic treatment of the burned domain it is quite clear that the model parameters of the two modeling approaches cannot be compared.

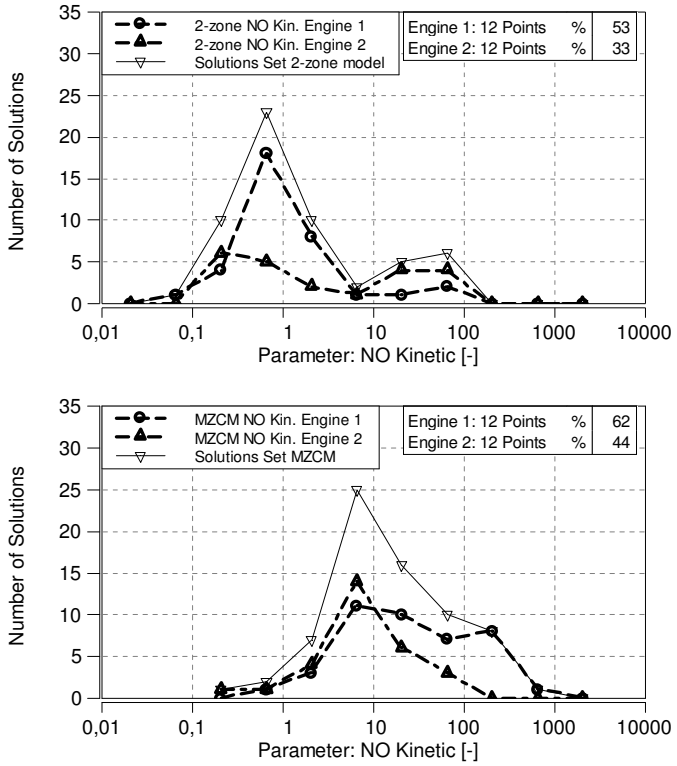

Figure 39: Frequency distribution NO kinetic parameter (top) 2-zone model (bottom) MZCM

6.4.5 Frequency Distributions of the Nonlinear Soot Parameter

Analogous to Figure 39, Figure 40 shows the frequency distributions of the model parameter for soot $C_{s,o}$. Again, the results for data with Engines 1 and 2 are given together with the relevant statistical information.

As expected, the differences between the two models are more distinctive for soot than for NO. This confirms that the approximation of a temperature and lambda distribution in the spray affects the mechanisms for soot formation more sensitively than those for NO formation.

The 2-zone model shows two frequency peaks for Engine 1 and no clear optimum for Engine 2 (Figure 40, top). Thus, it can be concluded that the parameters cannot be identified with sufficient quality on the basis of the 2-zone approach. In comparison to that, the multi-zone model has clear advantages (Figure 40, bottom). The frequency distributions show distinct peaks for both engines and, furthermore, the variety of solutions spreads within a smaller range. However, the two peaks are clearly allocated to different values of $C_{s,o}$ for the two engines.

The fact that two different soot oxidation parameters were identified for the two engines is not surprising, as the engines had e.g. different swirl levels, combustion chamber geometries and injection nozzles. All these parameters influence the soot emission but they cannot be considered by the model. Therefore, all these effects of such hardware parameters on soot emissions obviously impinge on the identified parameters.

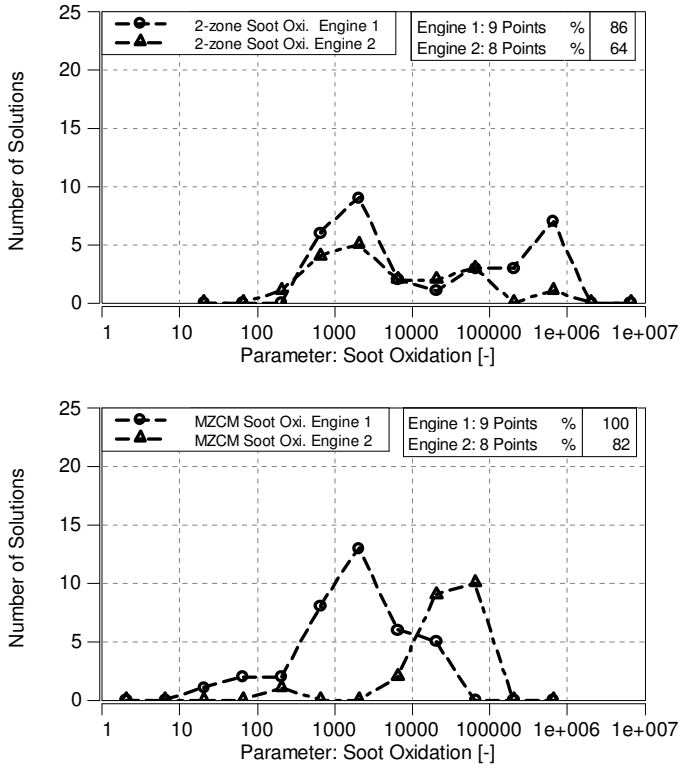

Figure 40: Frequency distribution of Soot oxidation parameters (top) 2-zone model (bottom) MZCM

6.4.6 Sensitivity of Identified Parameters on NO and Soot Emissions

Figure 41 and Figure 42 show the sensitivities of the calculated NO_x and soot emissions on the model parameters for both Engine 1 and 2. In each of these figures, the measured data points on the abscissa are plotted versus the corresponding calculated results on the ordinate. In these diagrams, the 45deg line represents the perfect fit of measurement and calculation. With respect to soot, these representations again show the high scattering of small soot values and the diminishing scattering towards higher values. The NO_x scattering is more uniformly versus its absolute values.

In general, the individual model parameters were varied within the neighborhood of the particular maxima of the frequency distributions presented above. For the soot emissions the full load points are emphasized. The figures clearly show how the values of the individual model parameters affect the arrangements of points around the line of perfect fit.

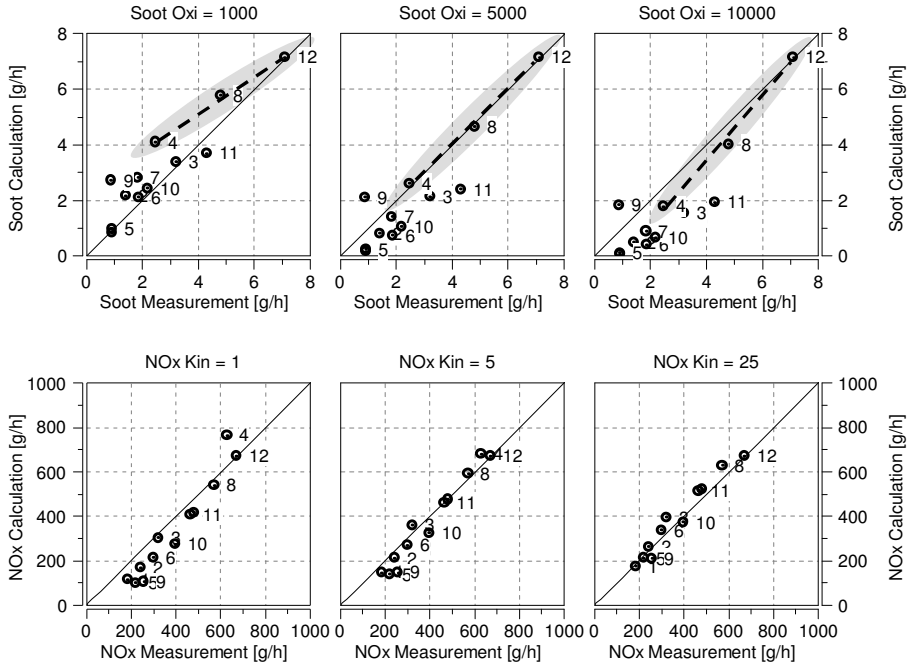

Figure 41: Result measurement vs. prediction emission parameter variation Engine 1 (top) Soot (bottom) NOx

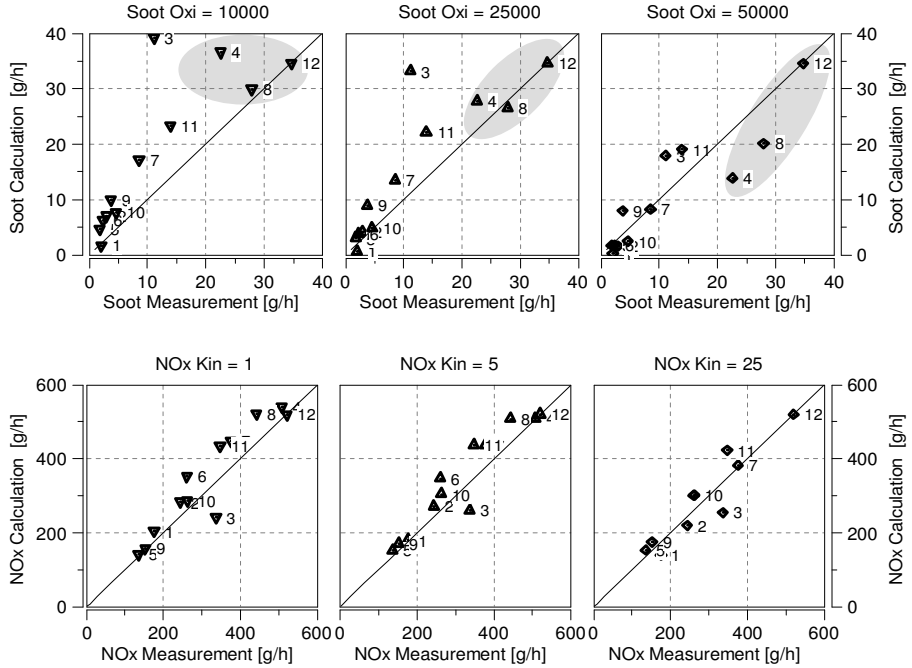

Figure 42: Result measurement vs. prediction emission parameter variation Engine 2 (top) Soot (bottom) NOx

7 Analysis of Engine Settings on the Combustion Process and Pollutant Formation

In the previous sections it has been demonstrated that the multi-zone approach is well suited to predict heat release and pollutant formation in a wide range of operating conditions. The following chapter analyzes the impact of different combustion strategies with the multi-zone model. Therefore, well directed measurements are conducted. The analysis concentrates on the following questions:

- Which are the main boundary conditions for the combustion and pollutant formation in diesel engines?
- How do these boundary conditions affect the process from a basic physical point of view? How are the changes represented in the multi-zone model?
- When and under which conditions are emissions predominantly formed?

7.1 Combustion Technologies for Reaching Present and Future Emission Targets

In the hands-on engine development process emissions are controlled by EGR and turbocharging, which both define the thermodynamic state and the composition of the cylinder charge at intake valve closing, and the injection characteristics with the main parameters: injection pressure and timing.

So far, the effects of these measures on the combustion process have been regarded from global results such as the heat release rate, cylinder pressure curve and the resulting emissions. However, the actual combustion processes and the mechanisms that are relevant for the emission formation take place in a high number of local reaction zones. The analysis in the present chapter concentrates on the impact of changing engine parameters on the distribution and development of thermodynamic conditions in these reaction zones. From the theoretical considerations in the previous chapters, 3 distinguished casual effects are identified which govern the combustion process and pollutant formation. These are:

1. Mixture formation of oxygen and fuel
2. Dilution of oxygen by inert gas species in the cylinder charge (e.g. by recycled exhaust gas)
3. Change of state during the combustion due to piston movement and heat release

Figure 43 demonstrated the impact of these causal effects on the thermodynamic characteristics of the spray zones, schematically represented by the arrangement in the field of temperature and lambda. Ad (1): The mixture formation process defines the concentration of reactants in the zones, which is expressed by the zone lambda value. The lambda value results from the interaction of the fuel evaporation and charge entrainment to the zone. A high entrainment rate leads to an increase of the zone lambda value, while fast evaporation has the opposite effect. Ad (2): As already discussed in Chapter 5.2 (Figure 21), charge dilution by EGR reduces the oxygen concentration which directly affects the theoretical combustion temperatures. This is represented by a shifting of the entire spray zone regime to the left. Ad (3): The third point summarizes the complex interaction of the combustion process with the compression / expansion stroke due to the piston movement. This was pointed out from the theoretical aspect in Chapter 5.2.2. The resulting thermodynamic change of state in the multi-zone model affects the entire process as it causes the boundary conditions for almost all running processes to change.

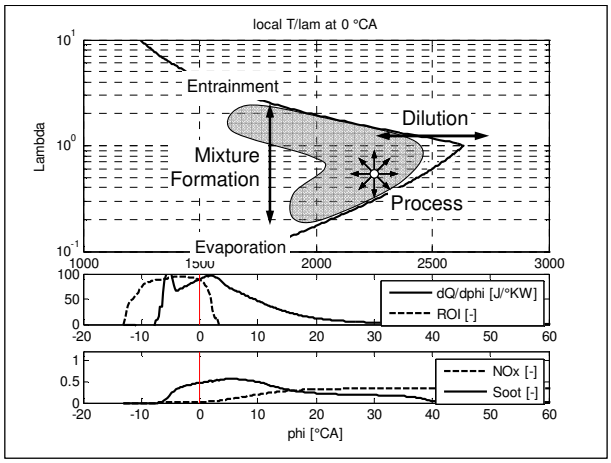

Figure 43: Schematic Representation of individual Causal Effects on Temperature and Lambda of the Reaction Zones

7.2 Measurement Database

7.2.1 Engine Map and Operating Conditions

The measurements used for the present investigation were taken on Engine 3 of Table 2. At first, the multi-zone model was calibrated to predict heat release and emissions in a reasonable range of operating conditions. The model parameters were identified on the basis of only a few measurements (5 points in the engine map). The method which is used for the parameter identification is discussed in detail in Chapter 6. The data for the parameter identification includes various engine operating points (engine speeds and loads) and covers reasonable ranges for the engine settings such as EGR rate, lambda, injection pressure, injection timing and boost pressure.

Figure 44 shows a comparison of measured and calculated results for the 5 operating points used for the parameter identification. The calculated results show a reasonably good agreement in the entire operating range.

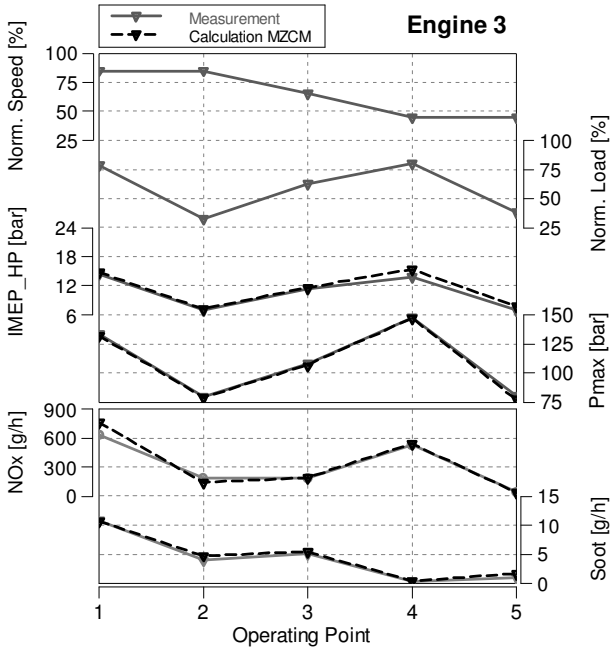

Figure 44: Results of Measurement vs. Calculation 5 Operating Points Engine 3

7.2.2 Special Measurements for isolated Physical Mechanisms

In the theoretical considerations to Figure 43, the mechanisms of the combustion process are clustered into 3 basic principles. Table 4 allocates these basic principles of the combustion mechanism to engine parameters. Any variation of one of these parameters (when all other parameters are kept at a constant level) predominately affects one or more of the mechanisms described above. In order to investigate them in greater detail, specific measurements were carried out which systematically varied the individual parameters as given in Table 4. At this point it has to be emphasized that usually the adjustment any single actuator (such as e.g. the EGR valve, VTG position etc.) of an engine on the test bed simultaneously changes several of the given engine parameters. Therefore, performing the parameter variations required careful manual adjusting of other actuators in order to keep the remaining parameters at constant values.

Table 4: Allocation of Combustion Mechanisms to Engine Parameters and Measured Variations

Engine Parameter	**EGR**	**Boost Pressure**	**Rail Pressure**	**Timing**
Principle of Combustion Mechanism	**Charge Dilution**			
		Mixture Formation		
			Process	
Variation 1	0 to 15%	const.	const.	const.
Variation 2	const.	const.	const.	-30 to 5 degCA
Variation 3	const.	const.	400 to 1600 bar	const.
Variation 4	const.	0.4 to 1.4 bar	const.	const.

The parameter variations were performed at two different engine operating points which were close to point 3 and 4 of Figure 44. With these variations the engine torque slightly changed because the injected fuel quantity was deliberately kept constant in order to create optimum comparable conditions for the combustion processes. In spite of this discrepancy, the load points are denoted as Point 3 and Point 4 in the investigations below.

The variations were made at the following boundary conditions:

- Variation 1: EGR
  at constant injection parameters and constant boost pressure
- Variation 2: Timing
  at constant IVC conditions (boost pressure, EGR) and constant injection pressure
- Variation 3: Rail Pressure
  at constant IVC conditions (boost pressure, EGR) and constant injection timing
- Variation 4: Boost Pressure
  at constant injection parameters and EGR rate

Figure 45 plots the parameter variations at Point 3 versus the relevant physical boundary conditions. Therefore, e.g. the engine settings for the EGR rate and global lambda are replaced by the relevant physical value oxygen concentration. For a qualitative representation of the trends the variations are shown in an isometric view (top). Additionally, the absolute values are represented in the bottom view which shows the variations projected in the coordinate planes.

There are three out of four variations shown which are analyzed in detail in the following chapters. For Point 3 the variations of rail pressure, timing and boost pressure were performed without EGR (EGR valve fully closed), so the charge oxygen concentration almost equals the value of fresh air (~0.232 % weight fraction).

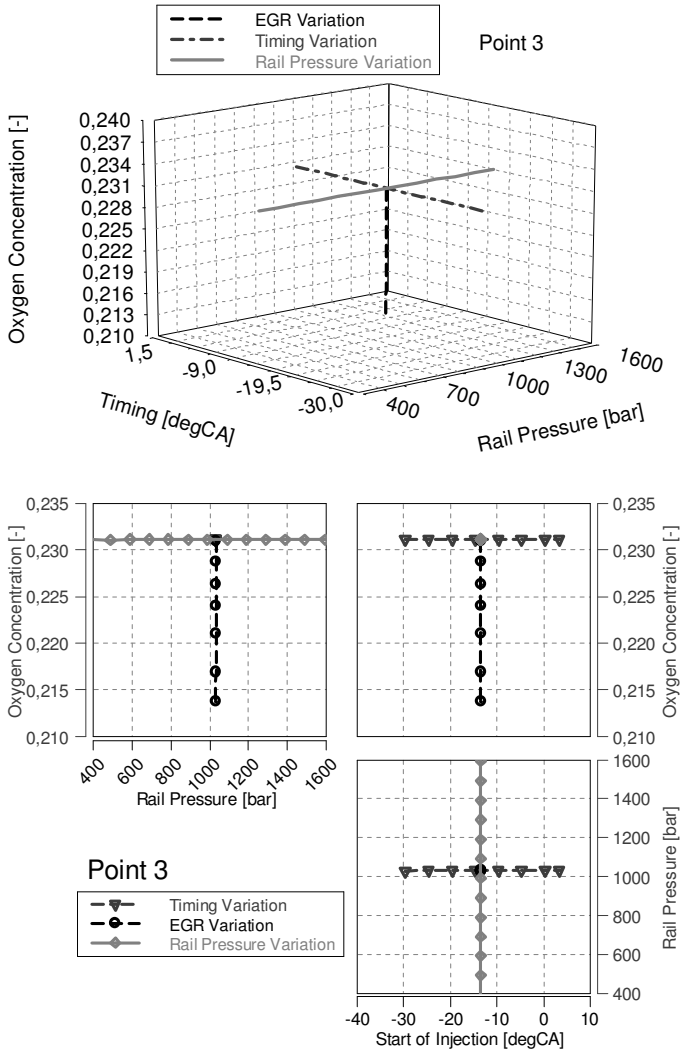

Figure 45: Variations of Engine Settings in Operating Point 3
(top) Isometric View (bottom) Projections in Coordinate Planes

The same variations are shown for Point 4 in Figure 46. In Point 4 the variations of rail pressure and timing were measured with EGR, while the boost pressure variation (not shown) was done without EGR. As observed in Figure 46, the oxygen concentration slightly drifts for the timing variation, as an absolutely constant EGR rate could not be achieved.

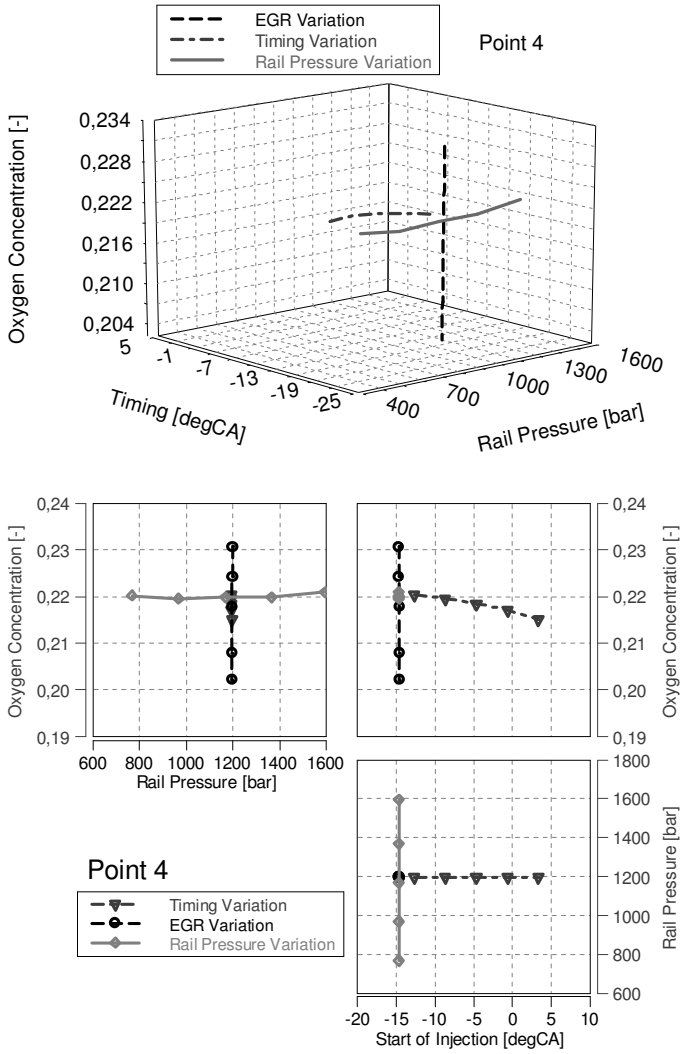

Figure 46: Variations of Engine Settings in Operating Point 4
(top) Isometric View (bottom) Projections in Coordinate Planes

7.3 Variation 1: Effect of Charge Dilution by Exhaust Gas Recirculation

7.3.1 Prediction of Heat Release by the Multi-Zone Model

Figure 47 illustrates that the model predictions show a good agreement with the measurements. For all points of the variation the identified combustion model parameters were constant. It can be observed that the effect of EGR on the heat release rate is not very significant (ROHR becomes slightly slower with increasing EGR-rate), but they are well reproduced by the model.

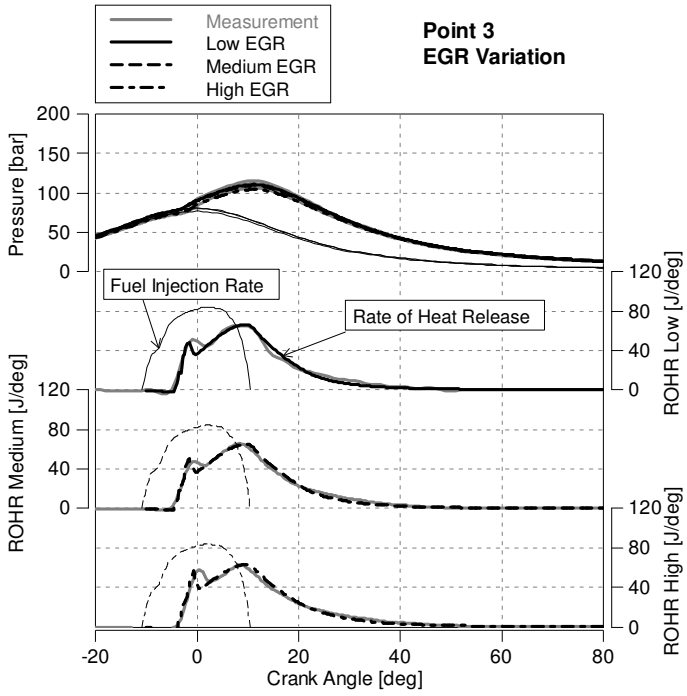

Figure 47: Change of Heat Release versus EGR rate

7.3.2 Prediction of Emissions by the Multi-Zone Model

Figure 48 shows the comparison of measured and calculated emissions. For these calculations again, one constant set of emission model parameters was used which had been identified from the 5 engine operating points of Figure 44. Basically, the agreement is reasonably good. There is one exception which concerns soot emissions at two variants of Point 4 (highest EGR rates). These two points depict the most extreme cases with the lowest global lambda values of below 1.2 (high fuel quantity and high EGR rate). At these points, the measured soot shows a sudden increase towards decreasing oxygen concentration which is far off the trend of the other measured points. These outliers are obviously not represented by the model. It is likely that this peculiarity originates from local rich areas due to insufficient charge exploitation. This is also a geometrical effect that cannot be accounted for by the 0-dimensional model.

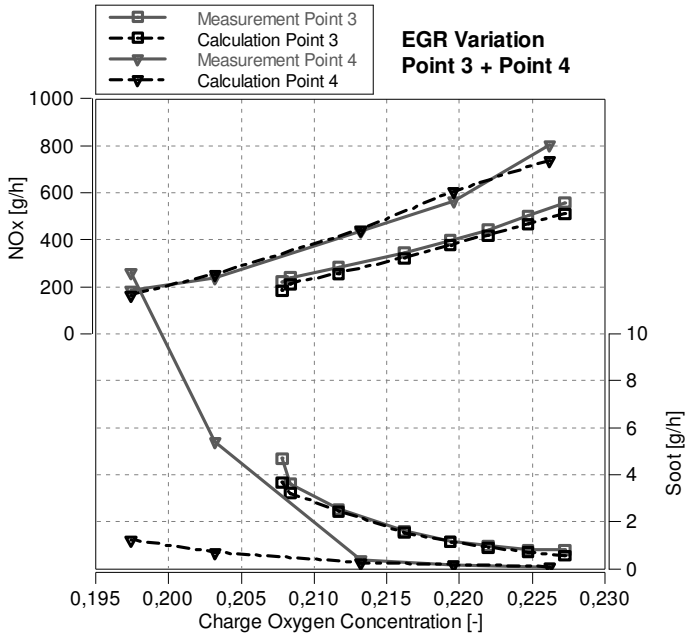

Figure 48: Calculated NOx and Soot Emissions and Comparison with Measurements

7.3.3 Effect of EGR on Charge Composition

It is well accepted [73] that an increasing dilution of oxygen by inert gas species causes a reduction of NO_x and an increase of soot. With respect to NO_x, the inert gases reduce the combustion temperature due to an increased thermal inertia and, furthermore, less oxygen is available for the formation of NO. The latter also hinders the oxidation of soot which is seen as one of the main reasons why soot emissions increase.

The actual oxygen content in the cylinder at IVC depends on the concentration of residual gas (due to internal and external EGR) and on the global Lambda (calculated from the total fuel and air massflow). Figure 49 shows the interrelation between global lambda, EGR rate and oxygen concentration, calculated according to eq. (3-11). The Figure also includes the measured values of the EGR variations in Point 3 and Point 4. As boost pressure was (by definition) kept constant, this example shows the pure effect of charge dilution.

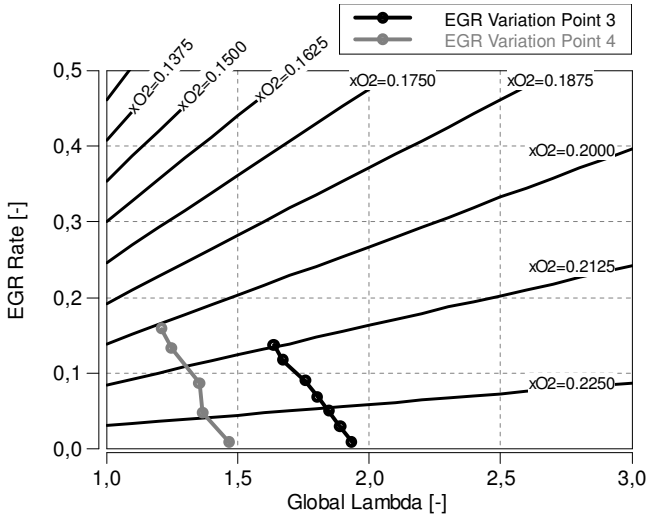

Figure 49: Intake Oxygen Concentration (wt) as a Function of Global Lambda and EGR Rate including Measured Values of an EGR Variation in 2 different Operating Points

7.3.4 Effect of EGR Variation on Mixture Formation

The effect of inert gases on mixture formation is depicted in Figure 50. The lower plot shows the increase of the overall spray mass (which also contains the mass of the burned zone). In the initial phase (during fuel injection), the major part of charge mass is entrained into the fuel spray. This entrainment process is of course independent from the EGR rate. The upper diagram shows the average lambda of all zones in the spray. It can be seen that EGR lowers the mean lambda primarily during the initial phase and towards the end of combustion. The only cause for this effect is the decreased oxygen concentration. The overall entrained mass is almost the same for all points, as shown by the characteristics of spray mass.

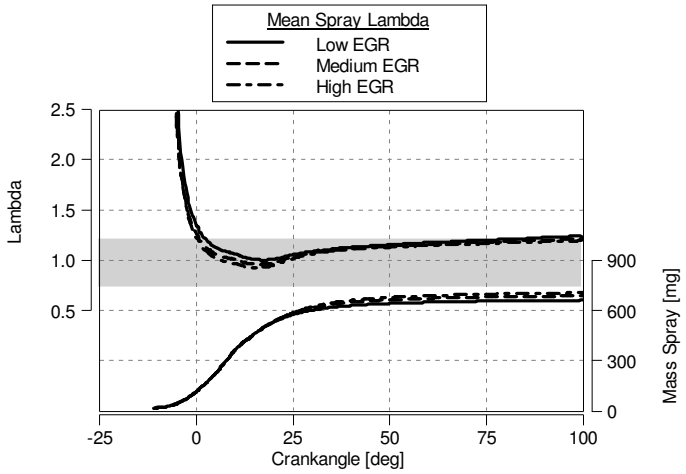

Figure 50: Progression of Mean Lambda of Spray and Spray Mass at Variation of EGR

7.3.5 Representation of Charge Dilution on NO_x Formation in the Multi-Zone Model

Figure 51 shows the effect of charge dilution on emission formation, as it is predicted by the MZCM. This figure compares the two extreme cases (maximum and minimum EGR as shown in Figure 48) and shows the distribution of zone temperatures and lambdas in a representation similar to Figure 28.

As the state histories of all zones cannot be easily visualized for the entire process, Figure 51 only demonstrates snapshots of the zone distributions. At this time around the end of fuel injection (i.e. at phi = 10° crank angle) the highest temperatures occur. The characteristics of fuel injection, rate of heat release, NO_x and soot formation are given in the lower diagrams of Figure 51. In the upper distribution plots of the figure every individual marker represents one zone. The marker size is proportional to the zone mass and the coloring indicates the NO_x formation rate (light indicates low and dark high NO_x formation rate). The continuous line shows the adiabatic isobaric flame temperature (AIFT, analogous to Figure 21) and thus represents a theoretical approximation for the combustion temperature.

The comparison of these two cases clearly depicts the effect of reduced oxygen concentration. In both cases, a major part of the spray zones lies in the area of lambda ~ 1. The lambda distribution of the zones with high EGR are slightly lower as already demonstrated by Figure 50 above. However, the most significant difference refers to the temperature distributions of the zones. With high EGR, the maximum combustion temperatures are approximately 100 K lower. Due to the non-linear temperature function of NO_x formation, this results in a NO_x reduction of 60%.

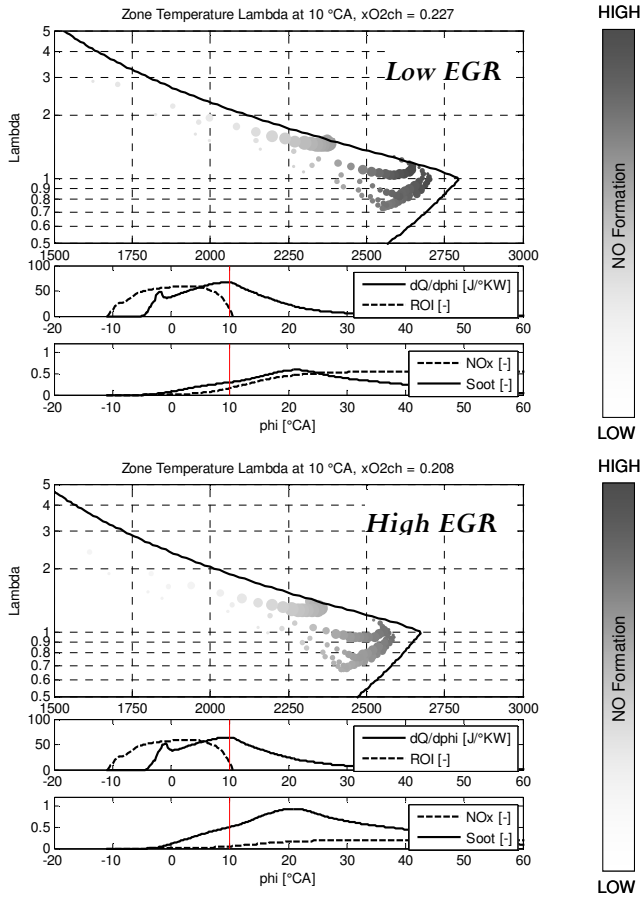

Figure 51: Distribution of Spray Zone Temperatures and Lambda Values at 10 deg a. TDC for different EGR Rates at Point 3

7.3.6 Characteristics of Soot Emission at a Variation of EGR

The soot formation and oxidation process is like no other process governed by local phenomena in the spray. An analysis of the impact of changing operating conditions on these highly transient processes is not reasonably possible on the basis of the high number of local zones in the spray. Thus, for the present analysis several spray-averaged quantities are depicted that qualitatively describe the relevant behavior.

In general, charge dilution by EGR leads to an increase of soot emissions which is caused by the reduction of oxygen concentration. This trend can be observed in the measurements and is also represented in the predicted emission shown in Figure 48.

In Figure 52 the lower plot shows the net in-cylinder soot which results from the difference of formation and oxidation reaction. All 3 curves show similar qualitative characteristics. Towards EVO a large part of overall formed soot is oxidized. Quantitatively, the highest peak and the highest engine-out emissions are observed at the high EGR rate.

Despite the lower average temperature in the spray, the soot formation reaction is enhanced at high EGR. This is caused by the fact that in the applied soot model (Hiroyasu [54]) the formation reaction is directly related to the presence of fuel vapor. At high EGR (low oxygen concentration) the local fuel vapor concentration during combustion is higher, as the combustion reaction is limited by the available oxygen. This behavior is very well reflected by the mean spray lambda value shown in the intermediate plot.

In addition to the higher soot formation, the soot oxidation is detained due to the lower oxygen concentration in the diffusion combustion and expansion phase. Therefore, the resulting engine-out emissions are even more pronounced at high EGR rates.

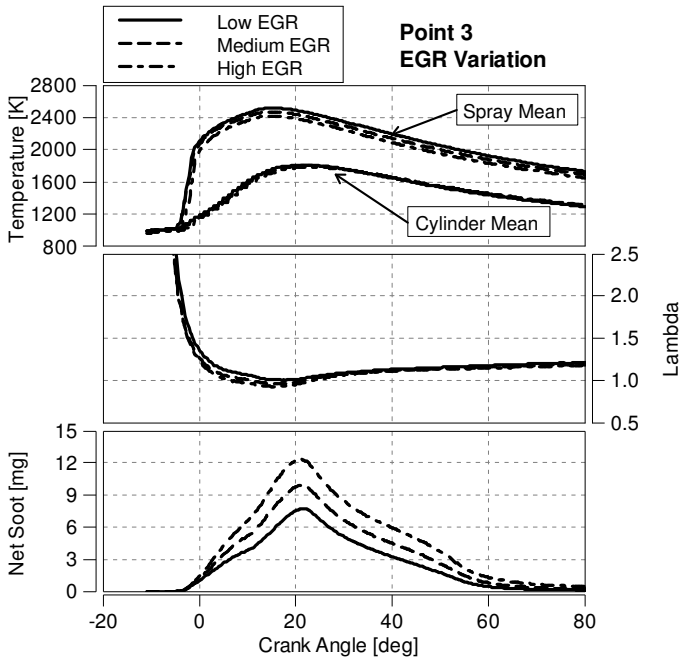

Figure 52: Characteristics of Soot at a Variation of the EGR Rate

7.4 Variation 2: Effect of Fuel Injection Timing

7.4.1 Prediction of Heat Release by the Multi-Zone Model

Figure 53 shows the results of heat release calculations with the MZCM for various fuel injection timings at the engine operating Point 3. Again, for all these calculations constant model parameters for charge entrainment and evaporation were used.

It can be observed that the shapes of the rate of heat release considerably change at a variation of the injection timing. Especially at very early and very retarded timings, the ignition delays get very long, leading to the fact that major parts of the combustion take place under premixed conditions. The multi-zone spray conception is intended to describe the heterogeneous mixing process in the spray. When the mixture becomes more and more homogeneous, the chemical reaction mechanism becomes dominant for the heat release towards the mixing process, which is not the main focus of the spray conception. Considering this fact it is notable that the multi-zone model predicts the heat release with reasonable good accuracy with one constant set of model parameters.

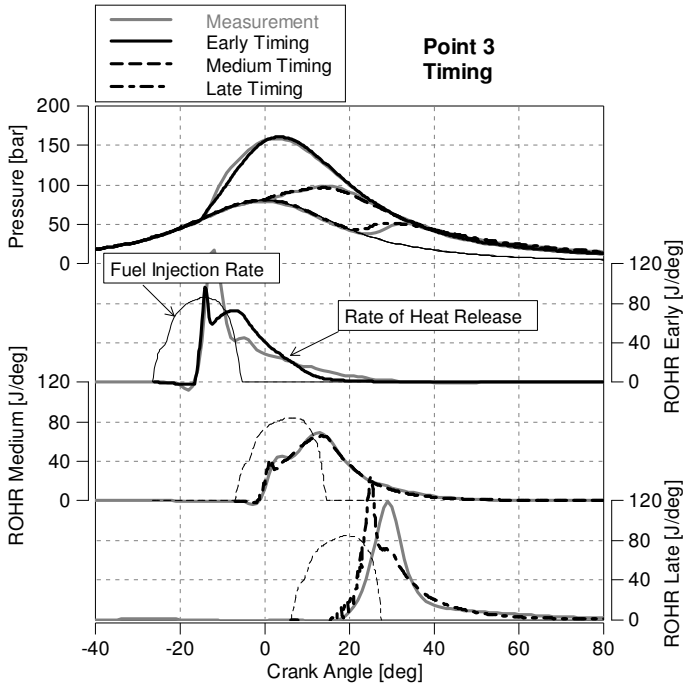

Figure 53: Change of Heat Release Characteristics versus Injection Timing

7.4.2 Prediction of Emissions by the Multi-Zone Model

A change of the injection timing has a significant impact on NO_x and soot emissions. In this example NO_x emissions vary even within one order of magnitude and the measured results are well predicted by the model (see Figure 54, left diagram). In real engines soot emissions frequently show a minimum versus timing which is partially caused by the changing interaction of the fuel spray with the piston bowl. As this latter phenomenon is not modeled by the 0-dimensional approach, the calculated results deviate from the measured soot emissions, but clearly approach them at one point (Figure 54, right diagram). This example very well demonstrates the overlapping of geometrical effects with pure thermodynamic characteristics of soot formation.

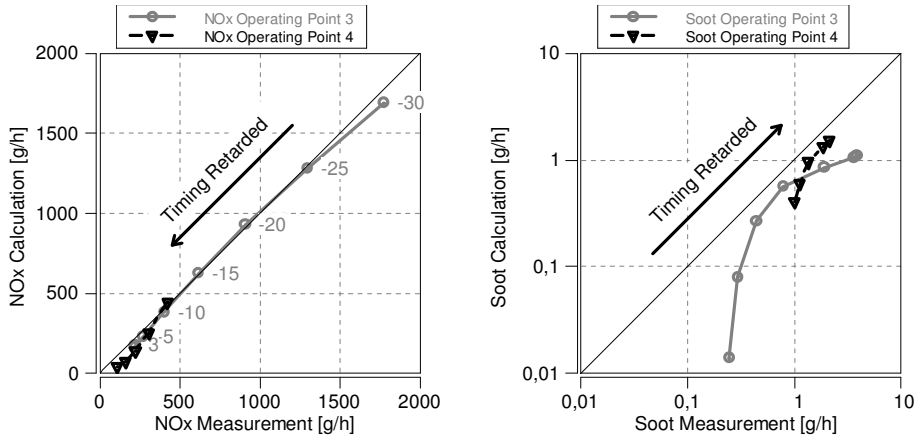

Figure 54: Measured vs. Calculated Emissions Injection Timing Variation Point 3 and Point 4

7.4.3 Effect of an Injection Timing Variation on Charge Composition

The injection timing variation at engine operation Point 3 was measured without EGR. This means that during this variation, the EGR valve was kept fully closed. In contrast to that, the variation at operating

Point 4 was measured with a constant EGR rate of 12 %, and in order to isolate the effect of timing variation, boost pressure (as postulated by Table 2) was additionally kept constant, which also results in the postulated constant global lambda in the combustion chamber. In this second case, both the EGR valve and the VTG position of the turbocharger had to be carefully adjusted at all variants in order to satisfy the postulated engine operating conditions. This way it can be assured that charge dilution has no influence on the investigated mechanisms.

7.4.4 Effect of Injection Timing Variation on Mixture Formation

Even though the boost pressure and boost temperature at IVC as well as the fuel injection pressure were kept constant, the boundary conditions for mixture formation change due to the compression / expansion characteristics enforced by the piston movement. Increasing charge density enhances both the charge entrainment and the evaporation rate as demonstrated in Figure 17 and Figure 19.

Analogous to the presentation of results in Figure 50, Figure 55 shows the histories of spray mass and mean spray Lambda during the combustion process. Basically, the characteristics are similar but have shifted according to the injection timing. However, the minima of the Lambda curves clearly fall with retarded injection timings. This phenomenon originates from the decreasing density in the expansion stroke (top dead center corresponds to 0° crank angle) leading to reduced charge entrainment.

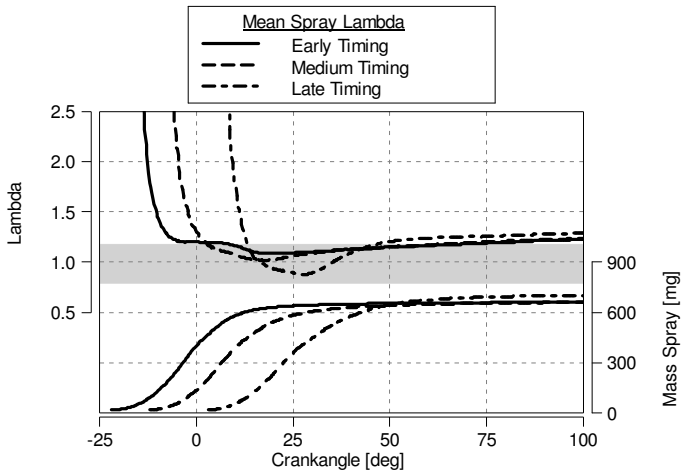

Figure 55: Effect of Injection Timing Variation on Mixture Formation

7.4.5 Effect of Compression and Expansion caused by Piston Movement

The effect of overlapping of the compression / expansion stroke is illustrated by the histories of three individual zones which are injected at different crank angle positions within one combustion process. This kind of representation has been introduced by Hountalas et al. in [74].

Figure 56 shows the histories of temperature and accumulated NO_x for 3 zones of the spray. These zones refer to fuel packages injected at the beginning, in the middle phase and at the end of injection. The accumulated NO_x is normalized to the overall fuel mass in the zone because the early and late packages have lower fuel masses compared to the intermediate package according to the injection rate shape. Two combustion processes with different injection timings ('early' and 'medium' timing) are compared.

In the early combustion process, the first fuel package is injected at -26 deg and combustion starts at -18 deg. The major part of NO_x is formed at temperatures above 2500 K which are reached between -12 to +5 deg. After this period the NO reaction freezes and the accumulated NO_x remains constant. The later injected packages remain at lower temperatures and, additionally, the NO reaction period shortens. Therefore, significantly less NO is formed.

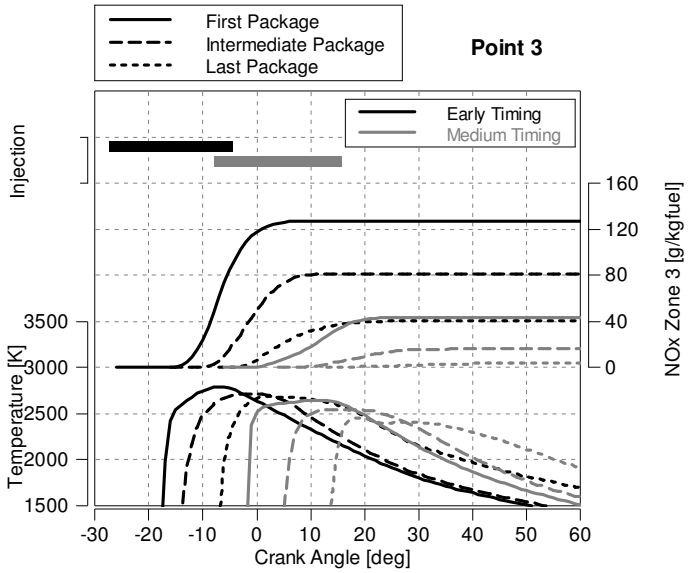

Figure 56: Traces of Temperature and NOx Formation as Function of Fuel Injection Timing

The characteristics of the temperature traces in Figure 56 provide very interesting findings on the thermodynamic change of state in the zones. After ignition the zones reach temperatures close to AIFT (~2500K) almost immediately. However, it can be observed that especially the earlier injected zones experience a further temperature increase which leads to higher peak temperatures. The further temperature rise is caused by the effect of the combined combustion and compression process discussed in Chapter 5.2.2 (Figure 23). Of course, this effect highly depends on the interaction of the combustion with the compression and expansion stroke. This leads to the presumption that all zones of an entire combustion process follow an overall trend which is related to injection timing.

This topic is investigated below by means of a detailed analysis of all tested fuel injection timing variants at both engine operation points 3 and 4 (see Figure 57). For reasons of simplicity, Figure 57 only shows the peak temperatures and the final accumulated NO_x. These values are plotted at that crank angle positions at which the zones were injected. Consequently, the temperature and NO_x lines match with the corresponding fuel injection periods in terms of their absolute crank angle positions. These results demonstrate the strong influence of the compression / expansion stroke on the combustion process and depict qualitatively a continuous NO_x vs. crank angle trend when varying fuel injection timing. The comparison between operating points 3 and 4 also shows the effect of EGR, which shifts the overall temperature and NO_x level downwards. Still, the qualitative trend remains comparable.

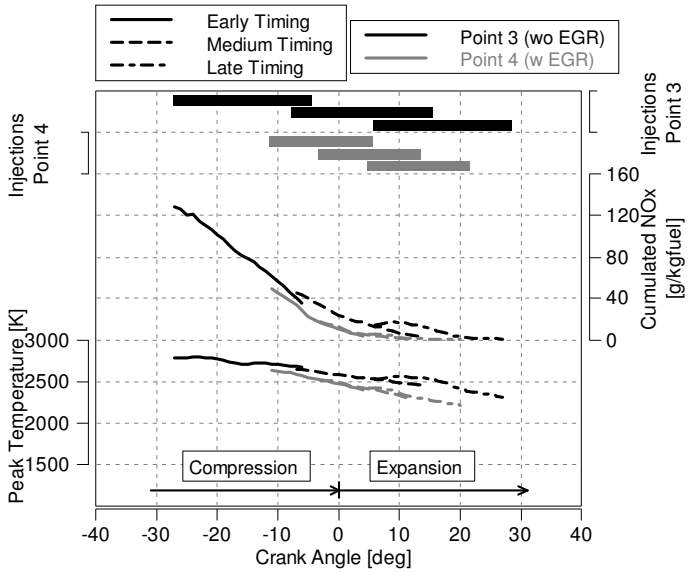

Figure 57: Peak Temperature and Accumulated NOx for individual Packages as Function of Fuel Injection Timing

7.4.6 Characteristics of Soot Emission at a Variation of Injection Timing

Figure 58 analyzes the impact of injection timing on soot. Therefore, the same considerations as made in Chapter 7.3.6 apply.

As discussed in chapter 7.3.6, the mean spray lambda value gives an indication for the fuel vapor and oxygen concentrations in the spray and these concentrations define the net soot formation rate. Such a behavior is also observed in Figure 58. For the later timings, mixture formation is detained which results in lower spray lambda values. This leads to a high peak of in-cylinder soot. Additionally, the injection timing affects the overall cylinder temperature level during combustion. At the late timing the mean temperature in the spray during diffusion combustion is significantly lower due to the piston expansion. Therefore, soot oxidation reaction is lower. These two effects lead to increasing soot emissions at retarded timings.

Of course, the 0-dimensional model only describes the 'thermodynamic' effect of a timing variation. An overlaying geometrical effect, which results from the interaction of the spray with the in-cylinder flow field and the piston bowl that probably affects mixture formation, cannot be considered.

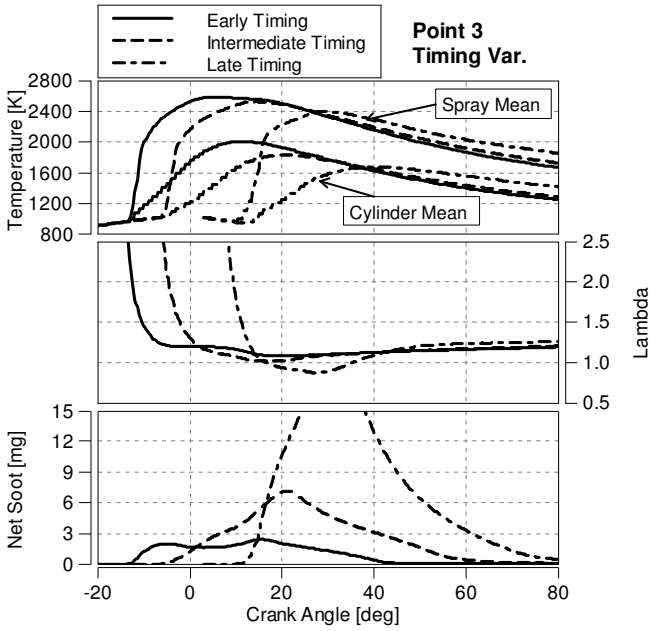

Figure 58: Characteristics of Soot at a Variation of Injection Timing

7.5 Variation 3: Effect of Fuel Injection Pressure

7.5.1 Prediction of Heat Release by the Multi-Zone Model

Figure 59 shows the cylinder pressures and heat release traces for various injection pressures at a constant fuel injection timing. With respect to the MZCM, the injection pressure predominantly affects the charge entrainment, as demonstrated in chapter 5.1.1, Figure 17. As the injection pressure variation was calculated with a constant entrainment parameter $C_{Entrain}$ it can be concluded that the model well predicts the charge entrainment. However, it was generally found that the simulated fuel evaporation rate had to be enhanced at low fuel injection pressures by slightly increasing the parameter C_{Evap}.

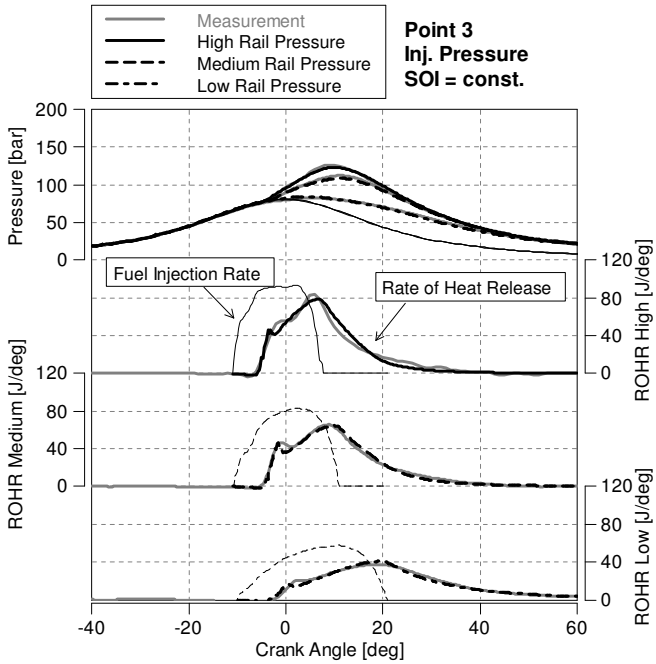

Figure 59: Change of Heat Release Characteristics versus Injection Pressure

7.5.2 Prediction of Emissions by the Multi-Zone Model

A comparison of calculated and measured NO_x and soot emissions is given in Figure 60. The qualitative trend is very well predicted by the model. Also the agreement of absolute values can be considered as satisfactory.

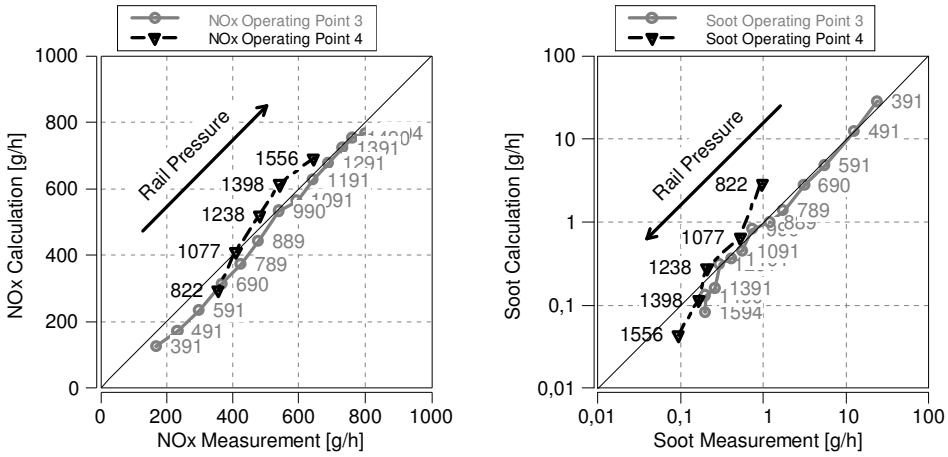

Figure 60: Measured vs. Calculated Emissions at a Variation of Rail Pressure Operating Points 3 and 4

7.5.3 Effect of Fuel Injection Pressure on Charge Composition

Similarly to the investigations on injection timing, the engine operation Point 3 was measured without EGR and the Point 4 with EGR. In both load points the charge composition was kept constant, thus it can be assumed that charge dilution does not affect the results of the injection pressure variations shown in Figure 59 and Figure 60 above.

7.5.4 Effect of Fuel Injection Pressure on Mixture Formation

The fuel injection pressure defines the initial velocity of the injected fuel parcel which subsequently decelerates due to the entrainment of mass from the cylinder charge. An increase of fuel injection pressure accelerates the charge entrainment. This is demonstrated in the lower diagram of Figure 61, showing a steepening rise of the spray mass versus increasing injection pressure. Furthermore, a high injection pressure also causes the initial droplet size to decrease which additionally enhances the fuel evaporation rate. As a result of all these phenomena, the whole combustion process accelerates. This is shown by the initial steep gradients of the 'Lambda' traces in Figure 61, upper diagram. Finally, it can be observed that the minimum Lambda falls with decreasing injection pressure, suggesting that the diminishment of charge entrainment with falling injection pressure is stronger than the slowing down of fuel evaporation.

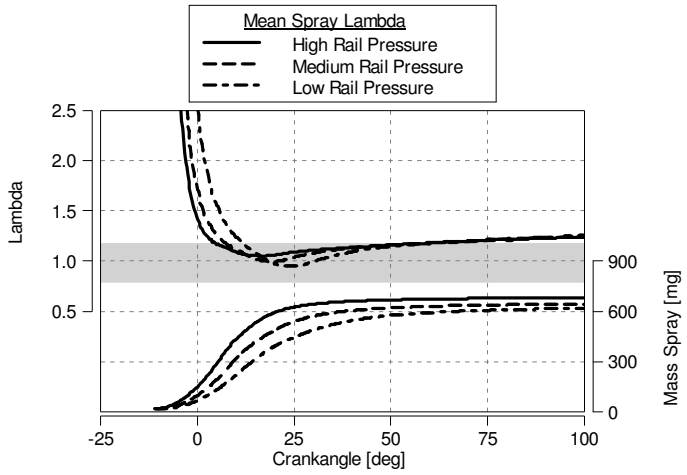

Figure 61: Effect of Fuel Injection Pressure on Mixture Formation

7.5.5 Effect of Compression and Expansion caused by Piston Movement

The discussion of this effect follows the procedure which was introduced in the previous chapter (see Figure 56 and Figure 57). Similar to Figure 56, Figure 62 shows the histories of three individual zones which are injected at different crank angle positions (start, middle phase, end) for a combustion with high and a combustion with low fuel injection pressure. It can be seen that both the peak zone temperatures and the cumulative NO_x traces show similar trends, as demonstrated with the pure variation of the injection timing. However, here it is the pure lengthening of injection which shifts the combustion more and more into the expansion stroke.

In addition to the effect of the pure shifting of the combustion process, the faster combustion also causes a steeper pressure rise. This of course affects the rise in temperature after the initial combustion which is overly enhanced at the high rail pressure.

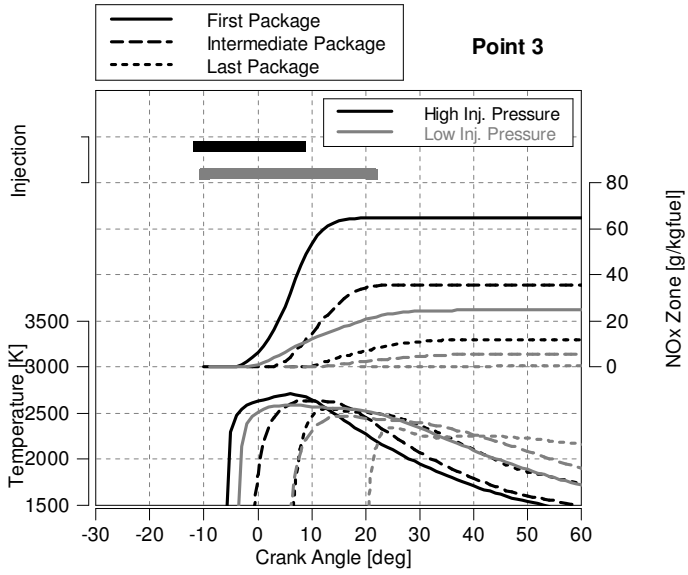

Figure 62 Traces of Temperature and NOx Formation as Function of Fuel Injection Pressure

Figure 63 shows these characteristics for various fuel injection pressures at two engine operation points. Analogous to Figure 57, it only plots the peak temperatures and the final accumulated NO_x. The values are again matched to the crank angle positions at which the zones are initiated. In this case, the peak temperature and accumulated NO_x traces do not show a similarly consistent trend, as was found for the fuel injection timing variation. The gradient of NO_x vs. injection crank angle is much steeper for the

high rail pressure. It can be assumed that these differences are caused by the overlaying effect of the piston movement together with a faster combustion. This topic is investigated below.

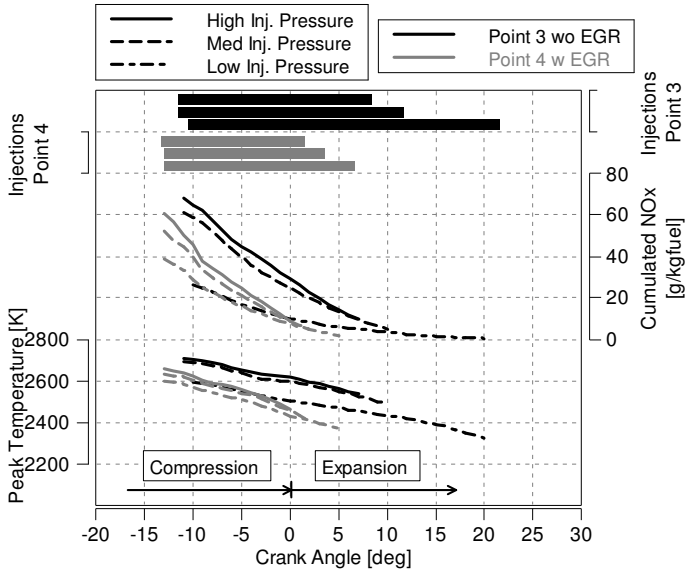

Figure 63: Peak Temperature and Accumulated NO_x for individual Packages as Function of Fuel Injection Pressure

Figure 64 shows the pressure characteristics, rate of heat release and injection timing for 3 Points out of the rail pressure variation in Point 3. At high rail pressure, the combustion is a lot faster which causes a faster rise in pressure and a higher peak pressure and temperature.

An adequate quantitative measure for this effect is the pressure increase of a zone related to the cylinder pressure at which the zone was injected. This is shown for all packages in the lower plot of Figure 64. The first packages are injected at -12 degCA at a pressure of approximately 60bar. At high rail pressure the cylinder pressure almost doubles from 60 to 120bar during combustion, while for the low rail pressure combustion is almost isobaric after TDC. The effect of this pressure rise especially concerns the initial zones and decreases for the later packages. This picture depicts very similar qualitative characteristics to the NO_x trend as shown in Figure 63.

It can be concluded that the increase of peak zone temperature (and therefore higher NO formation) is highly affected by the pressure rise during the process, caused by the piston movement and the combustion itself. For the variation of rail pressure at constant SOI there are two superposed effects: (1) the shifted center points of injection caused by a changing injection duration which reflects a shift of timing and (2) the shorter combustion duration which increases the peak pressure rise. Both of these effects are well covered by the model.

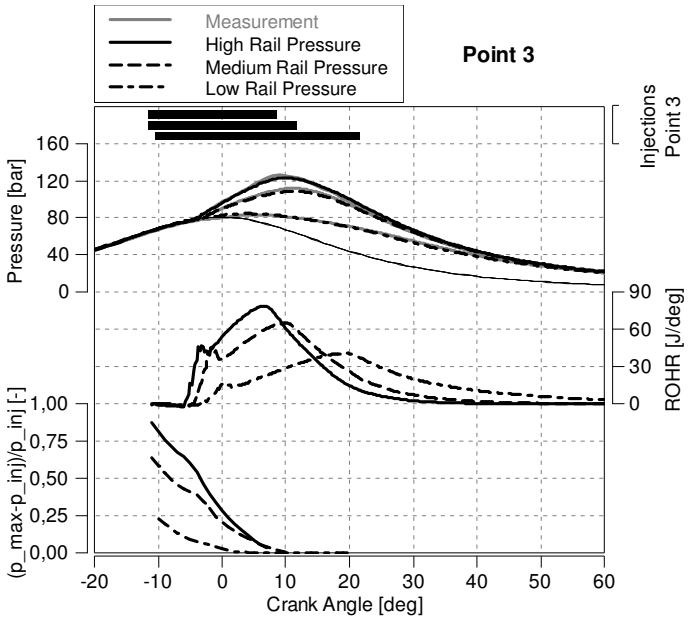

Figure 64: Cylinder Pressure, Heat Release and Pressure Rise at a Variation of Injection Pressure

7.5.6 Characteristics of Soot Emission at a Variation of Injection Pressure

Figure 65 analyzes the impact of injection timing on soot. Therefore, the same considerations apply as made in Chapter 7.3.6.

Injection pressure is the main source of spray momentum and hence one of the main parameters for the quality of mixture formation. This is directly reflected in the spray lambda characteristics at a variation of rail pressure shown in Figure 65. As discussed before (chapter 7.3.6), the mixture formation quality defines the species concentrations, which directly controls the net soot formation which is thus highest at the low rail pressure.

In addition to that, lowering the injection pressure leads to a prolongation of the injection duration which shifts part of the combustion process to a later phase in the expansion stroke. Thus, the time period for soot oxidation is shortened and the temperature level in that late phase is lower, which additionally reduces soot oxidation.

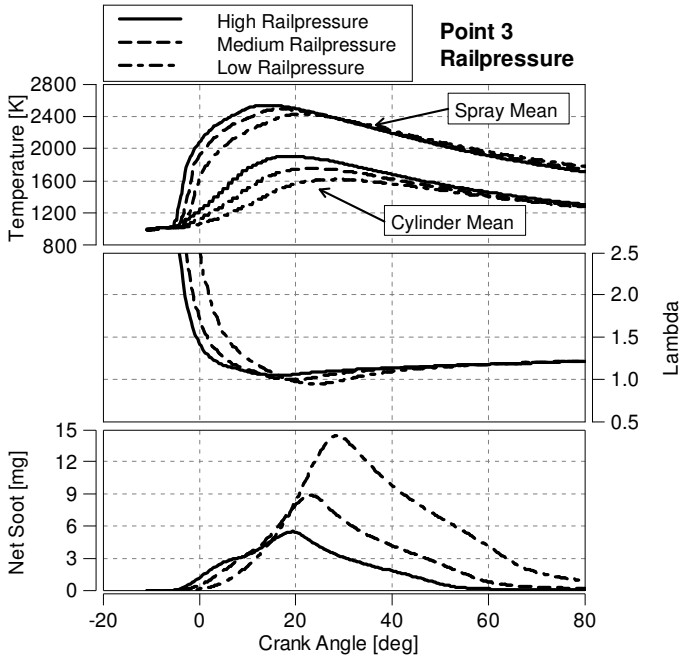

Figure 65: Characteristics of Soot at a Variation of Injection Pressure

7.5.7 Variation of Rail Pressure at Constant 50% Mass Fraction Burned

The previous results for injection pressure kept the start of injection constant, which leads to a shift of the injection center point towards late and thus causes a deterioration of the combustion process. For the present variation, the effect of this deterioration is compensated by shifting the injection timing along with rail pressure in order to achieve a constant 50% mass fraction burned point.

A comparison of these two approaches in terms of NO_x emissions is shown in Figure 66. The measurements at constant MFB50 were done without EGR, so the overall NO_x emission level is higher. The results are still comparable as the focus lies on the differences in the trends between the two approaches.

The variation of rail pressure at constant SOI from 1000 to 1600 bar leads to an increase of NO_x emissions by 50%. In the case of constant MFB50, the adjustment of timing compensates for a part of the NO_x characteristics as the injection starts earlier at lower rail pressures. Hence, the same rail pressure variation only causes a NO_x increase of 10%. So far, the effects of timing and rail pressure have been analyzed separately. It has shown that both effects are represented in the model. Consequently, the combination of both effects is also very well predicted by the MZCM.

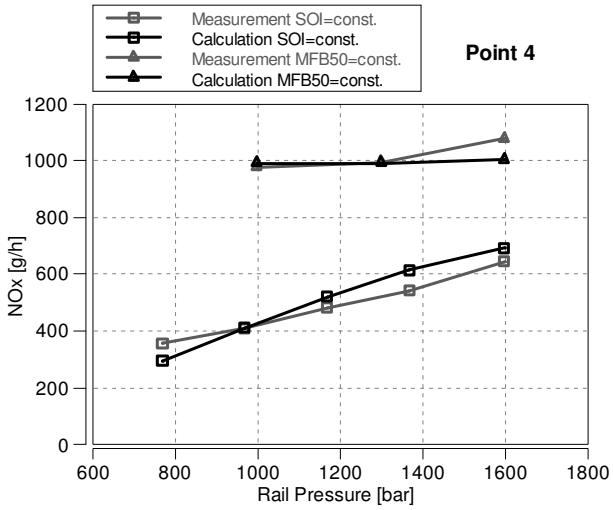

Figure 66: NOx Engine-Out Emissions Rail Pressure Variation
Comparison of Const. SOI vs. Const. MFB50

It was stated in advance that the temperature and NO_x formation which is characteristic for a variation of injection pressure and injection timing is caused by the cylinder pressure rise due to the piston movement and combustion. Figure 67 compares the cylinder pressure characteristics for the two different approaches of injection pressure variation.

In the plot on the left (constant SOI) one can clearly observe the differences in peak cylinder pressure caused by the deteriorated heat release. In the case of constant MFB50, the pressure traces and peak pressure show only little differences between the various points. These characteristics also reflect in the relevant value of relative pressure rise.

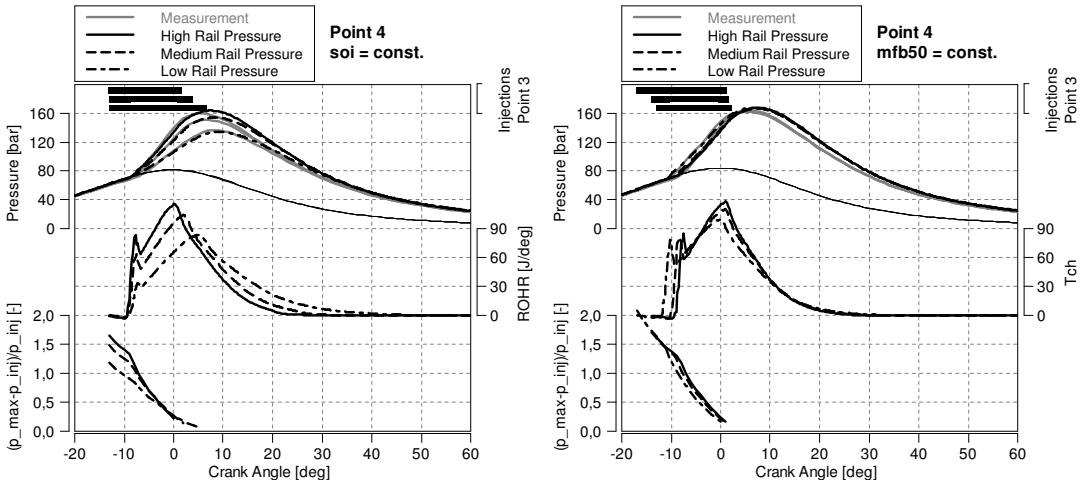

Figure 67: Cylinder Pressure, Heat Release and Pressure Rise at a Variation of Injection Pressure
Point 4: Comparison of (left) Const. SOI vs. (right) Const. MFB50

In the MZCM the effect of these different pressure characteristics can be observed in the peak temperature and cumulated NO_x histories of the packages over injection timing. At a variation of injection pressure at constant SOI, the gradient of cumulated NO_x vs. injection crank angle changes with injection pressure. In the case of constant MFB50, the lines run almost parallel for all points. There is just a crank angle offset that reflects the shifted SOI.

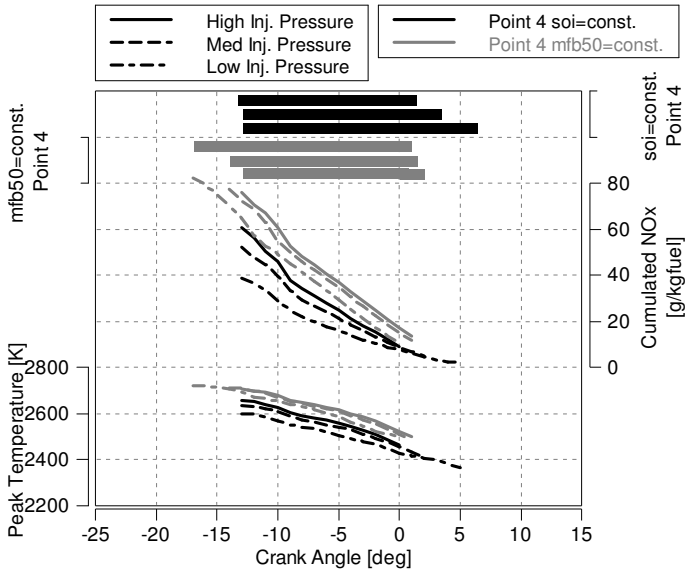

Figure 68: Cumulated NO_x and Peak Temperature of Zones at Variation of Rail Pressure Comparison of Const. SOI vs. Const. MFB50

7.6 Variation 4: Effect of Global Lambda by Variation of Boost Pressure

7.6.1 Prediction of Heat Release by the Multi-Zone Model

Figure 69 shows the cylinder pressures and heat release traces for a variation of boost pressure. With respect to the MZCM the main impact of increased boost pressure is the enhanced charge entrainment due to the influence of charge density on the spray penetration. This effect has already been demonstrated in chapter 5.1.1, Figure 17. The most accurate agreement of the measured and simulated curves is achieved, if the entrainment parameter $C_{Entrain}$ is slightly enhanced towards high boost pressure. All other parameters were kept at their baseline values.

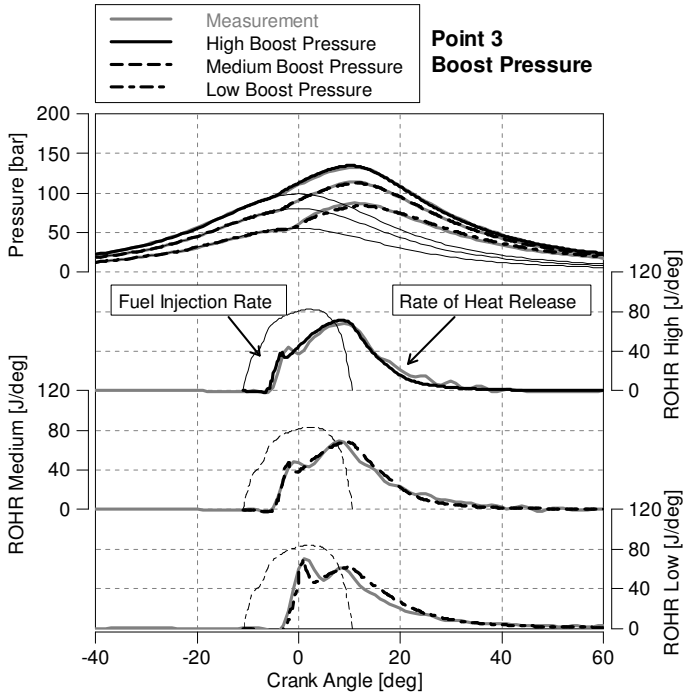

Figure 69: Change of Heat Release versus Boost Pressure

7.6.2 Prediction of Emissions by the Multi-Zone Model

A comparison of calculated and measured emissions is depicted in Figure 70. In terms of soot emissions, a reasonably good qualitative agreement can be observed. It needs to be considered that the operating points cover a range of several orders of magnitude (logarithmic view), and that the deviation especially regards the small absolute values. As discussed in the previous chapters, at low absolute values small measurement and calculation inaccuracies result in high relative deviations. Therefore, the agreement can be considered satisfactory.

A very interesting phenomenon can be observed for NO_x. Here, the measurement shows a clear increase of emissions with higher boost pressure. In contrary to that, the calculated NO_x emissions show exactly the opposite behavior. This results in an orthogonal crossing of the 45° line in the measurement vs. calculation plot. The described behavior can be observed similarly in both operating points. For that reason, the following sections will analyze these systematic trends on the basis of the relevant physical and thermodynamic effects.

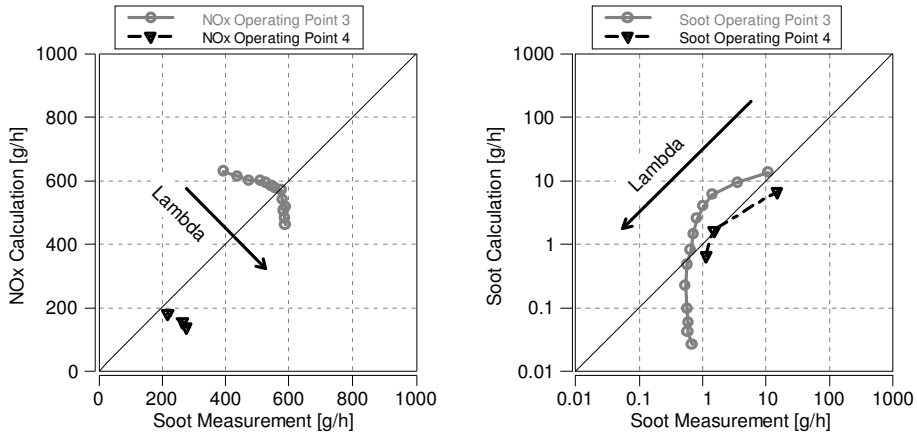

Figure 70: Measured vs. Calculated Emissions at a Variation of Boost Pressure Operating Points 3 and 4

7.6.3 Effect of Boost Pressure on Charge Composition

The boost pressure variations were measured without external EGR in both load points (EGR valve fully closed). Thus, the cylinder charge at IVC consists almost entirely of pure fresh air. On the engine testbed, the charge temperature is kept constant by a separate controller to compensate for the changing compressor outlet temperatures. Hence, the boost pressure directly controls the amount of aspirated air (constant volume flow) and is consequently directly proportional to the global lambda value.

The variation of total massflow and boost pressure leads to changing operating conditions of the turbocharger system. The related change of turbocharger efficiency affects the relative pressure drop from the intake to the exhaust, which is relevant for the scavenging process and thus can lead to a varying amount of trapped internal residual gases. Since the test engine was equipped with low pressure indication on the intake and exhaust side, it is possible to perform detailed 1-D gas exchange and combustion analysis as discussed in [75][4]. The calculations showed that differences in internal residual

[4] For this purpose, a simplified engine model is set up that consist only of a single-cylinder with intake and exhaust pipes. The boundary conditions at the pipe ends are defined by the measured crank angle resolved pressure and temperature traces. The in-cylinder heat release is calculated from the indicated high pressure trace. This allows analyzing in detail the gas exchange and combustion process without the need to set up a 1-D full engine model.

gas concentration are small (less than +/- 0.3%) and thus have minor effect on the overall process. This means that the effect is by far too small to explain the described behavior of NO_x emissions.

7.6.4 Effect of Boost Pressure on Mixture Formation

Analogously to the previous chapters, Figure 71 shows the histories of spray mass and mean spray lambda during the combustion process. In the present variation example, the boost pressure directly controls the charge density which leads to increased entrainment at high boost pressure. The effect of this can be observed in both the spray mass and lambda characteristics.

What is interesting to see is that at the highest boost pressure the mean lambda is throughout the process above lambda ~ 1. Of course, due to the heterogeneous lambda spreading the distribution in the spray covers a range around this mean value. However, the amount of spray mass which is present at near-stoichiometric conditions (high temperatures, high NO_x formation), is certainly lower at the high boost pressure. This leads to low calculated NO_x at high boost pressure which causes exactly the opposite behavior than shown in the measurements.

This discrepancy is regarded a relevant aspect for the systematic deviation of measurement and calculation. However, it is not easily possible to compensate for this effect (e.g. by tuning model parameters). The spray lambda characteristics are an output of the model which results from the interaction of the mixture formation mechanisms, entrainment and evaporation. According to the proposed method for model calibration shown in the previous chapter 6.3, there is only one exact solution for the set of model parameters. If these parameters were changed, it would also affect the heat release.

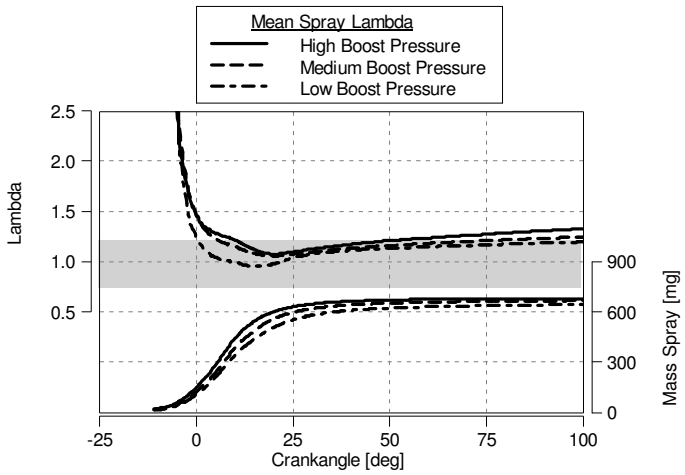

Figure 71: Effect of Boost Pressure Variation on Mixture Formation

7.6.5 Compression and Expansion caused by Piston Movement and Combustion

Figure 72 analyzes the thermodynamic characteristics of zone temperature and NO_x formation analogously to the previously established procedure (Chapter 7.4.5). In the present example, the injection characteristics (timing and duration) are almost identical for both considered operating points. Thus, the conditions for the combustion process in terms of the timing relative to the compression / expansion stroke are also very similar. The IVC state and also the motored temperature characteristics are in the range of a few degree K identical for all observed operating points. Hence, the theoretical, adiabatic combustion temperature should, according to the considerations made for Figure 22, also be similar.

Under these aspects it is interesting to see that there are significant differences in the temperature and NO_x formation characteristics. These differences especially regard the first injected package which has the highest contribution to the overall emissions. Here, the low boost pressure operating point shows the highest peak temperature and accumulated NO_x. Again, this trend goes exactly in the opposite direction than required to predict the measurements.

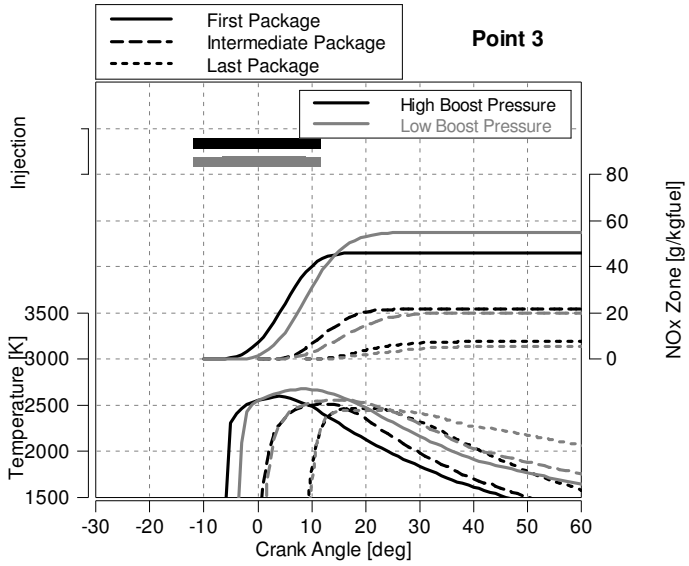

Figure 72: Traces of Temperature and NOx Formation as Function of Boost Pressure

The behavior shown in Figure 72 can also be explained from a thermodynamic point of view. As depicted in Figure 22 and Figure 23, it is not the absolute pressure level which is relevant for the peak combustion temperature, but the relative pressure rise during combustion. The quantitative measure for this effect is the relative pressure increase of a zone related to the cylinder pressure at which the zone was injected (compare Figure 64).

The pressure characteristics for the present variation example are shown in Figure 69. At the low boost pressure, the cylinder pressure almost doubles from 50 bar at the end of compression to a peak pressure of 90 bar, which makes a relative pressure rise of $(90\text{-}50)/50 = 0.8$. Contrary to that, at high boost pressure the relative pressure rise makes only a factor of $(140\text{-}100)/100 = 0.4$.

The resulting temperature increase due to compression is a direct result of the solution of the thermodynamic set of equations (Chapter 3.2.2). It cannot be compensated for by any mechanism or parameter of the combustion model.

7.6.6 Characteristics of Soot Emissions at a Variation of Boost Pressure

Figure 73 analyzes the impact of boost pressure on soot emissions. Therefore, the same considerations apply as made in Chapter 7.3.6.

The observed characteristics of the spray lambda distributions in Figure 71 directly impinge on the net soot formation which is throughout the process highest for the low boost pressure points. As mentioned, the changes of mixture formation might be overrepresented in the spray lambda characteristics, which is one possible explanation for the overestimation of the gradient of measured vs. calculated soot emission towards high global lambda values (Figure 70).

Figure 73 also depicts interesting information on the temperature characteristics. Due to the lower overall mass, the cylinder averaged temperature is highest at the low boost pressure. However, the average spray temperature is similar for all operating points, thus causing similar conditions for the soot oxidation reaction.

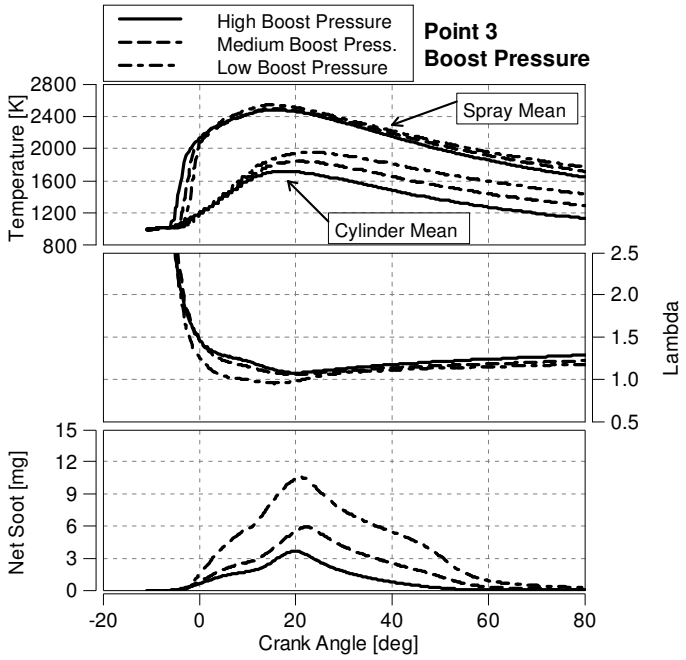

Figure 73: Characteristics of Soot at a Variation of Boost Pressure

7.6.7 Discussion and Interpretation of Results

In the previous sections, the systematically diverging trend of measured and calculated NO_x emissions was analyzed on the basis of fundamental thermodynamic and physical relations. The analysis has shown that there are two relevant effects that cause the observed undesired behavior: (1) the lambda distributions that result from the entrainment and evaporation characteristics (Figure 71) and (2) the thermodynamic effect of the combined compression and combustion process (Figure 72). The reason why these effects only come to the fore and distract the results at the boost pressure variation is, that for the other variation examples the causal effects of e.g. charge dilution or timing are by far more dominant. This shows that it is absolutely necessary to analyze each of the individual causal effects separately, which requires well directed measurements as shown in Figure 45 and Figure 46.

Being aware now of the physical effects that cause this undesired behavior, it is possible to discuss potential ways to overcome the discrepancies in the model. Therefore a closer look at the both effects mentioned above is taken.

Ad (2): The second effect is given by the thermodynamic solution and cannot be compensated for by any mechanism in the model. On the contrary: The analysis showed that this combined change of state of combustion and compression is the main relevant mechanism for the prediction of NO_x emissions versus variations of timing and injection pressure.

Ad (1): As discussed in chapter 7.6.4, the spray lambda distribution for the high boost pressure operating point exceeds the near-stoichiometric high temperature and NO formation region throughout the process. Shifting it to a lower region is only possible by either enhancing evaporation or suppressing the entrainment. It was also stated, that the heat release and thus the spray lambda characteristics result from the unambiguously identified mechanisms. When evaporation was enhanced, the initial phase of combustion was too fast. When entrainment was suppressed, the late phase of combustion was too slow. For this reason it is not possible to freely dispose of the spray lambda distributions due to the resulting incorrect prediction of the rate of heat release. However, more precisely it should have concluded that this is not possible – without making changes in the combustion model.

Adaption of Mechanisms in the Combustion Model

So far it has been assumed that entrainment and evaporation are continuous processes with constant parameters during the entire cycle. Reconsidering this restriction, the obvious consequence is to define a time dependent development of either of the mechanisms. By means of this measure it is e.g. possible to enhance evaporation, if it is at the same time compensated for by lower entrainment. Both entail a dropping of the spray lambda distribution.

For this purpose, evaporation is enhanced by increasing the parameter by a constant multiplier. To limit the heat release in the early phase of combustion, the entrainment needs to be suppressed by defining a low initial value. For the later diffusion combustion phase (in which evaporation is no more an issue) a higher value near the original one is required. From these considerations, the curve shown in Figure 73 is derived: At start of injection a relatively low initial value of 0.5 is defined. After the end of injection the parameter reaches the original value of 0.7, which is then constant. In-between a steady progression is obtained by defining an exponential transfer function.

Due to this general definition of the variable entrainment function based on characteristic and spray relevant parameters (SOI, EOI), the approach is directly applicable to changing operating conditions (e.g. variations of injection timing and duration). Furthermore, the trends of the other causal effects, e.g. charge dilution or the compression / expansion are still predicted correctly.

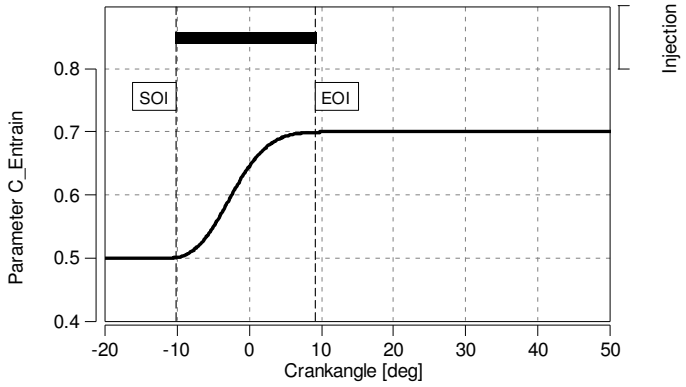

Figure 74: Development of Variable Entrainment Parameter During Injection

The resulting spray lambda characteristics are shown in Figure 75. Due to the enhanced evaporation and lower entrainment the mean spray lambda now passes the stoichiometric area in all cases.

At this point it has to be emphasized that despite the changes in the spray lambda characteristics the model still predicts the trend of soot emissions correctly. This is caused by the circumstance that the minimum spray lambda shifts to a later phase of combustion for the low boost pressure points. Additionally, it remains at a lower value during expansion which reduces the soot oxidation.

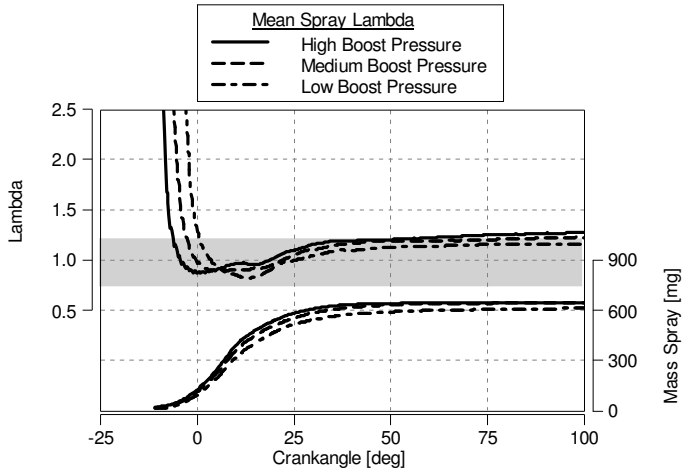

Figure 75: Mixture Formation with Variable Entrainment Approach

Figure 78 shows the comparison of measured and calculated NO_x emissions. In return of the changes in the model a good qualitative agreement of the trend is achieved. Still, a slight drift of the quantitative values can be observed at the lowest lambda (boost pressure) points. Considering the simplicity and general applicability of the variable entrainment approach, the overall agreement can now be considered reasonably good.

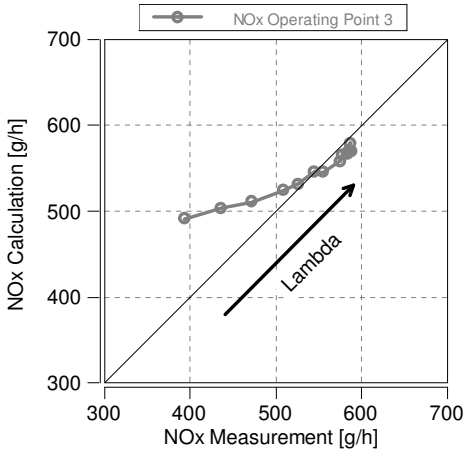

Figure 76: Measured vs. Calculated Emissions with Variable Entrainment Approach Operating Point 3

8 Conclusions

In the first chapter of the present work, several questions were raised that represent a central theme throughout this work. Finally, these questions provide a framework for the summary where the relevant topics are indicated by the corresponding abbreviations. Further topics that could not be examined in sufficient detail in the present work, but would be of interest for future research in this field are mentioned in the final section.

8.1 Summary

In the course of the present work a 0-dimensional combustion model is developed for the analysis and prediction of Diesel engine heat release and pollutant formation. The modeling conception is based on the well-established multi-zone package approach. In this type of model the injection spray is sub-divided into a high number of reaction zones. Each of these zones has its own history of state and composition. The model considers all relevant physical mechanisms for the description of the combustion process: fuel evaporation, fuel/air mixing (air entrainment) and chemical reactions for heat release and pollutant formation. These mechanisms are calculated within the individual reaction zones as integrated and continuous processes. Hence, the model offers a high degree of general validity.

A few modeling extensions that supplement the genuine multi-zone approach have been suggested. These especially concern the heat and mass transfer processes in-between the spray zones. This way, the model considers mixing of the spray with burned combustion products. This is achieved by introducing a new distinguished zone that summarizes all burned spray zones. These combustion products are further on together with the fresh charge recycled into the injection spray. This so-called Re-Entrainment mechanism is crucial for the combustion process in high-load operating points and for the prediction of trends in soot emissions. Furthermore, a heat transfer mechanism between the spray zones and the unburned charge zone is applied, which generates a homogenization of the in-cylinder temperature field towards exhaust valve opening. This mechanism is not only reasonable from physical aspects but also crucial for the prediction of engine performance. (*Q I.1, Q I.2*)

In the multi-zone model the heat release is mainly controlled by three relevant mechanisms: charge entrainment and fuel evaporation, which define the concentrations of reactants in the zones, and the chemical reaction. For each of the mechanisms, one appropriate model parameter is selected. Additionally, there is one parameter that controls the ignition delay which is calculated separately. This makes an overall number of only 4 main relevant parameters which are used to calibrate the combustion model for different engines and operating points. Furthermore, each of the emission models uses two parameters. (*Q II.1, Q II.2*)

A systematic method which identifies the parameters in two subsequent steps is presented: (1) For the identification of the main combustion parameters, a model based pressure trace analysis on the basis of the spray model was developed. This method screens the combustion process and evaluates the phases in which alternately the charge entrainment and the fuel evaporation mechanisms come to the fore. The variation of the chemical reaction parameter is used as an assessment criterion. In doing so, the method also considers the physical principles of the combustion process. Based on this, an algorithm is suggested which allows to automatically identify the entrainment and evaporation parameters. (2) On the basis of the predefined combustion process the emission model parameters are identified. An automatic algorithm estimates unambiguous mathematical solutions for the two emission model parameters for each pair of operating points. If this is done for a reasonably high number of measurements, a statistical evaluation of the identified solutions set allows to account for measurement outliers and calculation uncertainties. (*Q II.3*)

The method is applied to 3 different engines: two heavy-duty size engines and one passenger car size engine. The multi-zone model shows a high degree of universal validity. With identified model parameters engine performance, as well as NO_x and soot emissions can be predicted with high accuracy at various operating conditions. For all engines the combustion model parameters only varied in a small range. The systematic spreading of model parameters depicts evident physical effects, such as the increase of air entrainment with engine speed, pointing out the effect of charge motion due to swirl. It shows that identified NO_x parameters are in the same order of magnitude for similar engines. Contrary to that, soot parameters can most certainly not be transferred from one engine to another. Obviously, differences in the engine hardware, such as combustion chamber geometry and injection nozzle design, which are not considered by the model, impinge on the kinetic parameters of the soot emission model. (*Q I.3, Q II.4, Q II.5*)

The model has proven to predict engine performance and emissions for changing operating conditions, such as variations of EGR, turbocharging or injection characteristics with a high accuracy. From a physical point of view these operating conditions have fundamentally different effects on the combustion and pollutant formation processes. The analysis of these effects concentrates on the fundamental characteristic of the combustion in Diesel engines on the basis of the physical, thermodynamic and reaction kinetic mechanisms. Based on theoretical considerations, these effects are separated into three basic principles: mixture formation, charge dilution and the interaction of combustion and piston movement. (*Q III.1*)

In reality, there is always a complex interaction between all these mechanisms so the directed analysis of these principles requires special engine measurements that deliberately emphasize the individual principles.

The mixture formation process defines the lambda distribution in the spray, which is most significant for soot formation. On the other hand, due to the interrelation between the zone composition and the theoretical combustion temperature, it also defines the temperature distribution which together with oxygen concentration governs the NO_x formation. The highest rates are observed at near-stoichiometric conditions. The reduction of the oxygen concentration by charge dilution is the only way to control the theoretical combustion temperatures, and hence reducing NO_x formation. Furthermore, the oxygen availability is relevant for the soot the oxidation reaction. The thermodynamic change of state during the high pressure cycle results from the interaction of the combustion with the compression and expansion due to the piston movement. It defines the peak process temperatures at early combustion near TDC which are relevant for NO_x formation as well as the temperature level for the soot oxidation during the expansion stroke. The complex interaction of these mechanisms is well predicted by the model. (*Q III.2, Q III.3, Q III.4*)

8.2 Outlook

The results of the present work are sufficient cause to pursue the multi-zone approach for Diesel engine combustion modeling. The presented model and the developed automatable algorithms are seen as a starting point for further activities. In the near future, the focus lies on the integration of the model into the hands-on engine development process. Therefore, the first step is to implement the model into a 1-D cycle simulation code. The application of the model for various engines can build up a database of model parameters. This allows generating predefined sets of model parameters for different engine categories. Together with further experience this will possibly allows to predict so far unknown engines in combination with an estimation of the expected accuracy of results.

In the present work, various observed deviations between calculated and measured results are attributed to geometrical phenomena. However, 0-dimensional modeling is per definition limited to account for thermodynamic effects. This means that the spray model does not consider an interaction of the spray

with the in-cylinder flow field caused by swirl motion or the geometry of the combustion bowl. As a consequence, such geometric effects only impinge on the identified model parameters. From a scientific point of view, a detailed analysis of these geometrical phenomena and possible ways to consider their impact in the 0-D model would be of great interest. In this context, the information derived from detailed CFD calculations can deliver important information.

Another interesting topic that has not been addressed in the present work is the simulation of combustion concepts with multiple injections. In this regard, especially the interaction between separate injection sprays is seen as a crucial phenomenon. This interaction is most certainly governed by geometrical phenomena, which are difficult to consider in a 0-D model. However, the presented modeling approach with its Re-Entrainment mechanism basically provides the foundation to account for such phenomena. Especially with post injections, the interaction of the combustion and the gas exchange process due to turbocharging can lead to complex changes of operating conditions. Therefore, the detailed analysis of pollutant formation phenomena with multiple injections absolutely requires well-directed measurements.

9 References

[1] Merker, G. P.: Grundlagen Verbrennungsmotoren. Vieweg+Teubner, Wiesbaden, 2009

[2] Pischinger, R.; Klell, M.; Sams,T.: Thermodynamik der Verbrennungskraftmaschine. Springer, Wien, 2010

[3] Warnatz, J.; Maas, U.; Dibble, R. W.: Verbrennung: Physikalisch-Chemische Grundlagen, Modellierung und Simulation. 3. Auflage, Springer, Berlin, 2001

[4] Peters,N.: Skriptum: Technische Verbrennung. Technische Universität Aachen, Institut für Mechanik, Aachen, 2005

[5] Merker, G.; Schwarz, C.; Stiesch, G.; Otto,F.: Verbrennungsmotoren - Simulation der Verbrennung und Schadstoffbildung. 3. Auflage, Teubner, Wiesbaden, 2006

[6] Krome, D.: Charakterisierung der Tropfenkollektive von Hochdruckeinspritzsystemen für direkteinspritzende Dieselmotoren. Dissertation, Hannover, 2004

[7] Stahl, M.: Experimentelle und numerische Untersuchung des primären Strahlzerfalls von Druckzerstäubern. Dissertation, Darmstadt, 2008

[8] Hsiang, L. P.; Faeth, G.: Drop Deformation and Breakup due to Shockwave Disturbances. Int. Journal of Multiphase Flow, Vol. 21, 1994

[9] Arcoumanis, C.; Gavaises, M.: Linking the nozzle flow with spray characteristics in a diesel fuel injection system. Atomization and Sprays, Vol. 8, 1998

[10] Baddock, C.: Untersuchungen zum Einfluss der Kavitation auf den primären Strahlzerfall bei der dieselmotorischen Einspritzung. Dissertation, Shaker Verlag, Darmstadt, 1999

[11] Wierzba, A.: Deformation and breakup of liquid drops in a gas stream at nearly critical weber numbers. Experiments in Fluids, Vol. 9(1990):59-64, 1990

[12] Baumgarten, C.: Mixture formation in internal combustion engines. Springer, Heidelberg, 2006

[13] Semenov, N.: Chemical Kinetics and Chain Reactions. Oxford University Press, London, 1935

[14] Dec, J. E.: A Conceptual Model of DI Diesel Combustion Based on Laser-Sheet Imaging. SAE Technical Paper 970873, Detroit, 1997

[15] Flynn, P.; Durrett, R. P.; Hunter, G. L.; Loye, A.; Akinyemi, O. C.; Dec J. E.; Westbrook, C. K.: Diesel Combustion: An Integrated View Combining Laser Diagnostics, Chemical Kinetics, and Empirical Validation. SAE Technical Paper 1999-01-0509, Detroit, 1999

[16] Higgins, B.; Siebers, D.; Aradi, A.: Diesel-Spray Ignition and Premixed-Burn Behavior. SAE Technical Paper 2000-01-0940, Detroit, 2000

[17] Zeldovich, Y. B.; Sadonikov P. Y.; Frank-Kamenetskii, D. A.: Oxidation of Nitrogen in Combustion. Publ. House of the Acad of Sciences of USSR, Moscow Leningrad, 1947

[18] Heywood, J. B.: Internal Combustion Engine Fundamentals. McGraw-Hill, 1989

[19] Fenimore, C.: Formation of Nitric Oxide in Hydrocarbon Flames. 13th Int. Symposium on Combustion, The Combustion Institute, Vol. 13, pp. 373-379, 1971

[20] Sams, T.; Salzgeber, K.; Hausberger, S.: Skriptum: Schafstoffbildung und Emissionierung bei Kfz Teil I, Technische Universität Graz, Institut für Verbrennungskraftmaschinen und Thermodynamik, Graz, 2007

[21] Amnéus, P.; Mauß, F.; Kraft, M.; Vressner, A.; Johansson, B.: NOx and N2O formation in HCCI Engines. SAE Technical Paper 2005-01-0126, Detroit, 2005

[22] Wimmer, A.: Skriptum: Fahrzeug- und Motorenmesstechnik WS 2006/2007, Teschnische Universität Graz, Institut für Verbrennungskraftmaschinen und Thermodynamik, Graz, 2006

[23] Eastwood, P.: Particulate Emissions from Vehicles. John Wiley & Sons, West Sussex, 2008

[24] Hopp, M.: Untersuchung der Rußoxidation unter Dieselmotorischen Randbedingungen. Dissertation, Aachen, 2001

[25] AVL List GmbH: Rauchwertmessung mit der Filterpapiermethode, Rev. 02. AVL Application Notes, Graz, 2005

[26] Frenklach, M.; Wang, H.: Detailed Modeling of Soot Particle Nucleation and Growth. Twenty-Third Symposium (International) on Combustion, The Combustion Institute, pp. 1559-1566, 1990

[27] AVL List GmbH: BOOST Real-Time (RT) Users Guide Edition 12/2011, AVL List GmbH, Graz, 2011

[28] Allmer, I.; Petutschnig, H.; Sams, T.: Modellbasiertes Thermomanagement zur Verbrauchs- und Emissionsoptimierung für NFZ Anwendungen. 13. Tagung: Der Arbeitsprozess des Verbrennungsmotors, Graz, 2011

[29] Grill, M.: Objektorientierte Prozessrechnung von Verbrennungsmotoren. Dissertation, Stuttgart, 2006

[30] Engelmayer, M.: Simulationsmodell für Brennverlauf und NO-Bildung im Dieselmotor mit Direkteinspritzung. Dissertation, Technische Universität Graz, Graz, 2001

[31] Rakopoulos, C. D.; Gialoumis, E. G.: Diesel Engine Transient Operation. Springer, London, 2009

[32] Pirker, G.: Nulldimensionale Modellierung von Zündverzug und Brennratenverlauf bei direkteinspritzenden Dieselmotoren. Dissertation, Technische Universität Graz, Graz, 2006

[33] Faeth, G. M.: Current Status of Droplet and Liquid Combustion. Combustion Science, Vol. 3, Iss. 4, 1977

[34] Magnussen, B. F.; Hjertager, B. H.: On mathematical models of turbulent combustion with special emphasis on soot formation and combustion. Symposium (International) on Combustion, Vol. 16, Iss. 1, Trondheim, 1976

[35] Colin, O.; Benkenida, A.: The 3-Zones Extended Coherent Flame Model for Computing Premixed/Diffusion Combustion. Oil & Gas Science and Technology - Rev. IFP, Vol. 59, 2004

[36] Katrasnik, T.; Wurzenberger, J.; Schuemie, H. A.: On convergence, stability and computational speed for 0-D IC engine cylinder modeling. Springer, 2009

[37] Wimmer, A.; Glaser, J.: Indizieren am Verbrennungsmotor - Anwenderhandbuch, AVL List GmbH Handbuch, Graz, 2002

[38] Kožuch, P.: Ein phänomenologisches Modell zur kombinierten Stickoxid- und Rußberechnung bei direkteinspritzenden Dieselmotoren. Dissertation, Universität Stuttgart, Stuttgart, 2004

[39] Kerékgyártó, J.: Ermittlung des Einspritzverlaufs an Diesel-Injektoren. Dissertation, Otto-von-Guericke-Universität Magdeburg, Magdeburg, 2009

[40] Notz, H. W.: Beitrag zur experimentellen Ermittlung des Einspritzverlaufs am schnellaufenden Dieselmotor. Dissertation, Technische Universität München, München, 1986

[41] Woschni, G.; Anisitis, F.: Elektronische Berechnung des Einspritzverlaufes im Dieselmotor aus dem gemessenen Druckverlauf in der Einspritzleitung. Motortechnische Zeitschrift 30/7, pp. 238-242, 1969

[42] Austen, A. E.; Lyn, W.: Relation Between Fuel Injection and Heat Release in a Direct-Injection Engine and the Nature of the Combustion Process. Proceedings of the Institution of Mechanical Engineers, 1960

[43] Constien, M.: Bestimmung von Einspritz- und Brennratenverlauf eines direkteinspritzenden Dieselmotors. Dissertation, Technische Universität München, München, 1991

[44] Wolfer, H.: Der Zündverzug im Dieselmotor. VDI Forschungsheft Nr. 392, 1938

[45] Chmela, F. G.; Orthaber, G. C.: Rate of Heat Release Prediction for Direct Injection Diesel Engines Based on Purely Mixing Controlled Combustion. SAE Technical Paper 1999-01-0186, Detroit, 1999

[46] Magnussen, B. F.; Hjertager, B. H.: On Mathematical Modeling of Turbulent Combustion with Special Emphasis on Soot Formation and Combustion, 16th International Symposium on Combustion, 1976

[47] AVL List GmbH: BOOST Theory Guide Version 2011. Edition 07/2011, Graz, 2011

[48] Varde, K. S.; Popa, D. M.; Varde, L. K.: Spray Angle and Atomization in Diesel Sprays. SAE Technical Paper 841055, Detroit, 1984

[49] Sitkei, G.: Kraftstoffausbreitung und Verbrennung bei Dieselmotoren. Springer, 1964

[50] Andree, A.; Pachernegg, S. J.: Ignition Conditions in Diesel Engines. SAE Technical Paper 690253, Detroit, 1969

[51] Abramovich, G. N.: The Theory of Turbulent Jets. MIT Press, Cambridge, 1963

[52] Hohlbaum, B.: Beitrag zur Rechnerischen Untersuchung der Stickoxidbildung Schnelllaufender Hochleistungsdieselmotoren. Dissertation, Universität Karlsruhe, Karlsruhe, 1992

[53] Shahed, S. M.; Chiu, W. S.; Yumlu, V. S.: A Preliminary Model for the Formation of Nitric Oxide in Direct Injection Diesel Engines and its Application in Parametric Studies. SAE Technical Paper 730083, Detroit, 1973

[54] Hiroyasu, H.; Kadota, T.; Arai, M.: Development and Use of a Spray Combustion Modeling to Predict Diesel Engine Efficiency and Pollutant Emissions, Part I, Combustion Modeling. Bulletin of the JSME, Vol. 26, pp. 569-575, 1983

[55] Rakopoulos, C. D.; Hountalas, D. T.: Development and Validation of a 3-D Multi-Zone Combustion Model for the Prediction of a DI Diesel Engines Performance and Pollutants Emissions. SAE Transactions, Journal of Engines, Vol. 107, pp. 1413-1429, Detroit, 1998

[56] Stiesch, G.: Modeling Engine Spray and Combustion Processes. Springer, Berlin, 2003

[57] Reinhardt, H.: Modellierung des Zündverzuges bei Mehrfacheinspritzungen aufgeladener Dieselmotoren mit Direkteinspritzung innerhalb der thermodynamischen Prozessrechnung. Abschlussbericht, FVV Heft 870, 2008

[58] Borman, G. L.; Johnson, J. H.: Unsteady Vaporization Histories and Trajectories of Fuel Drops Injected into Swirling Air. SAE Technical Paper 620271, Detroit, 1962

[59] Jung, D.; Assanis, D. N.: Multi-Zone DI Diesel Spray Combustion Model for Cycle Simulation Studies of Engine Performance and Emissions. SAE Technical Paper 2001-01-1246, Detroit, 2001

[60] Rakopoulos, C. D.; Antonopoulos, K. A.; Rakopoulos, D. C.: Development and application of multi-zone model for combustion and pollutants formation in direct injection diesel engine running with vegetable oil or its bio-diesel. Energy Conversion and Management, Vol. 48, Issue 7, pp. 1881–1901, 2007

[61] Hountalas, D. T.; Lamaris, V.; Pariotis, E. G.; Ofner, H.: Parametric Study Based on a Phenomenological Model to Investigate the Effect of Post Fuel Injection on HDDI Diesel Engine Performance and Emissions – Model Validation using Experimental Data. SAE Technical Paper 2008-01-0641, Detroit, 2008

[62] Woschni, G.: A Universally Applicable Equation for the Instantaneous Heat Transfer Coefficient in Internal Combustion Engines. SAE Technical Paper 6700931, Detroit, 1967

[63] Woschni, G.: Einfluß von Rußablagerungen auf den Wärmeübergang zwischen Arbeitsgas und Wand im Dieselmotor. Tagung: Der Arbeitsprozess des Verbrennungsmotors, Graz, 1991

[64] Hohenberg, G.: Experimentelle Erfassung der Wandwärme von Kolbenmotoren. Habilitationsschrift, Technische Universität Graz, Graz, 1980

[65] Bargende, M.: Ein Gleichungsansatz zur Berechnung der instationären Wandwärmeverluste im Hochdruckteil von Ottomotoren. Dissertation, Technische Universität Darmstadt, Darmstadt, 1991

[66] Wimmer, A.; Pivec, R.; Sams, T.: Heat Transfer to the Combustion Chamber and Port Walls of IC Engines – Measurement and Prediction. SAE Technical Paper 2000-01-0568, Detroit, 2000

[67] Lavoie, G. A.; Heywood, J. B.; Keck, J. C.: Experimental and Theoretical Investigation of Nitric Oxide Formation in Internal Combustion Engines. Combustion Science Technology Vol. 1 pp. 313-326, 1971

[68] Tao, F.; Srinivas, S.; Reitz, R. D.; Foster, D. E.: Comparison of Three Soot Models Applied to Multi-Dimensional Diesel Combustion Simulations. JSME International, Series B, Vol 48, No. 4, 2005

[69] Schubiger, R. A.; Boulouchos, K.; Eberle, M. K.: Rußbildung und Oxidation bei der dieselmotorischen Verbrennung. MTZ Fachartikel 05/2002, 2002

[70] Thoma, M.; Stiesch, G.; Merker, G. P.: A Phenomenological Spray and Combustion Model for Diesel Engines with Pre-Injection. 5th International Symposium of Internal Combustion Diagnostics, pp. 90-101, Baden-Baden, 2002

[71] Castagna, E.; Biondo, M.; Cottrell, J.; Altenstrasser, H.; Beidl, C.; Koegeler, H. M.; Schuch, N.: Multiple Tier 3 Engine Applications on global modelling. MTZ Fachartikel 06/2007, 2007

[72] Haas, S. F.: Experimentelle und theoretische Untersuchung homogener und teilhomogener Dieselbrennverfahren. Dissertation, Universität Stuttgart, Stuttgart, 2007

[73] Sams, T.; Theissl, H.; Daum, S.; Glensvig, M.; Csato, J.: Möglichkeiten und Grenzen der Low-Nox Dieselverbrennung im Hinblick auf EURO 6. 11. Tagung: Der Arbeitsprozess des Verbrennungsmotors, Graz, 2007

[74] Hountalas, D. T.; Lamaris, V. T.; Pariotis, E. G.: Identification of the Error Introduced in DI Diesel Phenomenological Mutli-Zone Models from Assumptions Related to the Initial conditions at the Nozzle Exit. SAE Technical Paper 2010-01-0153, Detroit, 2010

[75] Leifert, T.; Nevado, F. M. Fairbrother, R.: Erweiterte Thermodynamische Analyse mittels AVL-GCA zur effektiven Unterstützung der Entwicklung und Kalibrierung von Verbrennungsmotoren. Tagung: Motorprozess und Aufladung II, IAV & Expert Verlag, Berlin, 2007

[76] Hrauda, G.; Strasser, R.; Aschaber, M.: Gas Exchange Simulation from Concept to Start of Production – AVL's Tool Chain in the Engine Development Process. THIESEL, Valencia, 2010

[77] Wenzel, S. P.: Modellierung der Ruß- und NOx- Emissionen des Dieselmotors. Dissertation, Otto-von-Guericke-Universität Magdeburg, Magdeburg, 2006

[78] Krueger, C.: Validierung eines 1D-Spraymodells zur Simulation der Gemischbildung in direkteinpritzenden Dieselmotoren. Dissertation, Technische Universität Aachen, Aachen, 2001

[79] Reitz, R. D.; Diwakar, R.: Structure of High Pressure Fuel Sprays. SAE Technical Paper 870598, Detroit, 1987

10 Appendix

10.1 Combustion Reaction

In chapter 4.2.4 the combustion reaction is given in the most general form by eq. (4-16). As mentioned, the values used for the model parameters and exponents given in the literature differ significantly. In general, the impact of the reaction on the overall combustion process is small, because in most phases the mixture formation is more dominant. Still, a sensitivity analysis is conducted by comparing different approaches. At first, the reaction equation is repeated in a slightly different form, where the Arrhenius-type approach comes to the fore (compare to eq. (2-3) and eq. (2-4)). In the reformulated eq. (10-1), the educts concentrations are expressed in terms of mass fractions of fuel vapor and oxygen. The reaction term *k* additionally considers the density and pressure in the pre-exponential term.

$$\frac{dx_{fb}}{dt} = \frac{d}{dt}\left(\frac{m_{fb}}{m_i}\right) = \underbrace{K_b \cdot \rho_{ch}^{\,a_{rho}} \cdot p^{b_p} \cdot e^{\frac{-E_a/R_m}{T_i}}}_{\text{Reaction Term 'k'}} \cdot \underbrace{x_{fv} \cdot x_{o_2}^{\,c_{O_2}}}_{\text{Educt Concentrations}} \tag{10-1}$$

Table 5 summarizes the parameter values of three approaches of interest. The first one is the model by Stiesch [56] which uses high values for the oxygen exponent c_{O2} and for the activation energy.

The second one is the model by Jung and Assanis [59] who consider two reaction steps: One for the 'premixed' part of combustion, which is applied for the fuel which evaporates during ignition delay (in each individual zone), and another one for the subsequent 'unmixed' reaction. The two reaction steps differ by very different values for the oxygen exponent. The activation energies are one order of magnitude lower compared to the approach of Stiesch.

The third approach was used for the present work, as it has shown to deliver good results.

Table 5: Overview of Model Parameters of the Combustion Reaction

		a_{rho}	b_p	c_{O2}	E_a/R_m
Stiesch [56]		0	0	5	12.000
Jung et al. [59]	premixed	1	0	5	1200
	unmixed	0	1	1	2500
Present Work		1	0	1.5	1200

The different approaches are compared on the basis of their Arrhenius plots, which show the reciprocal temperature *-1000/T* on the abscissa and the logarithm of the kinetic constant *ln(k)* on the ordinate. Therefore, eq. (10-1) is reformulated and expressed in logarithmic form with $K_b' = ln(K_b)$. For reaction mechanisms which are mainly governed by the exponential term, the reaction rate characteristics show straight lines in the Arrhenius plot.

$$\ln(k) = \frac{-E_a/R_m}{T_i} + \ln\left(\rho_{ch}^{\,a_{rho}} \cdot p^{b_p}\right) + K_b' \tag{10-2}$$

Figure 77 shows the Arrhenius plot for the reaction using the parameters suggested in the present work, i.e. $a_{rho}=1$, $c_{O2}=1.5$ and $E_a/R_m=1200$. The dashed lines represent the reaction rate characteristics versus temperature at constant zone concentrations defined by λ_Z, $x_{O2}^{\,ch}$ (given in the top section of the plot) and x_b (compare chapter 2.1.2). Surprisingly the reaction rate at constant *k* decreases with increasing temperature. This is caused by the consideration of the density in the pre-exponential term which is reciprocal to the temperature at constant pressure. According to [4], the density is especially relevant for bi-molecular and tri-molecular reactions where it impacts in the 2nd, respectively 3rd power.

The by far predominant effect however, is the decrease of the reaction rate with increasing x_b. In Figure 77 the full lines show the combustion characteristics under consideration of the interrelation of temperature and reactant concentrations during the reaction. On the basis of the Arrhenius law, one would assume that due to the temperature increase the combustion rate gets faster. However, at the same time fuel vapor and oxygen are consumed. This is mathematically represented in a weakening of the educts concentration term in eq. (10-1). Thus, it can be observed that the highest reaction rates occur at the beginning of combustion (i.e. at $x_b = 0$ *to* 0.1) due to the high concentrations of all educts. Towards the end of combustion the reaction rate drops significantly (logarithmic scaling!), as at least one of the reactant concentrations approaches zero asymptotically.

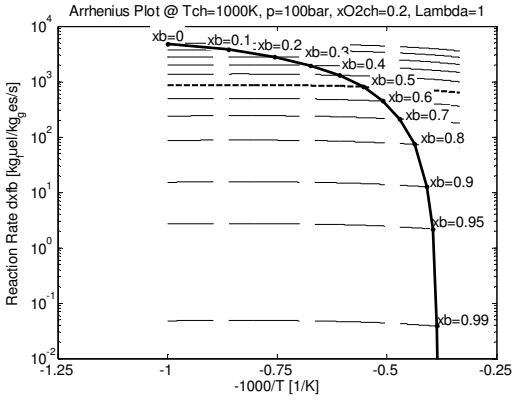

Figure 77: Reaction Mechanism used in this Work

Figure 78 shows the Arrhenius plot for the reaction mechanism of Stiesch. Here, the reaction rate at constant x_b indeed shows straight lines that increase with the temperature. This is caused by the high value for the activation energy and the neglecting of the density and pressure impact ($a_{rho}=0$ and $b_p=0$). Therefore, there is a peak in the reaction rate at $x_b=0.3$ to 0.4. After that, the reaction rate drops sharply which is caused by the high exponent of $c_{O2}=5$ in the oxygen concentration.

When using a high value for the oxygen exponent c_{O2}, it is necessary to increase the overall reaction parameter K_b to achieve a complete combustion. This is attributed to the fact that the zone oxygen concentration drops sharply towards the end of combustion for zone lambda values less or equal 1. Thereby, the reaction mechanism is much too fast under most conditions, which makes the overall heat release calculation rather insensitive to the reaction mechanism. This can lead to an undesirable behavior in the initial premixed combustion phase where the highest oxygen concentrations occur and at the same time the heat release is, in the theoretical conception, chemical kinetics controlled.

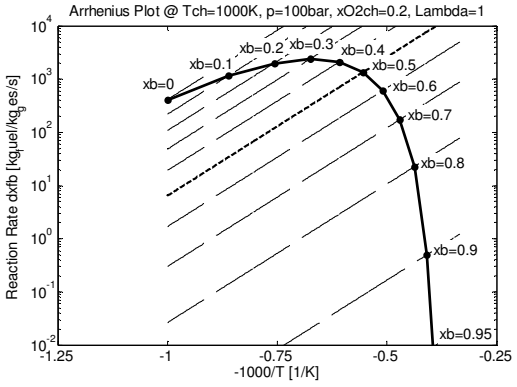

Figure 78: Reaction Mechanism of Stiesch

Jung and Assanis try to overcome this discrepancy by modeling the reaction mechanism in two steps. Figure 79 shows the reaction rate characteristics for both formulations. In the premixed phase (left), the

reaction rate is determined by the high value for the oxygen exponent and at the same time the gradient towards temperature is negative. Therefore the reaction rate drops very fast and abandons the ordinate scale at x_b=*0.8* to *0.9*.

Jung and Assanis deliberately choose a rather rapid reaction rate for the unmixed phase (right), as they assume that the later combustion phase is predominantly mixing controlled. This is achieved by choosing a low value for the oxygen exponent and pronouncing the temperature dependency by an increase of the activation energy.

The resulting characteristics for the combustion of a single zone are depicted in Figure 80. For the figure it was assumed that 20% of the fuel in the zone burns under premixed conditions.

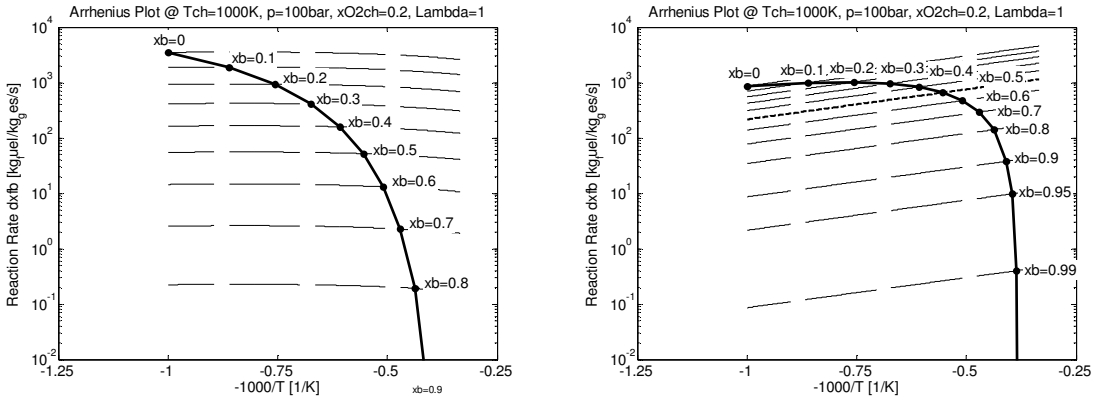

Figure 79: Reaction Mechanism of Jung and Assanis (left) premixed (right) unmixed

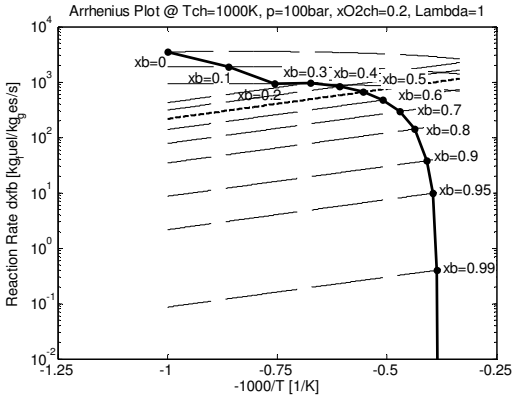

Figure 80: Combined Reaction Mechanism of Jung and Assanis
Combined Approach assuming a premixed Fraction of 0.2